Interferon Regulatory Factor 6 Determines Intestinal Epithelial Cell Development and Immunity

By

Austin Wright

A DISSERTATION

Presented to the Department of Molecular Microbiology and Immunology

and Oregon Health & Science University

School of Medicine

in partial fulfillment of

the requirements for the degree of

Doctor of Philosophy

June 2023

School of Medicine

Oregon Health &Science University

CERTIFICATE OF APPROVAL

This is to certify that the PhD dissertation of

Austin Paul Wright

Has been approved

Advisor_____ Timothy Nice _____

Member_____ William Messer _____

Member _____ Fikadu Tafesse _____

Member _____ Isabella Rauch _____

Member _____Lauren Rodda_____

Table of Contents

List of Figures

List of abbreviations

AIG1	androgen inducible 1
AKT	AT1 by inhibiting RAC-alpha serine/threonine-protein kinase
AMPs	antimicrobial proteins
AP-1	activator protein-1
ASC	apoptosis-associated speck-like protein containing a CARD
BATF3	Basic leucine zipper ATF-like transcription factor 3
BCL6	B cell lymphoma 6
BLIMP1	B lymphocyte-induced maturation protein 1
BMDM	Bone marrow derived macrophages
BMP2	Bone morphogenic protein 2
BV2	microglial cell line
CAMK1D	calcium/calmodium dependent protein kinase 1D
CAMP	cathelicidin antimicrobial protein
CBCs	crypt-based columnar stem cells
CCL5	C-C chemokine ligand 5
cDCs	conventional dendritic cells
cDNA	complementary DNA
ChIP-seq	chromatin immunoprecipitation sequencing
CLR	centered log-ratio
CM	conditioned media
CMV	cytomegalovirus
CRAMP	mouse cathelicidin
CRISPR	clustered regularly interspaced short palindromic repeats
DBD	DNA binding domain
DCs	dendritic cells
DEGs	differentially expressed genes
DLL1	Delta like ligand 1

DLL4	Delta like ligand 4
DMEM	Dulbecco's modified eagle medium
DMSO	dimethyl sulfoxide
DNA	deoxyribonucleic acid
C/EBP	CAAT-enhancer-binding protein
EECs	enteroendocrine cells
EGF	epidermal growth factor
EGFR	epidermal growth factor receptor
EICE	Ets-IRF composite element
EIF4G3	eukaryotic translation initiation factor 4 gamma 3
EMT	epithelial to mesenchymal transformation
EpCam	epithelial cell adhesion molecule
ERK	Extracellular signal-regulated kinase
FACS	fluorescence-activated cell sorting
FAE	follicle-associated epithelium
FBS	fetal bovine serum
FFPE	formalin-fixed paraffin-embedded
FISH	fluorescence in situ hybridization
FlaTox	flagellin toxin
FOXP3	foxhead box P3
FSL-1	fibroblast-stimulating lipopeptide 1
GALT	gut-associated lymphoid tissue
GAS	gamma-activated sites
GEO	gene expression omnibus
GFP	green fluorescent protein
GO	gene ontology
GRHL3	grainy head like protein 3
gRNA	genomic RNA

HBGAs	histo-blood group antigen
HEPES	4-(2-hydroxyethyl)-1-piperazineethanesulfonic acid
HIPK2	homeodomain-interacting protein kinase 2
HNoV	human norovirus
HSCs	hematopoietic stem cell
HTO	oligonucleotide-tagged antibodies
IAD	interferon regulatory factor-association domain
IAD1	interferon regulatory factor-association domain 1
IAD2	interferon regulatory factor-association domain 2
ICSBP	Interferon consensus sequence binding protein
IEC	intestinal epithelial cell
IFN	interferon
IFNAR	interferon alpha receptor
IFNAR1	interferon alpha receptor 1
IFNAR2	interferon alpha receptor 2
IFNGR	interferon gamma receptor
IFNGR1	interferon gamma receptor 1
IFNGR2	interferon gamma receptor 2
IFNLR1	interferon lambda receptor 1
IgA	immunoglobulin A
IgG	immunoglobulin G
IgM	immunoglobulin M
IL-1	interleukin 1
IL-23p19	interleukin 23 subunit alpha
IL-25	Interleukin 25
IL-36	Interleukin 36
IL-6	Interleukin 6
IL10RB	interleukin 10 receptor subunit beta

IL2RA	Interleukin 2 receptor alpha
IRAK1	IL-1 receptor-associated kinase-1
IRF	interferon regulatory factor
ISG	interferon stimulated gene
ISGF3	interferon stimulated gene factor 3
ISRE	IFN-stimulated response elements
ITK	inducible T-cell kinase
JAK	Janus kinase
JAM2	junction adhesion molecule 2
KC	keratinocyte chemoattractant
KDR	kinase insert domain receptor
KO	knock out
KPNA3	karyopherin subunit alpha 3
LL-37	cathelicidin
LPS	Lipopolysaccharides
LTBP1	latent transforming growth factor beta binding protein 1
LysM	lysozyme M
LysP	lysozyme P
M2C	intestinal epithelial cell line
MAPK	mitogen activated protein kinase
MDA5	melanoma differentiation-associated protein 5
MH2	Mad-homology 2
MHC	major histocompatibility complex
MNV	murine norovirus
MOI	multiplicity of infection
mRNA	messenger RNA
mTOR	mammalian targeting of rapamycin
MX1	myxovirus resistance 1

MyD88	myeloid differentiation primary response protein 88
NFAT	nuclear factor of activated T-cells
NFkB	Nuclear factor kappa-light-chain-enhancer of activated B cells
NGS	next generation sequencing
NK	Natural Killer
NLRP3	nod-like receptor family pyrin domain containing 3
NLRs	NOD-like receptors
NoV	Norovirus
NT	non-targeting
NTP	nucleoside triphosphate
ORFs	open reading frames
OVOL1	Ovo-like 1
P.I.	propidium iodide
PAMPs	pathogen associated molecular patterns
PBMCs	peripheral blood mononuclear cells
PBS	phosphate buffered saline
PCA	principal component analysis
PCR	polymerase chain reaction
pDCs	plasmacytoid dendritic cells
PFU	plaque forming units
PI3K	pathways and phosphoinositide 3-kinases
pIgR	polymeric immunoglobulin receptor
PIM1	proto-oncogene, serine/threonine kinase
PP	Peyer’s patches
PPAR	Peroxisome Proliferator Activated Receptor
PPS	Popliteal pterygium syndrome
PRRs	Pattern-recognition receptors
qPCR	quantitative polymerase chain reaction

RAG1	recombination activating gene 2
RAG2	recombination activating gene 2
RdRp	RNA dependent RNA polymerase
RIG-I	retinoic-acid inducible gene I
RIPK4	Receptor-interacting serine/threonine-protein kinase 4
RLRs	RIG-I-like receptors
RNA	ribonucleic acid
RNAseq	ribonucleic acid sequencing
ROS	reactive oxygen species
RSPO	R-spondin
RT	room temperature
SCT	secretin
SecPro	secretory progenitor
SIgA	secretory immunoglobulin A
SLIT2	slit guidance ligand 2
SMARCA1	SWI/SNF Related, Matrix Associated, Actin Dependent Regulator Of Chromatin, Subfamily A, Member 1
SNAI2	Snail homolog 2
SOCS1	Suppressor of cytokine signaling 1
SOCS3	Suppressor of cytokine signaling 3
STAT	signal transducer and activator of transcription
STING	stimulator of interferon genes
STS	staurosporine
TA	transit amplifying
TAK1	TGF-β–activated kinase 1
TBK1	TANK-binding kinase 1
TCR	T cell receptor
TFAP2A	activating enhancer binding Protein 2 alpha

TGF	transforming growth factor
TLR	Toll-like receptor
TNF	tumor necrosis factor
TRIF	TIR domain containing adaptor molecule 1
TYK2	tyrosine kinase-2
USP18	Ubiquitin specific protein 18
VF1	virulence factor 1
VP	viral protein
VPg	viral protein genome-linked
VWS	Van der Woude syndrome
WT	wild type
XBP1	X-box binding protein 1

Acknowledgments

Completing this PhD thesis has been a long and challenging journey, and I am deeply indebted to many individuals who have supported and encouraged me along the way.

First and foremost, I would like to express my sincere gratitude to my advisor, Dr. Tim Nice, for their unwavering support, insightful guidance, and constant encouragement throughout my research. Their expertise and patience have been invaluable, and their dedication to my success has been a driving force in the completion of this work.

I am also profoundly grateful to the members of my dissertation committee, Dr. William Messer, Dr. Fikadu Tafesse, and Dr. Isabella Rauch, for their thoughtful feedback, constructive criticism, and valuable suggestions which have greatly improved the quality of my research.

Special thanks go to my colleagues and friends in the Molecular Microbiology and Immunology department at OHSU. Your camaraderie, intellectual discussions, and moral support have made this journey both enjoyable and enriching. I am particularly thankful to Bryan Ramirez Reyes for assistance with qPCR of Irf6, Shelby Madden for assistance with organoid growth curve, Sydney Harris for assistance with qPCR and organoid size measurements, Ethan Mulamula for assistance with M2C growth curve, Dr. Alexis Gibson for assistance with FlaTox assay, and Dr. David Constant for assistance with RNA scope of Irf6 in the intestines.

I would like to acknowledge the financial support provided by the National Institute of Health. Without their generous funding, this research would not have been possible.

On a personal note, I am deeply thankful to my family for their love, patience, and unwavering belief in me. To my Mom and Step-Dad, thank you for your endless encouragement and for instilling in me the value of education and hard work. To my sweet little daughter Lilah who has filled my life with joy and laughter. To all my friends, your support and understanding have been my anchor during the most challenging times of this journey.

Lastly, I would like to dedicate this thesis to my late brother Michael, whose memory and inspiration have been a guiding light throughout my life. I wish you were still here to celebrate this with me.

Thank you all for making this achievement possible.

Abstract

Intestinal epithelial cell (IEC) responses to interferon (IFN) favor antiviral defense with minimal cytotoxicity, but IEC-specific factors that regulate these responses remain poorly understood. Interferon regulatory factors (IRFs) are a family of nine related transcription factors, and IRF6 is preferentially expressed by epithelial cells, but its roles in IEC immunity are unknown. In this study, Clustered Regularly Interspaced Short Palindromic Repeats (CRISPR) screens found that *Irf6* deficiency enhanced IFN-stimulated antiviral responses in transformed mouse IECs but not macrophages. Furthermore, knockout (KO) of *Irf6* in IEC organoids resulted in profound changes to homeostasis and immunity gene expression. *Irf6* KO organoids grew more slowly, and single-cell ribonucleic acid sequencing indicated reduced expression of genes in epithelial differentiation and immunity pathways. IFN-stimulated gene expression was also significantly different in *Irf6* KO organoids, with increased expression of stress and apoptosis-associated genes. Functionally, the transcriptional changes in *Irf6* KO organoids were associated with increased cytotoxicity upon IFN treatment or inflammasome activation. These data indicate a previously unappreciated role for IRF6 in IEC biology, including regulation of epithelial development and moderation of innate immune responses to minimize cytotoxicity and maintain barrier function.

Chapter 1: Introduction

Barrier Immunity

Physical and Chemical Barrier

The vertebrate innate immune system is comprised of several specialized cells and signaling molecules that detect and respond to pathogens in an immediate manner. The foundation of the innate immune system is the epithelial barrier separating the outside world from the inside organism and consists of a chemical, physical, and immunological barrier (**Fig 1.1**). At a macro level, the barrier defining the beginning and end of an organism seems obvious, but when we zoom in there is a complex system that has evolved to maintain this separation and ward of the constant barrage of physical damage, toxins, chemicals, and pathogens. Epithelial cells are burdened with the task of maintaining the physical barrier. To help prevent the colonization of invading pathogens and recover from damage, epithelial cells are constantly being sloughed off and replenished. Epithelial cells also play central roles in generating antimicrobial chemicals and cultivating commensal microbes.

The skin is a large barrier that utilizes keratinized cells to provide a dry tough environment that is not well suited for microbial colonization. Skin cells known as keratinocytes go through a differentiation process starting from a progenitor stem cell and ending in a dehydrated keratinized dead cell that eventually falls off the organism resulting in a dry hard surface that is difficult for microbes to penetrate. Terminally

differentiated keratinocytes known as corneocytes primarily act as the barrier stacked together in a “brick and mortar” fashion with lipids interspersed between them functioning as the “mortar” [1]. There are several antimicrobial proteins (AMPs) such as defensins and cathelicidins found on the skin which provide defense against pathogens and modulate the immune response [2]. Interestingly, the skin has an acidic pH of about 5.5 as a result of lactic acid in the sweat and urocanic acid produced by a histidine ammonia-lyase in corneocytes [3]. The epidermal barrier is so effective as a barrier that the most likely route of infection in the skin would be through penetration.

Mucus membranes are the other types of physical barriers that are required to defend against the outside world and are found in the digestive, respiratory, and reproductive systems, as well as sensory organs. Unlike the skin, mucus membranes are moist and soft, which allows for lubrication, nutrient absorption, gas exchange, transport and prevents dehydration of the epithelial cells that line the mucus membranes. Fluid flow and transport are also important functions of mucus membranes. For example, ciliated epithelium beat in a coordinated and polarized manner to generate fluid flow in the respiratory tract to help mucus flow over the surface, the ependyma facilitate the flow of spinal fluid in the brain ventricles, and the ovum is transported by ciliated epithelium in the oviduct as well. Instead of maintaining a constant supply of dry hardened cells, the mucus membrane produces mucus to retain moisture and provide a chemical barrier that is difficult for microbes to cross. Mucus also protects the epithelial cells from harmful substances like stomach acid and urine. The mucus layer is a

viscoelastic secretion comprised of glycoproteins, globulins, electrolytes, and lipids [4]. [5]

Mucin is the primary functional component of mucus. Mammals have 22 different mucins, and they can be classified broadly by either membrane bound or secreted. Mucins are highly glycosylated proteins and can be produced in monomers, dimers, and multimers to provide complex chemical structures that are difficult for invading pathogens to navigate. Apart from the gel like state of mucus, many antimicrobial proteins are important contributors to the effectiveness of mucus to provide protection to mucus membranes. The major defensive proteins found in the mucus are antimicrobial proteins (AMPs), enzymes, chelators, immunoglobulins, protease inhibitors, cytokines, and growth factors (Figure 1.1). Defensins are type of innate AMPs found in mucus that have been shown to disrupt the membrane of bacteria, inhibit cell wall synthesis, neutralize secreted bacterial toxins, disrupt viral entry, or inhibit viral uncoating after entry [6], [7], [8], [9], [10], [11].

Cathelicidins are another major class of proteins known to have antimicrobial properties found on both the skin and in mucus. Orthogonal cathelicidins are found in wide variety of vertebrates including fish, reptiles, birds, and mammals. Humans have one cathelicidin gene known as cathelicidin antimicrobial protein (*CAMP*) which gets cleaved into LL-37. Highly expressed in epithelial cells and immune cells, LL-37 is shown to generate pores in the membranes of bacteria, inhibits bacterial growth, disrupts biofilm formation, and neutralize viral particles through direct interaction [12], [13], [14], [15], [16], [17], [18]. In addition to direct inhibition of viral particle neutralization,

cathelicidin proteins were shown to enhance the expression of the antiviral cytokine interferon beta (IFN-β) by the astrocyte cell line U251 cells when they were incubated with either LL-37 or CRAMP (mouse cathelicidin), and the expression of (IFN-β) mRNA was enhanced when U251 cells were pretreated with cathelicidins before entrovirus 71 infection [18]. During wound healing, cathelicidins and other AMPs are highly produced in damaged tissues along with a non-coding RNA U1. Immune tolerance to U1 RNA is

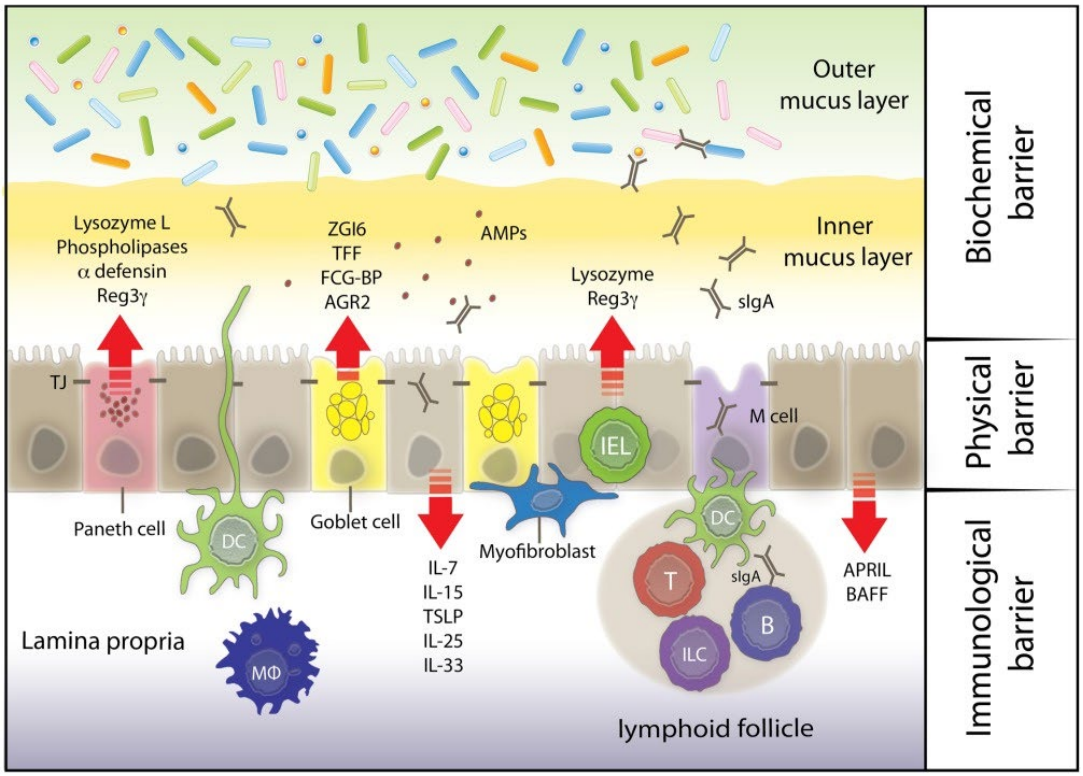

Figure 1.1 Biochemical, physical, and immunological barrier of mucus membranes.

Paneth cells, intraepithelial lymphocytes, and goblet cells produce and secrete protective antimicrobial proteins, enzymes, and mucins that make up the biochemical barrier. The physical barrier provided by polarized epithelial cells is held together by tight junctions and that allow for the regulation of specific uptake of nutrient. Dendritic cells, macrophages, intraepithelial lymphocytes, and innate lymphoid comprise the immunological barrier along with sIgA that is translocated through the epithelial cells into the mucus layer.

Adapted with permission from John Wiley and Sons: IUBMB Life Keeping bugs in check: The mucus layer as a critical component in maintaining intestinal homeostasis, Martin Faderl, Mario Noti, Nadia Corazza, Christoph Mueller, 2015.

broken when it binds to cathelicidin and activates the production of inflammatory

cytokines and interferons after being endocytosed through scavenger receptors [19].

Many different types of enzymes can be present in mucus. Digestive pancreatic

enzymes can be found in the mucus layer in the intestine, but lysozyme (muramidase) is

the most important defensive enzyme and is a cornerstone of innate immunity (Figure 1.1). Discovered by Alexander Fleming over 100 years ago, lysozyme was shown to be present in sputum, tears, and mucus and had antibacterial properties toward *Micrococcus lysodeikticus* [20]. Lysozyme causes bacterial cell lysis through hydrolysis of the glycosidic bond between the monomers that form the peptidoglycan layer of the cell wall [21]. In addition to hydrolysis, human lysozyme has a cationic nature that allows for pore formation of the negatively charged cell membrane of bacteria [22]. The digestion of bacterial walls and membranes releases bacterial products that enhance phagocytic activation while digestion of peptidoglycan by lysozyme has been shown to decrease inflammation. Lysozyme M knockout mice (*Lyz2*$^{-/-}$) have increased bacterial burden and decreased survival when infected with *Klebsiella pneumonia* despite compensation by the upregulation of LysP (the lysozyme preferentially expressed by Paneth cells) [23]. To determine the role of LysM on inflammation apart from controlling bacterial burden, which is inherently inflammatory, heat killed *Microcossus lutes* and purified peptidoglycan was subcutaneously injected into *Lyz2*$^{-/-}$and WT mice[24]. Lesions were larger and more prolonged in *Lyz2*$^{-/-}$mice indicating the digestion of peptidoglycan by Lysozyme in the lesion was playing an important role in decreasing the inflammatory response in addition to its role in controlling bacterial growth [24].

Iron is an essential nutrient that can be difficult for bacteria to acquire, and sequestering the available iron is one immunological strategy for inhibiting unwanted growth of a wide variety of pathological microorganisms[25]. Lactoferrin is an iron chelating protein known to have inhibitory effects on all types of microorganism

pathogens. Discovered through investigations into the antibacterial properties of cow's milk, lactoferrin withstood heat treatment but was destroyed by trypsin digestion and antibacterial properties were prevented by the addition of iron Fe^{2+} [26]. Lactoferrin chelates two ferric iron (Fe^{3+}) atoms and does not release the iron even at a low Ph. In addition to the chelating properties lactoferrin has been shown to inhibit viral infections through either direct interaction of the viral particle or by blocking the receptor proteins on the cell membrane [27]. Though found at all mucosal membranes, the cervico-vaginal fluid was found to have the highest concentration of lactoferrin, and levels fluctuate during the ovulatory cycles with lactoferrin levels being highest during ovulation [28], [29].

The chemical barrier is a crucial component of barrier immunity. By creating an environment that is hostile to pathogens, the chemical barrier prevents the colonization and proliferation of harmful microorganisms on bodily surfaces. Substances such as enzymes (e.g., lysozyme), antimicrobial peptides (e.g., defensins, cathelicidins), and acidic secretions (e.g., stomach acid) can directly kill or inhibit the growth of microbes. The chemical barrier helps maintain a balance in the body's microbiota, ensuring that beneficial microbes thrive while keeping pathogenic ones in check. Components of the chemical barrier can interact with and enhance adaptive immunity; for example, antimicrobial peptides can serve as adjuvants, enhancing the immune response to antigens. In summary, the chemical barrier is essential for immediate protection against infections, maintaining a healthy microbiota, and supporting both innate and adaptive

immune responses. Its role is fundamental in preventing pathogens from establishing infections and in orchestrating an effective immune response when breaches occur.

Immunological Barrier

Apart from the chemical barrier and the physical barrier there are many tissue-resident immune cells that survey the microbial and chemical environment directly in contact with each of the barrier membranes (Figure 1.1). The majority of immune cells reside near barrier sites spanning from innate immune cells (e.g., macrophages, eosinophils, dendritic cells, mast cells, and innate lymphoid cells) that directly kill invading pathogens to memory B and T cells that reside near sites of previous infection.

In the event of a pathogen getting past the chemical and physical barrier, tissue resident immune cells are quickly activated and begin to defend the host from the invasion. In the epidermis, specialized dendritic cells called Langerhans cells survey microbial presence and determine the appropriate immune response (either tolerance or inflammation) [30]. In the absence of pathogens, Langerhans cells promote the expansion of tissue resident regulatory T (Treg) cells [31], [32]. When Langerhans cells become activated in the presence of pathogens, they activate the innate immune response. Langerhans cells are constantly sampling the environment through their follicular dendrites and phagocytosis, they then migrate to cutaneous lymph nodes to present the antigens to $CD8^+$ and $CD4^+$ T cells resulting in either tolerance or inflammation [33], [34].

Tissue resident immune cells monitor the mucus membrane as well. Dendritic cells in the gut regularly sample the microbiome by extending their dendrites between epithelial cells [35]. These dendritic cells express tight junction proteins that allow for the membrane integrity to be maintained during the sampling [35]. Dendritic cells migrate to peripheral lymph nodes to present antigens to T and B cells in the germinal center.

Peyer's patches (PP) are secondary lymphoid tissues found primarily along the small intestine. The follicular associated epithelium around PP's contains specialized microfold cells (M cells) that continuously take up contents from the lumen[36]. Within the M cells are small pockets on the basal lateral side that typically houses a leukocyte and allows for DC to uptake the transcytosed antigen package (Figure 1.1)[36]. The antigen taken up by M cells is quickly transferred to dendritic cells and taken to the germinal center of the PP for antigen presentation to produce long-lived antibody producing plasma cells and memory B cells [36], [37], [38].

The antibodies produced in the PP, particularly IgA antibodies, are an essential part of defense in the intestine. B cells in the PP are activated after antigen presentation and differentiate into plasma cells that produce and secrete large amounts of IgA antibodies [38], [39]. While all types of antibodies can be found systemically, IgA antibodies are primarily utilized at barrier sites, being secreted into the mucus membranes and the skin through sweat glands [38], [39], [40], [41], [42]. Delivery of IgA to mucosal surface requires translocation through the epithelial layer. The polymetric immunoglobulin receptor PIgR binds to the J chain region of polymerized IgA and

transports it to the apical side of the epithelium [43]. Once secreted, IgA antibodies bind to antigens, such as bacteria, viruses, parasites, and food antigens to neutralize the pathogens.

Microbiome

The combination of the chemical, physical, and immunological barrier provides a strong defense against the constant barrage of environmental damage and pathogenic invasion, but beneficial microbes that have evolved to colonize barrier sites of organisms also have a barrier function. The microbiome has been shown to play an important role in preventing colonization by pathogens, promoting healthy development of epithelial cells, and maintaining the anaerobic environment in the intestinal lumen [44], [45], [46], [47], [48], [49], [50], [51], [52], [53]. The microbiome can differ greatly between individuals and can have wide variations in the same individual when sampled over time [54]. While there are large gaps in our knowledge of the composition of the microbiome and what role each organism plays in the health of the host, we know for sure that the healthy development of mucus membranes, skin, and the immune system requires the appropriate stimulation from the beneficial microbes residing within us and on our skin [47], [49], [50], [53]. Specialized ecological systems have evolved differently for each part of the body and microbes can be beneficial in one location while being problematic in a different location. For example, beneficial bacteria in the intestines can be severely damaging to other mucosal membranes. The combination of the microbiome, chemical,

physical, and immunological barrier allows for a strong defensive barrier to the outside world.

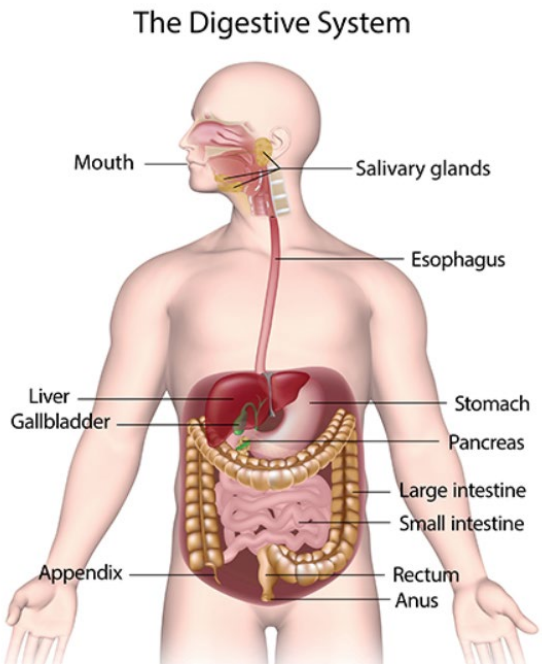

Figure 1.2 The digestive system.

The digestive system is comprised of several solid and hollow organs that break down and absorb food. The hollow organs that make up the gastrointestinal tract are the mouth, esophagus, stomach, small intestine, large intestine, and anus. The solid organs that make up the digestive system are the liver, pancreas, and gall bladder.

Adapted with permission from National Institute of Diabetes and Digestive and Kidney Diseases. Your Digestive System & How it Works, 2017.

Intestinal Epithelium

The Gastrointestinal Tract

Mucosal barriers are the most probable route of infection for all pathogens, and the gastrointestinal tract is the largest mucosal barrier. The digestive system is comprised of organs including the mouth, esophagus, stomach, liver, pancreas, gallbladder, small intestine, large intestine, and anus (Figure 1.2). Digestion begins in the mouth. Chewing or masticating is an important part of digestion as it physically breaks down food and mixes saliva to form a bolus. Saliva has many enzymes that break down food including carbohydrases, esterases, transferring enzymes, and proteolytic enzymes [55]. The sources of these enzymes can be glandular, microbial, or immunological[55]. The most prominent enzyme in saliva is amylase which breaks down starch molecules into smaller maltose molecules

[56], [57]. Saliva lubricates and solubilizes food which enhances taste and lubricates the bolus to help the food travel down the esophagus into the stomach without causing damage to the mucus membrane.

In the stomach, the bolus is mixed with gastric secretions and becomes chyme. The chyme is mechanically and chemically digested in the stomach before entering the small intestine. Oxyntic glands in the stomach contain parietal cells that produce hydrochloric acid which kill microorganisms, denature proteins, and activates the proteolytic enzyme pepsin. Mechanical digestion in the stomach occurs through peristaltic contractions of the stomach forcing the chyme against a constricted pylorus which only allows food smaller than about 2 mm to pass into the duodenum of the small intestine.

The intestines are divided into two major organs, the small and large intestine. The majority of the chemical digestion of the chyme occurs in the small intestine which is divided into three parts: the duodenum, the jejunum, and the ileum. The duodenum starts at the exit of the stomach and contains the ampulla of Vater where the pancreas and bile duct release their secretions that facilitate digestion. The Pancreas produces an alkaline secretion with many digestive enzymes including amylase, lipases, nucleases, and trypsin [58]. Bile is produced in the liver by hepatocytes then stored and concentrated in the gall bladder. Bile is a mixture of bile salts, cholesterol, fatty acids, bilirubin, and electrolytes which emulsify lipids in the small intestine and increases surface area for the lipase to break down the lipids [59], [60].

Directly after the duodenum is the jejunum which connects to the ileum. There is no clear distinction between where the jejunum ends, and the ileum begins. The ileum connects to the cecum, the beginning of the large intestine, at the ileocecal sphincter. The large intestine is subdivided into four parts the cecum, colon, rectum, and anus. Most of the digestion and nutrient absorption occurs in the small intestine and the large intestine primarily reabsorbs water and electrolytes while forming and expelling stool. While the bacterial microbiome can be found in the small intestine, the bulk of the microbial mass resides in the large intestine, where bacteria further digest the remainder of the food and produce vitamins.

Life cycle of Intestinal Epithelial Cells

The wall of the small intestine is defined by the presence of invaginations known as crypts and finger-like protrusions known as villi, lined with polarized cells that have microvilli. The presence of the microvilli increases the surface area of the intestinal epithelium to increase absorption efficiency. The wall of the large intestine is markedly different than the small intestine with no villi and far more intestinal glands lined with enterocytes and goblet cells. These goblet cells secrete mucus that lubricates the large intestine to facilitate movement of the feces. The colonic enterocytes absorb water, salts, and vitamins produced by the microbiome.

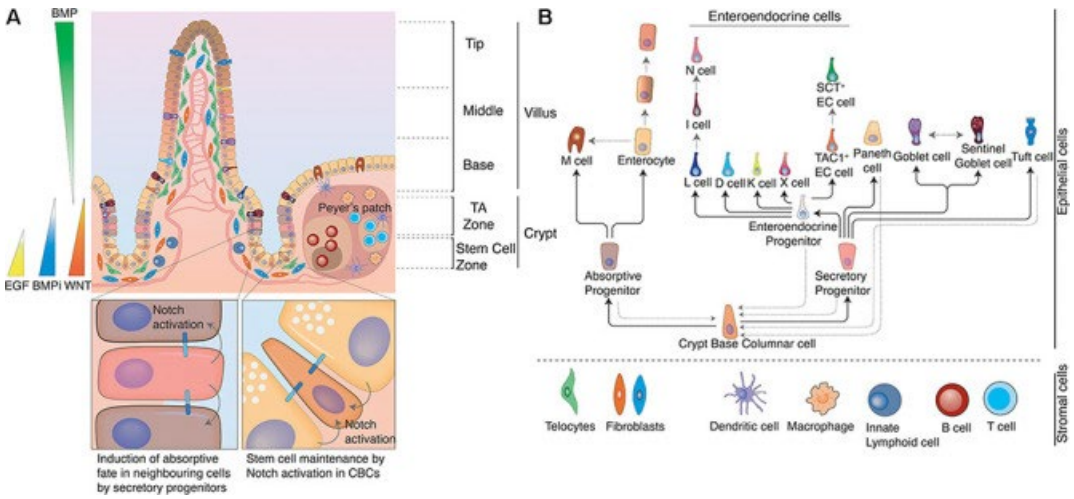

Figure 1.3 The differentiation pathways of intestinal epithelial cells.

Intestinal epithelial stem cells in the crypt replenish the intestinal epithelial lining of the intestine. (A) Cell type differentiation is determined by Notch, epidermal growth factor (EGF), bone morphogenic protein (BMP), and WNT concentrations. (B) When stem cells get pushed into the transit amplifying (TA) zone they begin differentiating down either the absorptive or secretory progenitor lineages. The absorptive cells include M cells and enterocytes. The secretory lineage includes Paneth cells, Goblet cells, Tuft cells, and enteroendocrine cells.

Adapted under creative commons from Frontiers in Cell and Developmental Biology. The Intestinal Epithelium – Fluid Fate and Rigid Structure from Crypt Bottom to Villus Tip, Vangelis Bonis, Carla Rossel, and Helmuth Gehart, 2021.

The intestinal epithelium is a single layer of polarized columnar cells, with different types of specializations that can be classified as either absorptive or secretory cells (Figure 1.3). Highly polarized, intestinal epithelial cells (IECs) have an apical membrane that faces the intestinal lumen, lateral membranes that interact with the other epithelial cells, and the basal membrane that interact with the underlying connective tissue or lamina propria. The polarized structure of IECs is important for their function, and protein trafficking to the different membranes is highly regulated [61]. Expression of proteins on the wrong membrane can result in poor nutrient absorption, lethal diarrhea, cancer development, and inflammatory bowel disease [61], [62], [63],

[64]. Enterocytes are the primary cell type that provides a physical barrier and absorbs nutrients, while M cells are specialized absorptive cells that continuously sample the lumen for immunological surveillance. Secretory cells found in the intestinal epithelium are Paneth, goblet, tuft, and enteroendocrine cells.

The crypts are comprised of crypt-based columnar stem cells (CBCs) and secretory Paneth cells. CBCs express the leucine-rich repeat-containing G-protein coupled receptor 5 (Lgr5), which is a membrane bound receptor that prolongs Wnt signaling when activated by its ligand R-spondin (RSPO) [65], [66], [67]. As the $Lgr5^{+}$ CBCs replicate, they essentially compete for stem factors Notch, epidermal growth factor (EGF), and Wnt, which are produced by Paneth cells and $Foxl1^{+}$ mesenchymal cells [68]. CBCs that cannot maintain a position in the crypt that has high in Notch and Wnt signaling get pushed out towards the edges of the crypt into the progenitor zone and begin to differentiate into transitional cells known as transit amplifying (TA) cells (Figure 1.3). CBCs that have no Notch but high Wnt signaling will differentiate into Paneth cells and remain in the crypt base [69].

Progenitor cells in the TA zone can replicate several times before entering the post-mitotic state and differentiating further, making up the bulk of intestinal epithelial cells [70]. As the cells fully differentiate, they travel towards the tip of the villi where they eventually are released from the villi and die from a form of apoptosis called anoikis, triggered by the loss of integrin-mediated cell-extracellular matrix signaling [71].

Turnover of the epithelium is very rapid, taking an average of 3.48 ± 1.55 days in humans [72]. The constant replacement of epithelial cells from a stem cell niche is an important aspect of maintaining a physical barrier. The digestive tract is a harsh environment that is specialized in breaking down organic material. The presence of volatile chemicals, digestive enzymes, reactive oxygen species, reactive nitrogen species, food antigens, bacteria, viruses, and parasites can lead to damage that needs to be quickly repaired. The gradient dependent signaling that determines differentiation of IECs allows for the rapid replacement of damaged or infected cells with fresh new healthy ones.

Absorptive Cells

Enterocytes

The majority of IECs differentiate into absorptive enterocytes, which are held together with tight junctions and have microvilli on the apical side that form the brush border. The tips of the microvilli are lined with mucin-like glycoproteins that form the filamentous brush border glycocalyx [73]. Held together by junctional complexes, enterocytes carefully regulate the permeability of the intestinal epithelium preventing unwanted passage of inflammatory molecules from the lumen [74]. The junctional complexes have three parts, tight junctions, adherens junctions, and desmosome junctions [75], [76], [77]. The basal membranes have hemidesmosomes that provide adhesion to the basement membrane [78].

Enterocytes have specialized transport proteins that selectively uptake nutrients and transport them into the blood stream through the capillaries within the villi. Though enterocytes are typically described as one type of cell, microdissection and single-cell RNA sequencing has shown that enterocytes have different nutrient uptake specialization depending on the location of the villi [79]. Near the bottom of the crypts amino acids transporters are more highly expressed, the middle expresses carbohydrate transporters, and the top express higher levels of peptide transporters, apolipoproteins, and cholesterol transporter proteins [79]. The glucose transporter Slc5a1 is low near the base, highest in the middle and decreases near towards the tip of the villi [79].

Though enterocytes are specialized to form a barrier while absorbing nutrients, sometimes bacterial products make it through. The apolipoproteins Apob, Apoa4, and Apoa1 were highest at the tip of the villi and are used to form chylomicrons that get secreted into the intestinal lymph during fat absorption [79], [80]. Lipopolysaccharides (LPS) can be absorbed from the lumen during fat absorption and Ghoshal *et al.* showed that chylomicrons can transport LPS from the gut lumen into the blood stream [81], [82]. In addition, it was shown that LPS binding protein associated with chylomicrons mediates LPS detoxification by decreasing the bioavailability of LPS to activate peripheral blood mononuclear cells (PBMCs) [83].

In addition to selective uptake of nutrients through transporters, enterocytes are capable of pinocytosis through four different mechanisms: clathrin-mediated endocytosis, micropinocytosis, caveolae-mediated endocytosis, and clathrin and caveolae independent endocytosis [84]. Paracellular transport has been observed as

well, where tight junction permeability is modified to allow small macromolecules to pass through the epithelium [85].

M Cells

M cells (microfold cells) are absorptive epithelial cells found within follicle-associated epithelium (FAE) directly above gut-associated lymphoid tissue (GALT) such as Peyer's patches (PP). M cells lack microvilli and are specialized for sampling antigens and pathogens in the lumen and then transporting them to the PP [86]. Like all other intestinal epithelial cells, M cells are replenished by crypt-based stem cells but mesenchymal cells in the GALT that express membrane bound RANKL induce the differentiation of M cells [87]. Specific deletion of RANKL in the mesenchymal cell found in the GALT resulted in no M cell differentiation [87].

There is a pocket that M cells form on the basolateral side where clusters of leucocytes reside [88]. $CD4^+$ T cells and B cells expressing IgM are the primary leucocytes found in the pocket of M cells but occasionally macrophages can be found there as well [88]. Mice without B cells have reduced numbers of M cells, and the development of FAE and PPs are disrupted as well [89]. B cells associated with M cell pockets remain there for the life of the M cell [89]. Dendritic cells are closely associated with the intestinal epithelium and can be found in the pocket of M cells taking up the cargo transcytosed by the M cell from the lumen [90], [91].

While macrophages and dendritic cells can sample luminal content, transcytosis of antigens through M cells is important for elicitation of secretory immunoglobulin A

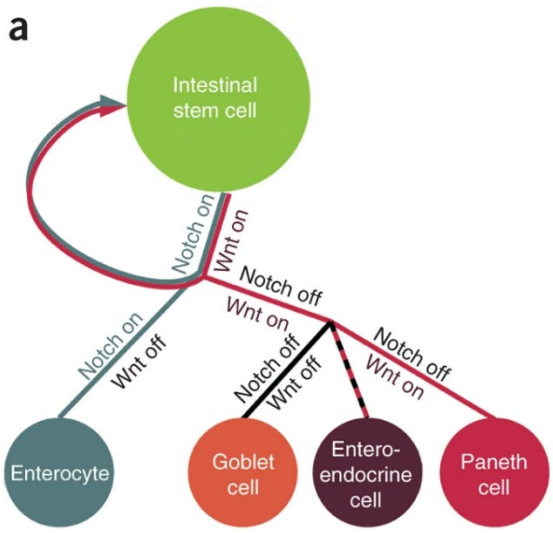

Figure 1.4 The role of Notch and Wnt signaling on intestinal epithelial differentiation.

Intestinal stem cells maintenance requires Notch and Wnt signaling. In the TA zone, if progenitor cells lose Wnt signaling but maintain Notch signaling, they go down the absorptive lineage and differentiate into enterocytes. If notch signaling is lost but Wnt signaling is maintained, progenitor cells go down the secretory lineage. The concentration of Wnt determines the secretory cell type.

Adapted with permission from Springer Nature: Nature Methods. Niche-independent high-purity cultures of Lgr5 intestinal stem cells and their progeny, Xiaolei Yin, Henner F Farin, Johan H van Es, Hans Clevers, Robert Langer, and Jeffrey M Karp, 2014.

(SIgA) production. In enterocyte specific RANKL KO mice the germinal centers of PPs, SIgA producing cells, and density of SIgA in the feces is reduced [92].

Secretory cells

Paneth cells

As stem cells are pushed into the transit amplifying (TA) zone, they differentiate into progenitor cells (Figure 1.3). When Wnt signaling is activated but Notch signaling is inhibited, the progenitor cells will differentiate into Paneth cells and move back down into the crypt (Figure 1.4) [93], [94], [95]. Deletion of atonal bHLH transcription factor 1 (Atoh1) and SRY-box transcription factor 9 (Sox9) inhibits the differentiation of Paneth cells [96], [97]. Paneth cells produce granules that contain a lot of antimicrobial proteins that get secreted into the lumen of the intestine, including α-defensins and lysozyme [98], [99], [100]. Paneth cells can be

ablated from the intestinal epithelium and the stem cell niche remains intact. However, Paneth cells have been shown to play an important role for homeostasis of the stem cell crypt as they express Delta like ligand 1 and 4 (DLL1 and DLL4) which bind to Notch on the intestinal stem cells [96], [100]. Though the primary source of Wnt for intestinal epithelial cells has been shown to be the subepithelial telocyte, Paneth cells are also capable of producing Wnt, and before the discovery the telocytes it was believed that Paneth cells were the primary source of Wnt [96], [101].

Goblet cells

Canonically, goblet cells are known for their production and secretion of mucus. In the crypt goblet cells produce a thick mucus that protects the stem cell crypt [102]. Villus goblet cells in the small intestine produce loose mucus very quickly that allows for nutrient penetration but still provides a protective chemical barrier [102], [103]. In the colon, the mucus produced by goblet cells is dense and impenetrable to small molecules and bacteria and provides lubrication to allow passage of the fecal matter [104]. The differentiation pathway for subtypes of goblet cells is complex, but in organoid culture inhibition of Wnt and Notch signaling resulted in goblet cell differentiation [95].

Tuft cells

Tuft cells are an interesting cell type that is marked by the unique morphology where they have long thick villi that extend from their apical membrane,

they have an oval shape being thinner at the apical and basal ends, and they have lateral protrusions that extend into the nuclei of the neighboring cells. Tuft cells have taste-chemosensory machinery and have been shown to detect the presence of pathogens through these receptors and activate the type II immune response in the presence of helminths [105]. Interleukin 25 (IL-25) is primarily released by tuft cells in the intestine, but tuft cells can also secrete acetylcholine and opioids [105], [106], [107].

Enteroendocrine cells

Enteroendocrine cells (EECs) are intestinal epithelial cells that produce hormones that respond to luminal stimuli to modulate glucose homeostasis, appetite, immunity, metabolism, and even control nutrient absorption [108]. There are over 20 EEC types described, each of which are classified by the specific hormone they primarily produce. For example, S cells primarily produce and secrete secretin (SCT) [109]. EECs were originally thought to be neural cells that developed from the neural crest, but it is now known that they develop from CBCs and come from the same secretory progenitor cells as goblet, tuft, and Paneth cells [108]. After differentiation into the secretory progenitor, neurogenin3 (Neurog3) drives EEC differentiation. Deletion of Neurog3 ablates the EEC population and over-expression of Neurog3 amplifies the population of EECs in the intestinal epithelium [110], [111].

Norovirus

Disease

Human norovirus is an enteric virus that causes vomiting and diarrhea. Noroviruses are non-enveloped positive-sense (+) RNA viruses that infect the intestinal epithelium and are transmitted through the oral fecal route. Though disease prevalence has been trending downward, diarrheal diseases are still in the top ten causes of disease in the world, and norovirus is the most common cause of gastroenteritis [112]. Typically, norovirus infections are not life threatening, and dehydration is the main complication resulting in death. Norovirus infection poses the greatest risk to children under 5 years old and the elderly 70 years and older [112]. Currently, the only treatment for norovirus infections is hydration supplementation. The disease burden is highest in developing countries, but in America, norovirus infections accounted for ~60% of all acute gastroenteritis [112]. Despite the burden of norovirus, research has been severely delayed due to difficulty growing human norovirus in the lab. Recent papers have been published showing human norovirus infections of intestinal organoids, but these infections are still relatively modest and incompatible with generation of defined viral stocks [113], [114], [115], [116], [117].

Structure

Norovirus (NoV) belongs to the *Caliciviridae* family which includes non-enveloped virions between 27-40 nm. *Caliciviridae* family viruses have icosahedral

symmetry, linear positive-sense RNA genomes between 6.4-8.5 kilobases and different open reading frames (ORFs) for non-structural and structural proteins [118]. Most NoVs genomes have three different open reading frames, except murine norovirus (MNV) which contains a fourth open reding frame [119]. The ORF1 encodes a large polyprotein that gets cleaved into six non-structural proteins (NS1/2, NS3, NS4, NS5, NS6, NS7) by viral protease NS6 [120]. ORF2 encodes viral protein 1 (VP1), ORF3 encodes VP2, and ORF4 overlaps with the VP1 sequence and encode virulence factor 1 (VF1) [119], [120], [121].

Norovirus infections have been shown to persist long after clearance of symptoms. The CR6 strain of MNV is a persistent strain that primarily grows in the intestines, whereas MNV strain CW3 does not persist, but is capable of systemically infecting the spleen [122]. Experiments switching the NS1/2 sequences from persistent MNV strain CR6 with the acute strain CW3 resulted in CW3 persistence in the colon [122]. Further investigation showed that NS1/2 gets cleaved by caspase-3 during infection and NS1 gets secreted [123].

NS3 is a NTPase that was shown to bind and hydrolyze nucleoside triphosphates (NTPs) [124]. NS4 is also known as p22 and has been shown to mediate Golgi disassembly and inhibits protein secretion [125]. NS5 is a viral protein genome-linked (VPg) that is covalently linked to the 5’ end of the MNV genome and acts as a primer for viral RNA synthesis mediated by the NS7 protein which is an RNA-dependent RNA polymerase responsible for genomic replication [119], [126].

VP1 is the main structural protein of the capsid, which is made of 90 VP1 dimers and forms a T=3 icosahedral capsid. VP1 has two domains: the shell (S) domain forms the icosahedral shell of the capsid [127]. The protruding (P) domain extends from the shell and interacts with histo-blood group antigen (HBGAs) found on the surface of epithelial cells [127]. VP2 is the minor structural protein that locates on the inside of the capsid and provides stability to the capsid [128]. VF1 is only found in MNV and has been shown to not be required for infection but does inhibit apoptosis and contributes to viral fitness during persistent infection [129], [130].

Life Cycle

Norovirus typically enters the host through the fecal-oral route. MNV has been used as a model to study HNoV as they are genetically similar, but how HNoV infiltrates cells is unknown. Once the virus has entered the host, MNV interacts with HBGAs found on the surface of enterocytes, goblet cells, tuft cells, stem cells, and transit amplifying cells . Interaction with HBGAs is thought to help concentrate the virus onto the cell surface. The virion then binds to the phagocytosis receptor CD300lf expressed exclusively on tuft cells and is endocytosed, after which the viral genomic positive (+) strand RNA is uncoated via endosomal uncoating [131], [132], [133]. The positive strand RNA serves as messenger RNA (mRNA) that is translated into viral proteins. The VPg capping the RNA recruits cell host translation factors and the first viral proteins are made before any replication [134], [135]. After post-translational cleavage of the polyproteins, the intracellular membrane bound replication complex forms and begins replicating

genomic (gRNA) and sub-genomic RNA (sgRNA) [136]. The replication of positive strand RNA first requires synthesis of a negative (-) strand to be the template. The replication of the (-) RNA is thought to be initiated *de novo* and the (+) RNA replication is mediated through VPg priming [136], [137].

The generation of sgRNA has been thought to occur through early termination of RdRp synthesis, but it has also been suggested that a highly conserved step-loop formation disrupts the RNA synthesis [138], [139]. The sgRNA typically contains ORF2, ORF3, and ORF4 coding for the major and minor capsid proteins [139]. After the (+) gRNA is capped with the VPg, it is packaged into viral particles [136]. MNV is a lytic virus, and egress of viral particles occurs when NS3 creates pores in the mitochondria cell membrane [140]. The released viral particles are spread to other hosts through feces and saliva [112], [113], [119], [141], [142], [143].

Murine norovirus as a model for studying immunity

Until recently, MNV was the only norovirus that could be grown in cell culture. MNV serves as a mouse model to study viral immunity in the intestines [119], [141], [144]. MNV was originally reported in 2003, found in severely immune compromised mice lacking recombination activating gene 2 (RAG2), required for B and T cell maturation, and signal transducer and activator of transcription 1 (STAT1), a key innate immune transcription activator. These mice spontaneously died from a viral infection that could be passaged by intracerebral inoculation [145]. Sequencing and phylogenetic

analysis determined the unknown virus was most similar to previously identified species of noroviruses [145].

To determine the role B and T cells played on the new norovirus, *Rag1*$^{-/-}$ mice were inoculated with MNV, but none of them died [145]. However, *Stat1*$^{-/-}$ mice or mice lacking the interferon alpha receptor (IFNAR) and the interferon gamma receptor (IFNGR) died following MNV inoculation, indicating that the STAT1-dependent innate immune response was required for preventing lethal infection of MNV [145].

MNV and reovirus (another IEC-tropic virus) infections in conditional interferon lambda receptor (IFNLR) KO mice showed that IFNLR expression on IECs was critical for controlling enteric viral infections, confirming further that the intestinal epithelium had a compartmentalized IFN response [146]. Despite type I and type III interferons signaling through the same canonical pathways, these experiments indicate they are not redundant and that IFN-λ signaling in the intestinal epithelium has a distinct role from type I IFN. Using the MNV model, we were able to further define cell type specific signaling factors that regulate the IFN response in IECs.

Interferons

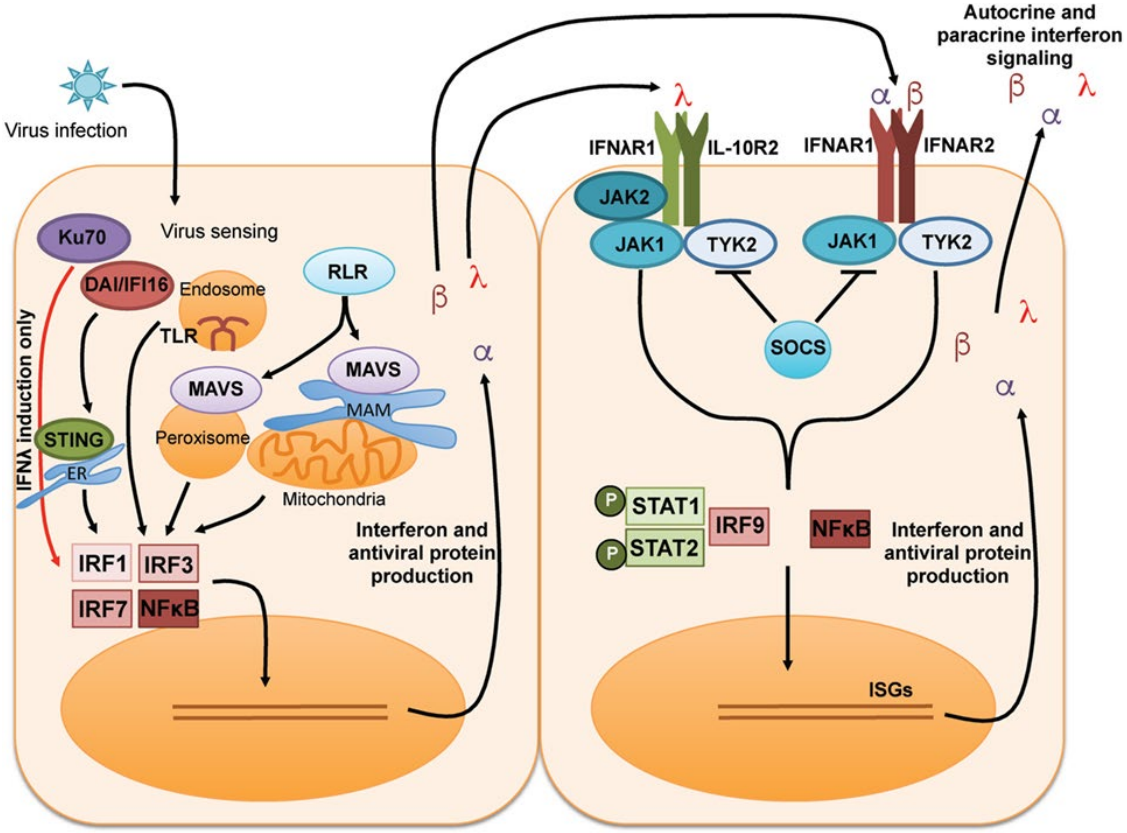

Figure 1.5 The canonical signaling pathway for type I and type III interferons.

After the entry of a viral particle intracellular pattern recognition receptors activate transcription factors IRF1, IRF3, IRF7, or NFκB which turn on the production and secretion of type I and type III IFNs. Interferons interact with the membrane bound receptors to activate the JAK-STAT pathway. The ISGF3 complex (STAT1:STAT2:IRF9) induce the expression of ISGs leading to the antiviral state.

Adapted under creative commons from Frontiers in Immunology. Interferon Lambda Genetics and Biology in Regulation of Viral Control, Emily A. Hemann, Michael Gale Jr, and Ram Savan, 2017.

Interferons (IFNs) are signaling molecules produced during viral infections that activate the antiviral response and inhibit the growth of viral pathogens. There are three type of IFNs: type I (IFN-α/β), type II (IFN-γ), and type III (IFN-λ). IFN classifications are based on the membrane-bound receptor that the secreted cytokine signals through. Type I interferons bind to interferon alpha receptor 1 (IFNAR1) and interferon alpha

receptor 2 (IFNAR2) (Figure 1.5). In humans, there are several type I interferons which include 13 IFN-α subtypes, IFN-β, IFN-ε, IFN-κ, and IFN-ω. Type II interferons bind to the interferon gamma receptor 1 (IFNGR1) and interferon gamma receptor 2 (IFNGR2). There is only one IFN-γ which forms a homodimer and binds to a four-chain bundle of IFN-γ receptors [147]. Type III interferons bind to interferon lambda receptor 1 (IFNLR1) and interleukin 10 receptor subunit beta (IL10RB) (Figure 1.5). In humans there are four IFN-λ ligands that have been described IFN-λ1-4 and two in mice IFN-λ2 and IFN-λ3 [148], [149].

Canonical signaling

Pattern-recognition receptors (PRRs) identify the presence of pathogen associated molecular patterns (PAMPs) inside the cell and induce the production of type I and type III interferons (Figure 1.5) which are secreted from the cell and bind to their respective receptors on neighboring cells. IFN stimulation induces the expression of hundreds of genes known as interferon stimulated genes (ISGs), which leads to the antiviral response that prevents viral entry, inhibits viral replication, and enhances MHC antigen presentation.

Type II interferons are primarily secreted by activated T cells and natural killer cells to modulate numerous immune responses to infection and cancer [150]. Type II interferons are different from type I and type III interferons because the receptor is homodimeric with Jak1 binding to the α-chain and Jak2 binding to the β-chain. When the interferon associates with the four chains of the IFN-γ receptor, the JAKs

phosphorylate STAT1 which homodimerizes, translocates to the nucleus, and binds to gamma-activated sites (GAS) on the genome [151]. While type II IFNs are important for the innate and adaptive immune response to viral infections, analyzing the differences between type I and type III IFNs in IECs was the primary goal of the research presented here and they will be reviewed in more detail.

IFN-α/β and IFN-λ are regulated by and signal through similar mechanisms. Canonically, upon virus sensing, interferon regulatory factor 3 (IRF3), interferon regulatory factor 7 (IRF7), and nuclear factor-κB (NF-κB) transcription factors turn on production of IFN-α/β and IFN-λ (Figure 1.5). Receptor-associated kinases Janus kinase 1 (JAK1) and tyrosine kinase-2 (TYK2) bound to the intracellular tails of the IFN receptors phosphorylate STAT1 and STAT2. These phosphorylated STAT proteins recruit IRF9 to form the interferon stimulated gene factor 3 (ISGF3) complex. The ISGF3 complex translocate to the nucleus and binds the IFN-stimulated response elements (ISRE) in the promoter region of ISGs (Figure 1.5) [152].

While there are hundreds of ISGs, IFN-induced protein with tetratricopeptide repeats (IFIT1) and ISG15 are two prominent ISGs that directly inhibit viral replication. IFIT1 inhibits the translation of viral proteins by binding to the eukaryotic initiation factor 3 (eIL3) complex which regulates translation initiation [153]. Binding of IFIT1 to eIL3 inhibits the formation of the 43S-mRNA complex formation preventing mRNA translation [153]. ISG15 is an ubiquitin-like protein that is covalently conjugated to target proteins (ISGylation) to inhibit viral replication and egress [154]. The ISGylation of nascent viral proteins can inhibit their interactions with host proteins, prevent their oligomerization,

or disrupt their function [154]. Host proteins are also ISGylated during the antiviral response but the conjugation of ISG15 to host proteins can be reversed by the ubiquitin specific protein 18 (USP18) [154].

Prolonged IFN signaling can have detrimental inflammatory effects. Dysregulated type I IFN signaling has been implicated in diseases such as systemic lupus erythematosus, rheumatoid arthritis, systemic sclerosis, and juvenile dermatomyositis [155]. To prevent these harmful effects, negative feedback loops tightly regulate the expression patterns of ISGs. The down-regulation of IFN signaling is mediated by inhibition of kinase activity and down-regulation of membrane expression of the receptor.

Suppressor of cytokine signaling 1 (SOCS1) inhibits type I and type III IFN signaling by inhibiting Tyk2 activity at the receptor (Figure 1.5) [156]. SOCS3 inhibits type I IFN signaling by blocking substrate phosphorylation of JAK1 [157]. Additionally, Type I IFN signaling is also inhibited by USP18, which blocks the association of JAK1 to the interferon alpha receptor 2 (IFNAR2) and interferon lambda receptor 1 (IFNLR1) subunits [158].

While these canonical signals have been well established in the field, the roles of highly related gene family members with cell type-specific expression patterns are not well understood.

Non-canonical signaling

The canonical signaling of type I and type III IFNs, involving JAK/STAT/IRF signaling cascades, have been extensively studied for decades. However, non-canonical IFN signaling, which often occurs in a cell type specific manner, is less understood. For example, IFN-λ was shown to inhibit reactive oxygen species (ROS) generation by neutrophils in a DSS-colitis model by inhibiting RAC-alpha serine/threonine-protein kinase (AKT) through JAK2 [159]. In fibroblasts, IFN-λ was shown to activate mitogen activated protein kinase (MAPK) independent of STAT1 [160]. In brain microvasculature endothelial cells from STAT1 KO mice, both IFN-α/β and IFN-λ increased trans-endothelial electrical resistance [161].

Several studies have indicated that type I interferon stimulation activates MAPK-pathways and phosphoinositide 3-kinases (PI3K)/mammalian targeting of rapamycin (mTOR) pathways [162]. STAT3 phosphorylation provides a docking site for PI3K to be activated by IFN-α and it was shown under IFN-β stimulation PI3K lead to phosphorylation of AKT [163].

In humans, there are four JAK (JAK1-3 and Tyk2) and seven STAT (STAT1-6, STAT5a and STAT5b) homologs [164], [165], [166]. Various non-canonical STAT complexes can form under IFN stimulation [167], [168]. For instance, type I IFN stimulated STAT2 homodimers interact with IRF9 to form an ISGF3-like complex [166]. STAT2-IRF9 heterodimers can drive the activation of a common ISG, RIG-I [169]. Additionally, STAT2/STAT3 heterodimers and STAT2/STAT6 heterodimers have also been shown to

induce ISG expression under IFN-α/β stimulation [170], [171]. Type I IFN-induced growth inhibition was shown to occur through the formation of a STAT5:Crkl complex that binds to GAS elements [172].

These various non-canonical STAT complexes formed under IFN stimulation induce the expression of smaller subsets of ISGs than the ISGF3 complex [167]. Despite extensive research on the IFN signaling pathway, the non-canonical pathways are much less understood and further research is required to determine their roles.

Cell type specific signaling

Though IFN-α/β and IFN-λ both signal through the ISGF3 complex, they do not both turn on all the same ISGs in all cell types [173], [174]. For example, in human vaginal epithelial cells a subset of ISGs were more highly expressed under IFN-λ than IFN-β [175]. In primary human vaginal epithelial cells treated with IFNs, 162 ISGs were induced by both IFN-λ and IFN-β, six genes were only induced by IFN-β, and 89 genes were only induced by IFN-λ [175]. In contrast, neonate mouse IECs showed 63 ISGs induced by both IFN-λ and IFN-β, one was only induced by IFN-β and 147 were only induced by IFN-λ [176]. The cell-specific ISG expression is likely influenced by epigenetic status, as[177] IECs treated with histone deacetylase blockers enhanced ISG expression under IFN-λ stimulation but not IFN-β [177].

IFN signaling plays a vital role in the immune system, with specific effects on different types of immune cells. In T cells, type I IFN stimulation increases expression of IL2RA, MYC, and PIM1 corresponding to the proliferative effects of IFN stimulation of T

cells [178]. In B cells, it was shown that IFN-α stimulation can activate STAT6, resulting in STAT2:STAT6 dimerization, which can recruit IRF9 to form an ISGF3-like complex [179]. Activation of STAT1 under type I IFN stimulation in NK cells induces the expression of Fasl and perforin [163]. Extracellular signal-regulated kinase (ERK) dependent activation of activator protein-1 (AP-1) was induced by IFN-β in microglia cells [180]. Interferons exert distinct and critical effects on various immune cell types, tailoring the immune response to effectively combat infections and malignancies. Understanding cell type-specific signaling pathways is essential for developing targeted therapies in immune-related diseases.

Cell type specific regulatory pathways are important for clearance of viral pathogens as we have seen with MNV viral infections. For instance, MNV infections can be inhibited by either IFN-λ or IFN-α/β, depending on the virus strain. Specifically, the infection of intestinal epithelial cells by MNV is controlled by IFN-λ, while MNV infection of macrophages is controlled by IFN-α/β. [181]. Furthering our understanding of the regulatory mechanisms responsible for the compartmentalization of IFN signaling by cell type was the primary goal of my dissertation and the experiments presented in following chapter.

Role of interferons in the intestines

The role of IFNs in the intestinal epithelium is complex and compartmentalized. What is interesting about the intestines is that IECs preferentially respond to type III IFNs

and are not responsive to type I interferons despite the presence of IFNAR1 and IFNAR2 expression [182]. The mechanism that inhibits the responsiveness to type I interferons is unknown. We know that type I and type III IFNs are not redundant and that Type III IFNs are preferentially utilized by epithelial barriers. The current hypothesis as to why IECs utilize type III interferons is that they elicit a less cytotoxic and inflammatory response than type I IFNs, which allows for a targeted antiviral response that does not disturb the commensal microbiota or break down the physical barrier of the intestinal epithelium [176], [183]. The experiments in the following chapter were designed to further understand the cell type specific signaling that regulates the IFN response in IECs.

Apoptosis of IECs is highly specialized to prevent the formation of breaks in the barrier that could lead to infection. There would be negative selective pressure on evolution of an innate immune response that impaired the barrier function when activated. While all other nucleated cells respond to type I IFNs, IECs rely on IFN-λ for antiviral defense [184], [185]. Deletion of IFNAR1 and IFNGR1 have no impact on IEC infection but deletion of IFNLR1 or STAT1 causes a significant increase in norovirus replication within IECs [186]. In Rag1 knock-out mice, IFN-λ treatment was capable of sterilizing noroviral infections despite these mice having no adaptive immunity [186]. Norovirus infections could not be sterilized by IFN-λ in Rag1 knock-out mice that also had IFNLR1 deleted in the IECs implicating the essential role IFN-λ had in inhibiting MNV infection in the intestine [146]. Deletion of the two type III IFN genes (Ifnl2 and Ifnl3) in mice phenocopies the IFNLR KO mice. Reovirus and norovirus strains that infect IECs exhibited increased growth similar to what is seen in the IFNLR KO mice [187]. This

finding demonstrated that the known type III IFN cytokine are indeed the essential cytokines signaling through IFNLR with no alternative ligands required for the antiviral response.

Rotavirus, is a major cause of severe diarrhea in children, specifically infecting IECs. Murine models have shown that murine rotavirus strain EDIM induces IFN-λ production and endogenous IFN-λ has antiviral effects [188]. Pretreatment of of exogenous IFN-λ prevents the establishment of a robust infection of EDIM-murine rotavirus [188]. Previously, the Nice lab has shown that microbiota-dependent IFN-λ signaling occurs in discrete pockets (also known as “hot pockets”) that prophylactically inhibit enteric viral infections [189]. These hot pockets were dependent on the presence of the IFNLR1 on IECs and were activated by bacterial products of the microbiome [189]. Ablation of the homeostatic IFN-λ stimulation through IFNLR1 deletion on IECs resulted in hyper-susceptibility to initial murine rotavirus infections [189].

In addition to antiviral properties type III IFNs have been shown to play an important role during infections of the obligate intracellular parasite *Cryptosporidium parvum*[190]. To identify host genes required for *Cryptosporidium* infection and host response Gibson *et al.* utilized a genome wide CRISPR screen that identified IFN signaling genes were enriched. *Cryptosporidium* infection of human IECs induced the production of IFN-λ but did not induce IFN-β production [190]. *In vivo* mouse infections of *C. parvum* induced IFN-λ and exogenous IFN-λ treatment protected mice from severe infection [190].

IECs face a unique immunological problem as they are bombarded by immunological stimulations in the lumen but are required to differentiate between commensal microbes and pathogens while allowing nutrient and macromolecule transport pass the intestinal barrier. The study of canonical and non-canonical IFN signaling in the intestines allows us to further understand the cell type-specific innate immune response to viral infections in the intestinal epithelium. The experiments in the following data chapter give further insight into the compartmentalized cell-type specific IFN signaling that helps maintain the intestinal barrier during viral infections.

Interferon regulatory factors

Interferon regulatory factors (IRFs) are a family of homologous transcription factors that each share a conserved DNA binding domain (DBD) that binds to a consensus sequence known as the IFN-stimulated response element (ISRE). IRFs have different post-translational modifications that regulate their activity. Though IFNs were discovered in 1957 the first IRF wasn't reported until 1988 [191], [192].

IRF1 was discovered through a DNA affinity column chromatography experiment looking for proteins that bound to upstream sequences of the IFN-β gene [192]. It later came to light that IRF3 and IRF7 were the primary activators of IFN-β and IRF9 was part of the ISGF3 complex. Interestingly, interferon regulatory factors evolved before IFNs with homologs being present in invertebrates and phylogenetic analysis indicates the appearance of IRFs coincides with animal multicellularity [193]. Early on, IRF1 and IRF4 diverged evolutionarily, and now the IRF family can be subdivided into two groups that

share similar C-terminal domains [193]. The IRF1 sub-group contains the c-terminal IRF association domain 1 (IAD1) and IRF4 sub groups have the IAD2 [193]. In mammals there have been ten IRFs identified. However, IRF10 has either been lost or silenced in mice and humans.

Structure of Interferon Regulatory Factors

The structure of the IRF protein family includes a DBD and an activation domain. The most conserved domain of IRFs is the N-terminal helix-turn-helix DBD, which contains five tryptophan repeats, three of which bind to IFN regulatory element (IRE, NAANNGAAA) and the IFN-stimulated response element (ISRE, A/GNGAAANNGAAACT) [194], [195]. The activation domain is different between each of the IRFs but they all include a linker region and an IAD which is similar to Mad-homology 2 (MH2) domains of the SMAD family [196]. IRF3, IRF4, IRF5, and IRF7 have known auto-inhibitory regions [195]. The IAD domain is the region of the IRF that binds to other proteins to either form homo/heterodimers or transcriptional complexes.

Role of interferon regulatory factors in interferon signaling

Interferon signaling is highly effective against viral infections, but dysregulated signaling can result in pathology. To maintain homeostasis, many regulatory mechanisms allow for controlled IFN signaling only when appropriate. IRFs are crucial regulators of IFN signaling, being involved during initiation of IFN production, ISG expression, and down-regulation of IFN signaling.

During infections, PRRs, such as toll-like receptors (TLRs), C-type lectin receptors (CLRs), RIG-I-like receptors (RLRs), and NOD-like receptors (NLRs) recognize PAMPs and activate the production of IFNs. When double-stranded RNA binds to toll-like receptor 3 (TLR3) or when LPS is detected by TLR4, TRIF activates TANK-binding kinase 1 (TBK1) which phosphorylates IRF3 to initiate the production of IFNs [197]. TLR7 and TLR9 detect single-strande RNA and CpG DNA, respectively, in the endosome, where myeloid differentiation primary response protein 88 (MyD88) activates both IRF5 and IRF7 to produce type I IFNs [197]. IRF4 down regulates IRF5 signaling by competing for the IRF5 binding site on MyD88 [198]. The antifungal response can be activated when β-glucans produced by fungus are detected by CLR Dectin-1 where IRF5 is activated to induce IFN-β production in dendritic cells (DCs) [199]. Cytosolic PRRs that recognize double stranded RNA (RIG-1 and melanoma differentiation-associated protein 5 (MDA5)) activate the production of IFNs. Double-stranded DNA detection results in activation of stimulator of interferon genes (STING), which subsequently activates IRF3, IRF5, and IRF7 through TBK1 [197].

Activation of NF-κB leads to newly transcribed IRF1 mRNA which activates IFN production [200]. The role of IRF1 during IFN signaling is not fully understood but it has been shown to be important for epigenetic regulation, NLRP3 inflammasome activation, tumor necrosis factor (TNF)-mediated IFN signaling, and positive feedback regulation of ISG responses [200]. IRF2 competes for IRF1 binding sites and has been shown to inhibit IRF1 transcriptional activation [201].

During type I and type III IFN signaling STAT1 and STAT2 heterodimers recruit IRF9 to form the ISGF3 complex to activate the antiviral response (Figure 1.5). IRF1, IRF7, IRF8, and IRF9 are all induced by IFN signaling [202]. Much remains unknown about the cell type specific regulatory roles of IRFs during interferon signaling.

Developmental roles of IRFs during hematopoiesis

IRFs were discovered and named for their regulatory role during interferon signaling, but many of them have been shown to play an integral role during hematopoiesis. All hematopoietic cells are generated from a common pluripotent hematopoietic stem cell (HSC). These HSCs can differentiate into either lymphoid or myeloid lineages. Lymphocyte progenitor cells can mature in T cells, B cells, innate lymphoid cells, and Natural Killer (NK) cells. Myeloid progenitors can differentiate into granulocytes, monocytes, megakaryocytes, and erythrocytes. Most dendritic cells derive from myeloid progenitor cells, but some have been shown to arise from common lymphoid progenitors.

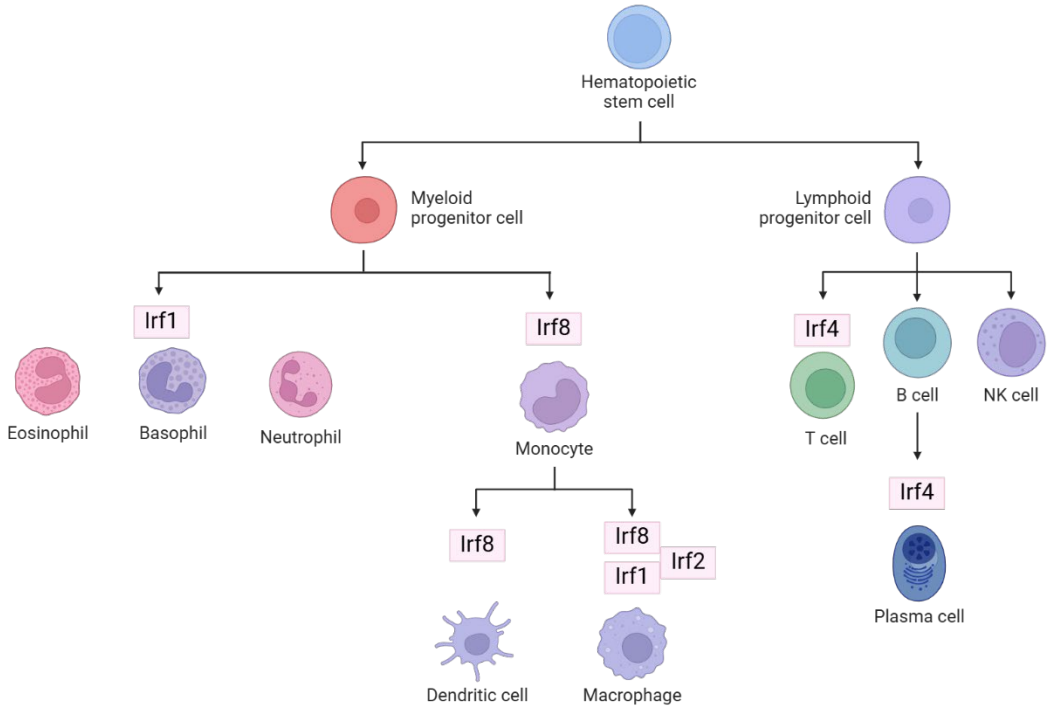

Figure 1.6 Role of Irfs during hematopoietic stem cell differentiation

Irf1 expression drive granulocyte differentiation. Irf8 expression determines monocyte, dendritic cell, and macrophage maturation. Irf4 expression is essential for T cell and plasma cell development. During macrophage development Irf8 can heterodimerize with Irf1 or Irf2.

Created with BioRender

IRF1 during hematopoiesis

IRF1 KO mice have several immunological deficiencies, but the role of IRF1 in hematopoiesis has not yet been shown to be cell intrinsic or a secondary effect. Mice lacking IRF1 are not able to develop mature $CD8^+$ T cells or NK cells, fail to mount a Th1 response, and their Treg differentiation is skewed [203]. However, bone marrow

chimeras indicate that the decrease in $CD8^+$ T cells and NK cells was dependent on the *Irf1*$^{-/-}$ microenvironment [204].

Granulocytes are a class of myeloid cells that contain granules in their cytoplasm that can contain AMPs, enzymes, low pH, reactive oxygen species, or nitric oxide. During granulocyte maturation, IRF1 expression increases [205]. Over-expression of IRF1 in myeloid progenitor 32Dcl3 cells increased granulocyte differentiation and blocking IRF1 expression decreased maturation [205]. Bone marrow cells from IRF1 KO mice had decreased granulocyte and macrophage colonies [206]. It was shown that IRF1 regulates the granulocyte master regulators CAAT-enhancer-binding protein (C/EBP)-ε and -α [206].

IRF4 during T cell differentiation

IRF4 regulates the differentiation of various immune cells, including B cells, T cells, dendritic cells, and macrophages. Naïve CD4+ T cells differentiate into specialized subsets with distinct effector functions and cytokine profiles in response to antigen recognition and cytokine signals. This subdivision is governed by lineage-specific transcription factors acting as "master regulators" for each Th subset. The differentiation of T cell subsets hinges on the levels of IRF4, which, in turn, are influenced by the strength of T cell receptor (TCR) signaling [207], [208]. This signaling strength is modulated by the activity of mTOR and inducible T-cell kinase (ITK) [207], [208]. Additionally, C-REL, NFAT, FOXP3, STAT3, and STAT6, along with T-BET, play roles in modulating IRF4 expression in various T cell subsets (Figure 1.6) [209]. BATF and IRF4

promote chromatin opening which allows STAT and SMAD signaling that induce the expression of lineage specific transcription factors [209], [210]. These signals induce the expression of lineage-specific transcription factors, which, either independently or in collaboration with IRF4, guide the expression of lineage-specific gene sets.

IRF4 regulates plasma cell differentiation.

IRF4 is also important for B cell differentiation. Centrocytes are a pre B cell found in the germinal center. During selection of centrocytes, NF-κB is activated by a high affinity antigen receptor and CD40 signaling from T cells [211]. The activation of NF-κB induces IRF4 expression, which then inhibits B cell lymphoma 6 (BCL6) expression by directly binding its promoter region [212]. The inhibition of BCL6 allows for the expression of B lymphocyte-induced maturation protein 1 (BLIMP1) [211]. IRF4 and BLIMP1 activate X-box binding protein 1 (XBP1) expression, and high levels of these three genes promotes plasma cell differentiation [211].

IRF8 regulates myelopoiesis.

IRF8, also known as Interferon consensus sequence binding protein (ICSBP), has been shown to play an essential role in the differentiation of myeloid cells including monocytes, dendritic cells, macrophages, and granulocytes. Expression of IRF8 suppresses neutrophil production and promotes dendritic cell lineage commitment [213]. *Irf8*$^{-/-}$ mice develop immunodeficiencies and a chronic myeloid leukemia-like

disease [214]. In humans, a K108E mutation in IRF8 causes severe immunodeficiency with a complete lack of circulating monocytes and dendritic cells [215]. The T80A mutation in IRF8 had less severe immunodeficiency but showed depletion of $CD11c^+$ $CD1c^+$ circulating dendritic cells [215].

Dendritic cells (DCs) are antigen presenting cells that are crucial for initiation of the innate and adaptive immune response. While DCs are heterogenous population they are usually classified as either conventional dendritic cells (cDCs) or plasmacytoid dendritic cells (pDCs). cDCs can be subdivided into cDC1 which are crucial for activating the CD8 T cell response and cDC2 prime the CD4 T cell response. IRF8 is highly expressed in pDCs and cDC1 cells, and is low or negative in cDC2 cells, where IRF4 expression is more important [216]. The balance of IRF4 and IRF8 expression by early DC progenitors determines the pre-DC fate [216]. Basic leucine zipper ATF-like transcription factor 3 (BATF3) regulates IRF8 expression in pre-DCs and mature DCs [217]. BATF3 also maintains IRF8 autoactivation in DCs [218]. It was shown that IRF8 defined the epigenetic and transcription state of pDCs regardless of the microenvironment [219].

IRF8 is essential for monocyte/macrophage differentiation. In Granulocyte-monocyte progenitors in the bone marrow, mTOR inhibits STAT5 activation, subsequently increasing IRF8 and CD115 expression [220]. CD115 is the receptor for colony stimulating factor-1 which plays a crucial role in the differentiation of monocytes into macrophages. The transcription factor PU.1 forms a complex with IRF8, which binds to the Ets-IRF composite element (EICE) sequence. IRF8 also heterodimerizes with IRF1 or IRF2 to bind ISRE sequences activating macrophage differentiation genes [221].

Taken together, the lineage specific role of IRF8 is dependent on the dimerization of other transcription factors that determines the genes activated by IRF8. Dendritic cell differentiation is dependent on IRF8 cooperating with BATF3 and monocyte/macrophage differentiation is dependent on IRF8 interacting with PU.1, IRF1, and IRF2. Indicating that cell type specific roles of IRFs can have major differences in gene expression despite the DNA binding domain being highly conserved between the nine IRF family members.

IRF6

Interferon regulatory factor 6 (IRF6) is the only IRF required for murine viability, with KO in mice being embryonic lethal. Much less is known about the role of IRF6 in the immune response. The majority of IRF6 research has been done on its role in fetal development, as mutation in IRF6 are associated with craniofacial developmental disorders that result in cleft lip or cleft palate. Orofacial clefts are the most common craniofacial birth defect, and Van der Woude syndrome (VWS) is the most common orofacial cleft syndrome, with a prevalence of 1/35,000-1/100,000 live births [222]. Non-random mutation in IRF6 account for about 70% of VWS [223].

Popliteal pterygium syndrome (PPS) is a rare disease that presents with orofacial clefts but has more severe deformations such as pterygium, a wing like membrane, of the popliteal fossa, the depression in the back of the knee. Individuals with PPS may also have syndactyly (fusion of two or more digits), ankyloblepharon (fusion of the upper and lower eye lids), sygnatia (fusion of the upper and lower jaws), and abnormal external genitalia. Mutations in IRF6 were shown to account for 97% of PPS [223].

Mutations in IRF6 were recently shown to potentially cause spina bifida which is a generalized term for when the neural tube fails to close [224]. IRF6 has also been implicated in several cancers including breast, ovarian, gastric, and acquired immunotherapy resistance in pancreatic ductal adenocarcinoma [225], [226], [227], [228].

IRF6-related disorders are inherited in an autosomal dominant manner. No instance of a human with two disrupted IRF6 alleles has been reported. IRF6 is comprised of nine exons with a start codon on the third exon and the stop codon on the ninth exon [229]. Exons one and two are the untranslated region, three and four are the DBD, five and six is the linker region, seven and eight are protein binding region, and exon nine is the c-terminal domain [229]. Point mutations that cause VWS are significantly over-represented in exons three, four, seven, and eight. Mutations associated with PPS were more likely to occur in exons three and four. The most common mutation associated with PPS is arginine 84 switch to a cystine (R84C) that inhibits binding of IRF6 to the DNA and sequesters the unmutated protein expressed from the second allele [229], [230], [231].

IRF6 regulates palatal fusion

IRF6 is structurally similar to other IRFs with a DBD, linker region, IAD1, and a serine-rich auto-inhibitory region. The majority of IRF6 mutations associated with VWS occur either in the DBD or the IAD regions but other mutations have been reported that affect an enhancer region that is involved in p63-mediated transcriptional regulation of

IRF6 [232], [233]. During murine embryonic development it was shown that IRF6 is highly expressed in secondary palates dissected from day 14.5-15 and adult skin [232].

IRF6 was shown to regulate the epithelial to mesenchymal transformation (EMT), a process that is important for palatal fusion. In mammals, the fusion of the secondary palate occurs by two palatal shelves migrating toward each other, making contact, and forming the medial edge seam at the midline. The midline epithelial cells must undergo apoptosis, EMT, or migrate away from the seam, and disruption in the palatal fusion process results in a cleft palate [234]. Ablation of IRF6 was shown to delay the transforming growth factor beta (TGFβ)-mediated palatal fusion [235], [236]. IRF6 has been shown to regulate both EMT and apoptosis during palatal fusion. TGFβ signaling increases IRF6 expression through SMAD and MAPK dependent pathways [236]. IRF6 promotes the expression of homeodomain-interacting protein kinase 2 (HIPK2) which is phosphorylated by TGF-β–activated kinase 1 (TAK1). Activated HIPK2 phosphorylates ΔNp63, resulting in its degradation, which increases protein cyclin-dependent kinase inhibitor 1 (p21), activating apoptosis [234], [236], [237], [238].

TGFβ-induced EMT is known to be regulated by the transcription factors Snail homolog 2 (SNAI2) and TWIST. Blocking TGFβ signaling delays palatal fusion. IRF6 knock-down on palatal shelves delays palatal fusion, and decreases SNAI2 but not TWIST [235]. Ectopic expression of IRF6 after blocking TGFβ rescues palatal fusion and increases SNAI2 expression [235]. These data indicate that IRF6 is downstream TGFβ signaling and that SNAI2 is regulated by IRF6.

IRF6 regulates keratinocyte differentiation

Keratinocytes are the primary cell type in the outermost layer of the epidermis. The stem cells in the basal layer constantly reproduce and differentiate to replenish the upper layers. IRF6 has been shown to play an essential role in keratinocyte differentiation. Deletion of IRF6 results in severe loss of epidermal barrier function, epidermal hyperproliferation, and soft tissue fusions that result in neonatal lethality [239], [240].

[236][236] While the exact role of IRF6 during keratinocyte differentiation is still largely unknown, investigations have shed light on IRF6's DNA binding regions, gene networks, and post translation modifications. AP-2A (TFAP2A) and p63 regulate IRF6 expression by interacting with the enhancer region *MCS9.7,* and mutations in the *MCS9.7* region that disrupt protein binding recapitulate IRF6 mutation phenotypes [229], [241], [242]. In turn, IRF6 activation leads to p63 degradation by the proteosome in a feed-back-loop that allows keratinocytes to exit the cell cycle [243]. RIPK4 was shown to phosphorylate serine residues 90, 413 and 424, activating IRF6 [240], [241]. Disruption of the RIPK4-IRF6 axis dysregulates lipid composition of the stratum corneum leading to loss of the epidermal barrier [240].

ChIP sequencing of IRF6 in squamous cell carcinomas showed potential binding sites within 2233 genes, but only 56 genes overlapped with the 332 differentially-expressed genes identified in a IRF6-dependent microarray; Ovo-like 1 (OVOL1) was

confirmed to be directly regulated by IRF6 [244]. Bone morphogenic protein 2 (BMP2) and epidermal growth factor receptor (EGFR) were identified in the ChIP sequencing, but not confirmed [244]. While these genes were not confirmed to be regulated by IRF6, they are relevant to this thesis because they have extremely important roles in IEC development.

Over-expression of IRF6 causes more severe deformations than ablation. In an IRF6 over-expression mouse model, IRF6 was identified to have an inverse relationship to TAP2A and grainy head like protein 3 (GRHL3) [224]. This TFAP2A-IRF6-GRHL3 developmental axis was shown to important for neurulation [224]. These experiments connected oral facial development and neurulation two developmental distinct events to the same pathway [224]. Overexpression of IRF6 has more severe defects than under-expression, but expression of just the DBD was shown to be even more lethal than overexpression of the full protein in Zebra fish embryos. Injections of the IRF6 DBD into zebrafish embryos caused dominant negative phenotypes of epiboly arrest, loss of gene expression characteristic of the enveloping layer, and rupture of the embryo at late gastrula stage [245].

The complex developmental disruption resulting from IRF6 mutations and dysregulated expression have made studying IRF6 difficult. Cell type-specific conditional KO models may be required for defining post-developmental functions of IRF6.

Role of IRF6 in the immune system

The majority of IRF6 research has been done on its role in development because of the known connection to VWS, PPS, and the neonatal lethality of IRF6 ablation. However, a few studies have connected IRF6 to pathogen defense mechanisms. In 2012 Kwa M *et al.* showed that IRF6 is activated during TLR2 stimulation in epithelial cells [246]. MyD88 and IL-1 receptor-associated kinase-1 (IRAK1) both activated IRF6 but only IRAK1 was co-precipitated with IRF6 [246]. Co-expression of IRAK1 and IRF6 increased expression of C-C chemokine ligand 5 (CCL5) [246]. In primary keratinocytes, IRF6 was shown to inhibit TLR3-induced IFN-β expression and IL-23p19 expression [247].

In human oral epithelial cells IRF6 was shown to regulate the expression of the proinflammatory IL-1 subfamily protein IL-36γ. *Porphyromonas gingivalis* exposure increased expression of IRF6 and IL-36γ [248]. Gene silencing of TLR2 inhibited expression of IL-36γ but not IRF6 [248]. However, knockdown of IRF6 inhibited expression of IL-36γ after exposure to *P. gingivalis*[248]. This study suggests that IRF6 expression is not regulated by TLR signaling but does promote inflammation in response to *P. gingivalis* [248].

Conditional KO mice lacking IRF6 in innate immune cells were more sensitive to endotoxic shock [249]. IRF6 was shown to negatively regulate TLR4-mediated cytokine production, inhibit NFkB activation, and constrains neutrophil migration [249]. Bone marrow derived macrophages (BMDM) deficient in IRF6 had increased expression of keratinocyte chemoattractant (KC) and IL-6 after LPS exposure [249]. IRF6 expression is

reduced in macrophages upon M2 polarization and knock-down of IRF6 enhanced M2 polarization in BMDMs [250]. Peroxisome proliferator–activated receptor-γ (PPARγ) was shown to be directly regulated by IRF6 in BMDM regulating the M1/M2 polarization [250].

Taken together, these data indicate that IRF6 can have either a proinflammatory or anti-inflammatory role in response to pathogenic ligands and the role of IRF6 is cell type dependent. Interestingly, the function of IRF6 has been shown to play such a complex and essential role in other cell types but has been completely missed in the intestinal epithelium. In the following data chapter, I show that IRF6 is a critical factor for IEC homeostasis, differentiation, immunity, and cell death.

Chapter 2: Interferon Regulatory Factor 6 (IRF6) Determines Intestinal Epithelial Cell Development and Immunity

Authors

Austin P. Wright[1], Sydney Harris, Shelby Madden[1], Bryan Ramirez Reyes[1], Ethan Mulamula, Alexis Gibson[1], Isabella Rauch[1], David A. Constant[1], and Timothy J. Nice[1#]

Affiliations

1 Department of Molecular Microbiology and Immunology, Oregon Health & Science University, Portland, OR, USA

Correspondence to: nice@ohsu.edu (T.J.N.)

Contributions

Austin P. Wright: Conceptualization, Formal analysis, Investigation, Writing – original draft, Writing – review & editing.

Sydney Harris: Investigation.

Shelby Madden: Investigation.

Bryan Ramirez Reyes: Investigation.

Ethan Mulamula: Investigation.

Alexis Gibson: Investigation.

Isabella Rauch: Funding acquisition, Writing – review & editing.

David A. Constant: Investigation, Writing – review & editing.

Timothy J. Nice: Conceptualization, Funding acquisition, Investigation, Supervision, Writing – original draft, Writing – review & editing.

Acknowledgements

Integrated Genomics Laboratory, Massively Parallel Sequencing Shared Resource, Advanced Light Microscopy Core, and Flow Cytometry Core.

Funding

T.J.N. and A.P.W. were supported by National Institutes of Health grant R01-AI130055 and the Medical Research Foundation of Oregon. T.J.N. was additionally supported by the Kenneth Rainin Foundation (Grant #20220034), and OHSU School of Medicine. I.R. was supported by National Institutes of Health grant R01 AI167974. The funders had no role in study design, data collection, and interpretation, or the decision to submit the work for publication.

Citation

A. P. Wright *et al.*, “Interferon regulatory factor 6 (IRF6) determines intestinal epithelial cell development and immunity,” *Mucosal Immunol*, Apr. 2024, doi: 10.1016/j.mucimm.2024.03.013.

Introduction

The interferon (IFN) family of cytokines are a first line of defense against viral pathogens. Activation of IFN receptors initiates a signaling pathway resulting in transcription of IFN-stimulated genes (ISGs), which include many direct-acting antiviral effectors [251], [252]. There are three types of IFN, which are defined by their use of distinct membrane-bound receptors [253]. The transcriptional profiles (ISGs) induced by each IFN type overlap substantially, but there are cell type-specific differences in antiviral protection. Type I IFN can act on nearly every nucleated cell in the body, but type III IFN (IFN-λ) primarily acts on epithelial cells of barrier tissues, and intestinal epithelial cells (IECs) preferentially respond to IFN-λ [254], [255], [256], [257], [258], [259], [260]. For example, interferon lambda receptor KO (*Ifnlr1*$^{-/-}$) mice fail to control intestinal replication of murine norovirus (MNV) [258], and homeostatic antiviral responses in the intestinal epithelium are absent in *Ifnlr1*$^{-/-}$ mice [259]. Thus, understanding the factors that regulate IFN-λ responsiveness of IECs is of particular importance to intestinal health.

Type I and III IFN receptors can utilize the same canonical signaling pathway [253]. Receptor-associated Janus kinase 1 (JAK1) and tyrosine kinase 2 (TYK2) phosphorylate signal transducer and activator of transcription 1 (STAT1) and STAT2. Interferon regulatory factor 9 (IRF9) joins with STAT1 and STAT2 to form IFN-stimulated gene factor 3 (ISGF3), which translocates to the nucleus and binds IFN-sensitive response element (ISRE) motifs in ISG promoters [253]. One major difference between

type I and III IFNs is the strength of signaling, with type III IFN resulting in a more moderate but sustained level of gene expression [261], [262], [263]. Thus, a modest response stimulated by type III IFN in epithelial cells benefits tissue homeostasis by maintaining antiviral protection with minimal epithelial cytotoxicity [182]. However, IEC-specific factors that regulate the IFN response remain poorly understood.

IEC-specific regulators of the interferon response may include relatives of canonical signaling factors, such as members of the JAK, STAT, and IRF families. There are nine IRF proteins that share a conserved N-terminal DNA binding domain (DBD) that interacts with a conserved GAAA consensus DNA sequence that is part of the ISRE motif [264], [265]. The C-terminal regions are more divergent and include regulatory motifs. IRFs 3-9 encode an IRF-association domain (IAD) and an autoinhibitory region that facilitate dimeric interaction and inhibition of dimerization, respectively. Despite the discovery of IRFs as regulators of IFN, and their homology in the DBD, some IRFs have been shown to regulate development of specific cell types. For example, IRF4 and IRF8 regulate leukocyte development [266], [267], [268], [269], and IRF6 regulates keratinocyte development [270], [271], [272]. IRF6 is expressed by all epithelial lineages, but developmental and immunological roles in the intestine have not been previously described.

To identify the presence of IEC-specific factors that regulate the antiviral IFN response, we designed a CRISPR screen that targeted canonical IFN signaling factors and homologous family members. We found that *Irf6* KO enhanced IFN-stimulated antiviral immunity of IEC cell lines but not macrophages. RNAseq analysis of *Irf6* KO IEC cell lines

revealed substantial baseline changes in growth and development pathway genes, and dysregulated ISG expression that correlated with antiviral protection. We found that *Irf6* was highly expressed in primary IEC organoids and intestinal tissues. *Irf6* KO in primary IEC organoids reduced growth and developmental gene expression, with enhanced production of particular ISGs and increased IFN-stimulated cytotoxicity. These data suggest a previously unappreciated role for IRF6 in IEC development and immunity.

Results

Protection against virus-triggered death by IFN treatments in macrophage and epithelial cell lines

To study genetics of IFN-stimulated antiviral protection, we used murine BV2 and M2C-CD300lf cell lines that represent myeloid-lineage and intestinal epithelial-lineage, respectively [273], [274]. First, we directly compared the efficacy of type I and III IFNs in these cells by performing dose-response titrations using recombinant murine IFN-β and IFN-λ (**Fig. 2.1**). Both BV2 and M2C cells were treated with IFN for 24 hours before being challenged with a lytic strain of murine norovirus (MNV) [275], [276], which kills cells by apoptotic or lytic mechanisms [277], [278]. The BV2 cells were infected at an MOI=10 resulting in <1% viability, and the M2C cells were infected at an MOI=50 resulting in ~9% viability. IFN-β treatment protected MNV-infected M2C from death, reaching ~100% viability at 10 ng/mL (**Fig. 2.1A**, squares). IFN-λ treatment also protected MNV-infected M2C from death, but with a lower maximum survival rate of ~30% (**Fig. 2.1A**, circles). The BV2 macrophages had a survival rate of ~10% when treated with

10ng/ml IFN-β, but showed no increase in survival when pretreated with any dose of IFN-λ, as expected (**Fig. 2.1B**). To compare differences in responsiveness between IFN type and cell type in the subsequent CRISPR screen, we selected doses that moderately increased viability following MNV infection: **1)** 10ng/ml IFN-λ-treated M2C IECs, **2)** 0.01 ng/ml IFN-β-treated M2C IECs, and **3)** 10ng/ml IFN-β-treated BV2 macrophages (**Fig. 2.1**, dashed lines).

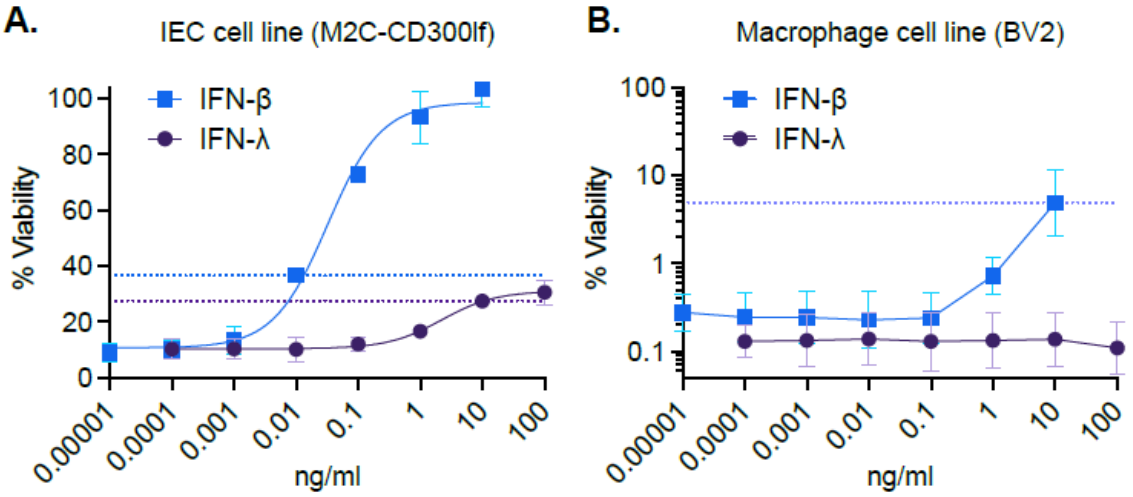

Figure 2.1 Protection against norovirus-triggered death by interferon treatments in macrophage and epithelial cell lines.

M2C-CD300lf epithelial cells (A) and BV2 macrophage cells (B) were plated and treated with serial dilutions of IFN-β or IFN-λ followed by determination of viability using the ATP-Glo assay. Viability for each dose was normalized as a percent of uninfected, untreated cells. Dashed lines indicate doses selected for use in subsequent screens. Data is represented as mean and standard deviation of two (M2C) or three (BV2) replicates. ATP = adenosine triphosphate; IEC = intestinal epithelial cell; IFN = interferon.

CRISPR screens for IEC-specific regulators of the IFN response

To determine requirement of candidate genes for IFN-stimulated protection, we knocked out genes within JAK, STAT, NF-κB and IRF families using CRISPR lentivirus transduction (two gRNAs/gene). For each IFN treatment and cell type, we saw that gRNA

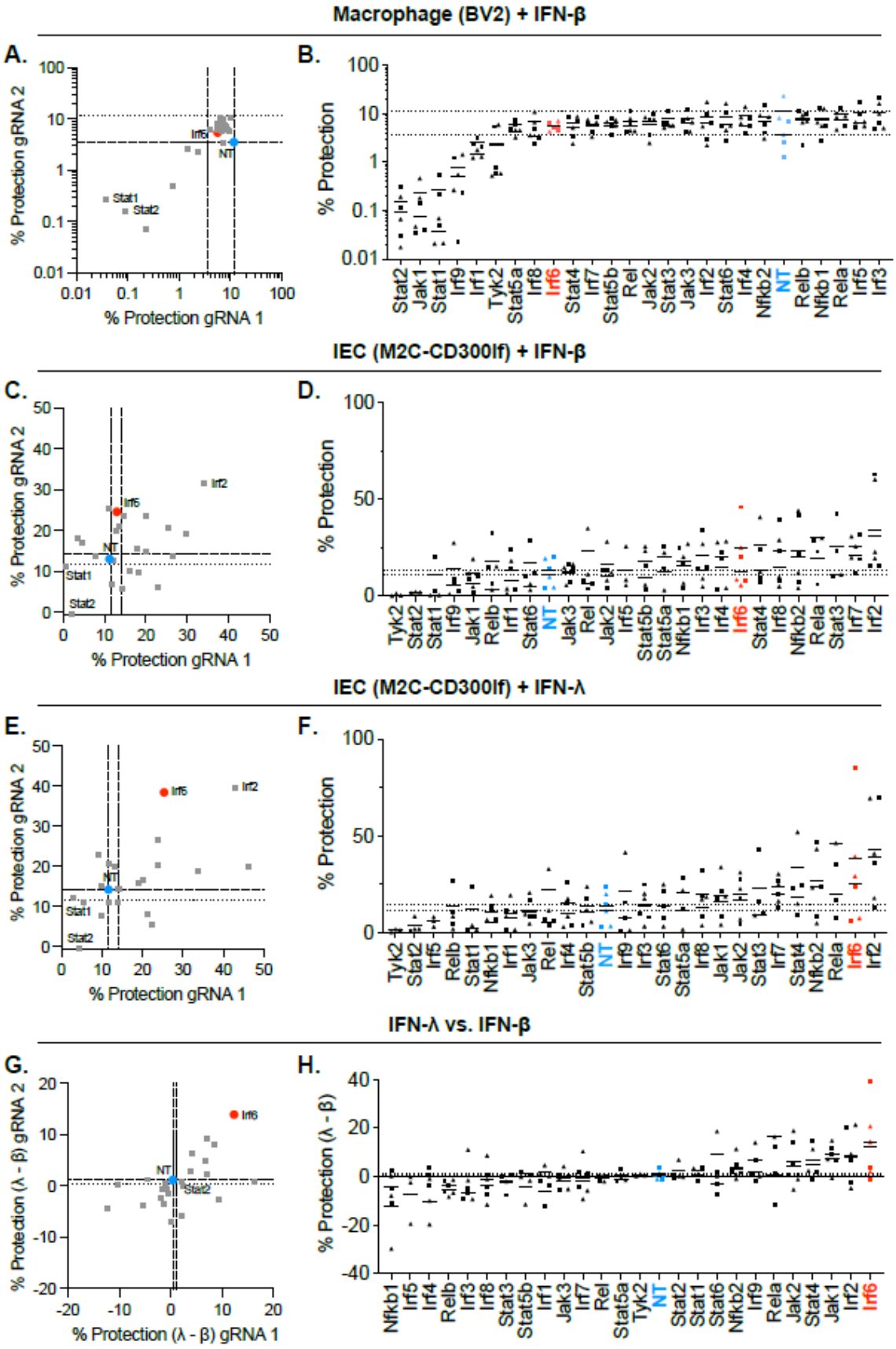
Macrophage (BV2) + IFN-β
A.
% Protection gRNA 2
% Protection gRNA 1
Irf6
NT
Stat1
Stat2
B.
% Protection
Stat2 Jak1 Stat1 Irf9 Irf1 Tyk2 Stat5a Irf8 Irf6 Stat4 Irf7 Stat5b Rel Jak2 Stat3 Jak3 Irf2 Stat6 Irf4 Nfkb2 NT Relb Nfkb1 Rela Irf5 Irf3
IEC (M2C-CD300lf) + IFN-β
C.
% Protection gRNA 2
% Protection gRNA 1
Irf2
Irf6
NT
Stat1
Stat2
D.
% Protection
Tyk2 Stat2 Stat1 Irf9 Jak1 Relb Irf1 Stat6 NT Jak3 Rel Jak2 Irf5 Stat5b Stat5a Nfkb1 Irf3 Irf4 Irf6 Stat4 Irf8 Nfkb2 Rela Stat3 Irf7 Irf2
IEC (M2C-CD300lf) + IFN-λ
E.
% Protection gRNA 2
% Protection gRNA 1
Irf6
Irf2
NT
Stat1
Stat2
F.
% Protection
Tyk2 Stat2 Irf5 Relb Stat1 Nfkb1 Irf1 Jak3 Rel Irf4 Stat5b NT Irf9 Irf3 Stat6 Stat5a Irf8 Jak1 Jak2 Stat3 Irf7 Stat4 Nfkb2 Rela Irf6 Irf2
IFN-λ vs. IFN-β
G.
% Protection (λ - β) gRNA 2
% Protection (λ - β) gRNA 1
Irf6
NT
Stat2
H.
% Protection (λ - β)
Nfkb1 Irf5 Irf4 Relb Irf3 Irf8 Stat3 Stat5b Irf1 Jak3 Irf7 Rel Stat5a Tyk2 NT Stat2 Stat1 Stat6 Nfkb2 Irf9 Rela Jak2 Stat4 Jak1 Irf2 Irf6

Figure 2.2 CRISPR screen for interferon-stimulated protection of macrophage and intestinal epithelial cell lines.

CRISPR KO cells and NT control cells were screened for differences in IFN-stimulated protection from MNV-triggered death using the ATP-Glo viability assay. IFN-stimulated protection was calculated by subtracting viability of untreated controls from IFN-treated cells (% protection, A–F), and differences between IFN types were determined by subtracting IFN-β-stimulated protection from IFN-λ-stimulated protection (λ–β, G–H). Data is plotted as individual replicates (B, D, F, H) or as the mean values from three replicate experiments for each of two independent gRNAs per gene (A, C, E, G). (A–B) IFN-β-stimulated protection of BV2 macrophages. (C–D) IFN-β-stimulated protection of M2C-CD300lf IECs. (E–F) IFN-λ -stimulated protection of M2C-CD300lf IECs. (G–H) Difference between IFN-λ- and IFN-β-stimulated protection of M2C-CD300lf IECs. Genes positioned in the bottom left quadrant of G are more protected by IFN-β than IFN-λ and genes positioned in the upper right quadrant are more protected by IFN-λ than IFN-β. Dotted lines in all plots represent the mean values of NT control gRNAs (blue). Shapes for individual replicate datapoints represent each independent gRNA. Mean values are indicated for each gRNA. Data represents three experimental replicates. ATP = adenosine triphosphate; CRISPR = Clustered Regularly Interspaced Short Palindromic Repeats; IEC = intestinal epithelial cell; gRNA = guide ribonucleic acid; IFN = interferon; KO = knockout; MNV = murine norovirus; NT = non-targeting.

targeting of canonical signaling factors resulted in lower protection provided by IFN treatments, validating our screening approach (**Fig. 2.2**). In particular, IFN-β treatment of BV2 cells with gRNA targeting *Stat1, Stat2, Irf9,* and *Jak1* resulted in nearly no protection (0.01-1%), whereas treatment of non-targeting controls resulted in 3-11% protection (**Fig. 2.2A-B**). gRNA targeting *Irf1* and *Tyk2* may have a more modest effect on IFN-stimulated protection of BV2 cells, resulting in an intermediate amount of protection (1-3%) following IFN-β treatment (**Fig. 2.2A-B**). None of the CRISPR targeted BV2 cell lines showed increased IFN-β-stimulated protection relative to controls.

Similar to BV2 cells, M2C-CD300lf cells with gRNA targeting *Stat1* and *Stat2* were among the least protected cells following IFN-β treatment (**Fig. 2.2C-D**). Likewise, IFN-λ treatment of M2C-CD300lf cells with gRNA targeting of *Stat1* and *Stat2* resulted in

reduced protection relative to non-targeting controls (**Fig. 2.2E-F**). However, unlike the BV2 cells, there were several genes where gRNA targeting increased the IFN-stimulated protection of M2C-CD300lf cells, including *Irf2* and *Irf6*. Targeting of *Irf2* resulted in increased protection of M2C-CD300lf cells pretreated with either IFN-β or IFN-λ (**Fig. 2.2C-F**), indicating that *Irf2* may inhibit IFN signaling in these epithelial cells. This is consistent with the previously described inhibitory activity of *Irf2* [279]. Targeting of *Irf6* resulted in increased protection of M2C-CD300lf cells pretreated with IFN-λ (**Fig. 2.2E-F**), but appeared to have a more modest or inconsistent effect on M2C-CD300lf cells pretreated with IFN-β (**Fig. 2.2C-D**), and had no effect on BV2 macrophages (**Fig. 2.2A-B**).

To quantify differences between IFN-λ and IFN-β treatments, we determined the difference in IFN-stimulated protection for each CRISPR gRNA in M2C-CD300lf cells (**Fig. 2.2G-H**). Notably, this comparison was between IFN types within the same cell lines, thereby minimizing effects of variation in MNV susceptibility between cell lines. We found that *Irf6*-targeted cells had the largest difference between IFN-λ and IFN-β treatments, with greater protection provided by IFN-λ than IFN-β (**Fig 2.2G-H**). These results suggested that *Irf6* is a novel regulator of the IFN-stimulated antiviral response in IECs.

To increase confidence in selecting candidate genes for further study, we complemented the viability CRISPR screen with an orth

Figure 2.3 Pooled CRISPR screen for interferon-stimulated antiviral response in macrophage and intestinal epithelial cell lines.

(A) Pooled CRISPR-transduced cells were screened for genes that altered IFN-stimulated protection from MNV infection by cell sorting the top 10% of infected cells based on staining for MNV NS1-2 protein production. (B) Representative FACS plots of NS1-2 staining. (C) MFI of MNV NS1-2 staining 8 hours post-infection of cells pretreated for 24 hours with no IFN, 1 ng/mL IFN-β, or 100 ng/mL IFN-λ, as indicated. Each dot represents the mean fluorescence intensity of a single replicate. (D–G) Plotted values indicate abundance of each gRNA in untreated cells divided by abundance of the same gRNA in cells pretreated with IFN-β. Dashed line indicates mean of NT control. (D, F) Mean values of the two gRNAs for each gene plotted on x- and y-axes. (E, G) Plotted values of each replicate, with the gRNAs for each gene represented as distinct symbols. Mean values for each gRNA are indicated. Genes are ranked from left to right in order of enhancement to inhibition of the IFN response. Data represents two experimental replicates. CRISPR = Clustered Regularly Interspaced Short Palindromic Repeats; FACS = fluorescence-activated cell sorting; gRNA = guide ribonucleic acid; IEC = intestinal epithelial cell; IFN = interferon; MFI = mean fluorescence intensity; MNV = murine norovirus; NT = non-targeting.

ogonal FACS-based pooled CRISPR screen (**Fig. 2.3A**). Pooled CRISPR-transduced cells were pre-treated with IFN types, infected with MNV, and cells with the greatest production of MNV protein (top 10% NS1/2-positive) were sorted for quantification of gRNA abundance (**Fig. 2.3A**). MNV NS1/2 protein staining at 8 hours post-infection was consistently detected in the BV2 and M2C-CD300lf pools (**Fig. 2.3B-C**, 'no IFN' group),

indicating that these cell lines are similarly capable of supporting MNV replication. IFN-β treatment resulted in lower fluorescence intensity of MNV NS1/2 in both BV2 and M2C cells (**Fig. 2.3B-C**). However, IFN-λ treatment of M2C cells did not significantly reduce

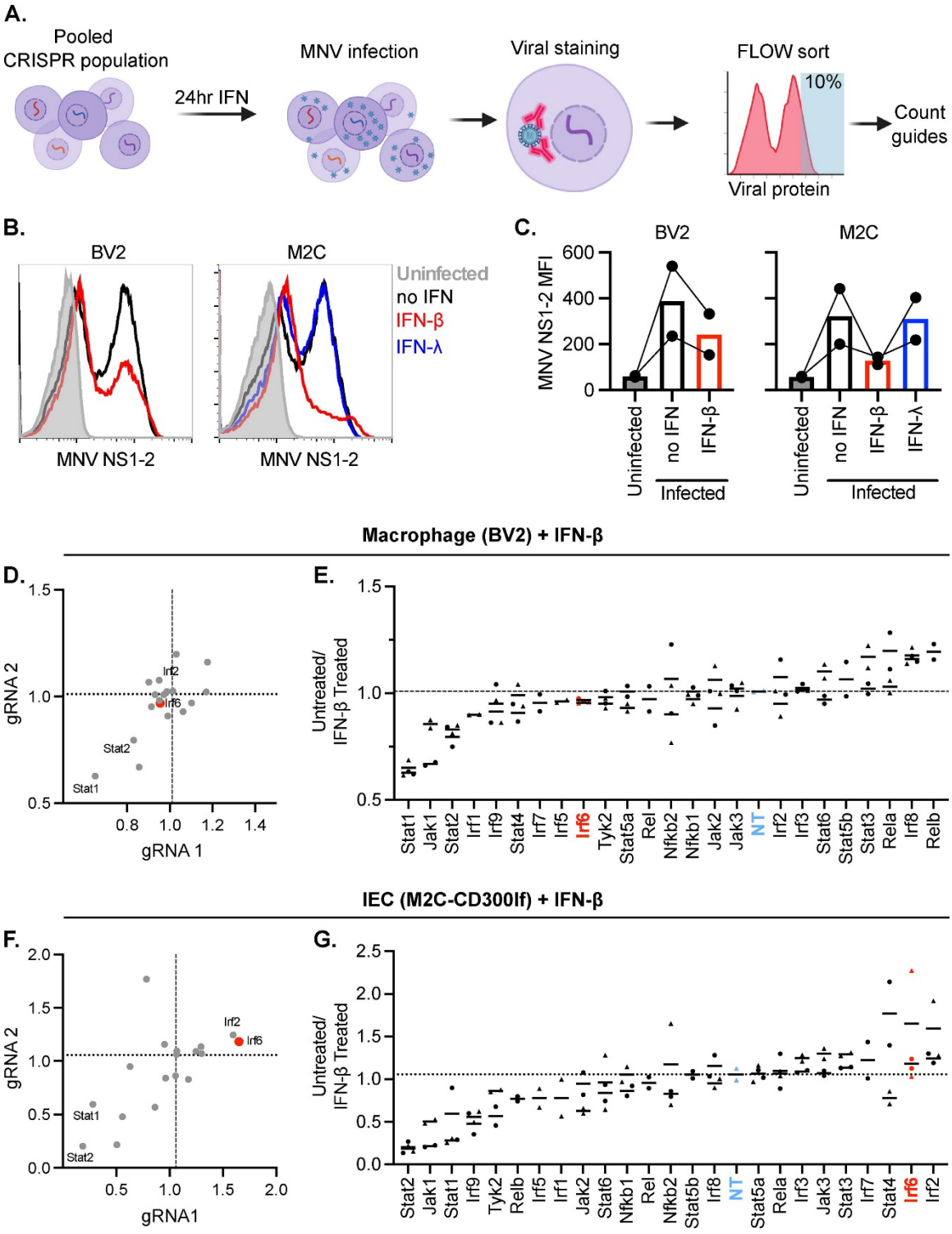

MNV NS1/2 protein staining, confounding our ability to identify genes that influence IFN-λ activity by this screening method. Notably, these data suggest that actions of IFN-λ to protect cells from MNV-triggered death (**Fig. 2.1-2.2**) are distinct from those that block initial translation of viral protein (**Fig. 2.3B-C**). Therefore, IFN-λ-treated cells were not further considered in analysis of this pooled CRISPR screen.

We sequenced gRNAs present within the top 10% of MNV NS1/2-positive cells, and compared gRNA counts between groups. Genes that promote IFN-stimulated antiviral immunity were expected to have correspondingly decreased gRNA counts within untreated groups relative to IFN-treated groups. Indeed, canonical genes (*Stat1*, *Stat2*, *Jak1*) were decreased within untreated M2C and BV2 cells relative to paired IFN-β-treated groups, whereas non-targeting control gRNAs were equally represented (**Fig. 2.3D-G**). These expected outcomes validate our screen results. Analogous to the results of the viability screen (**Fig. 2.2C-D**), *Irf2* was increased within untreated M2C relative to the paired IFN-β-treated groups (**Fig. 2.3F-G**), but was not different in BV2 cells (**Fig. 2.3D-E**). Likewise, *Irf6* was increased within untreated M2C relative to the paired IFN-β-treated groups (**Fig. 2.3F-G**), analogous to the results from IFN-λ-treated cells in the viability screen (**Fig. 2.2E-F**). Thus, both CRISPR screening approaches suggested a novel and cell type-specific role for *Irf6* in the regulation of IFN-stimulated antiviral response of IECs.

Irf6 KO slows growth and alters IFN-stimulated protection of an IEC cell line

Both CRISPR screens suggested that targeting of *Irf6* resulted in greater IFN-stimulated antiviral protection of M2C IECs. To further test the role of *Irf6*, we generated monoclonal cell lines targeted by the two *Irf6* gRNAs used in the screen, and sequence-verified disruption of the *Irf6* locus. *Irf6* gRNA 1 cut directly before the conserved DNA binding domain, and *Irf6* gRNA 2 cut near the beginning of the predicted IRF-association domain (**Fig. 2.4A**). We selected monoclonal cell lines with mutations that resulted in frame shift and early stop codons (**Fig. 2.4A**). *Irf6* qPCR from the KO cell lines indicated undetectable (gRNA 1, KO1) or significantly reduced (gRNA 2, KO2) *Irf6* mRNA expression (**Fig. 2.4B**). Notably, the baseline abundance of *Irf6* mRNA was low in all M2C cells (greater than 1000-fold less abundant than the housekeeping gene *Rps29*, **Fig. 2.4B**),

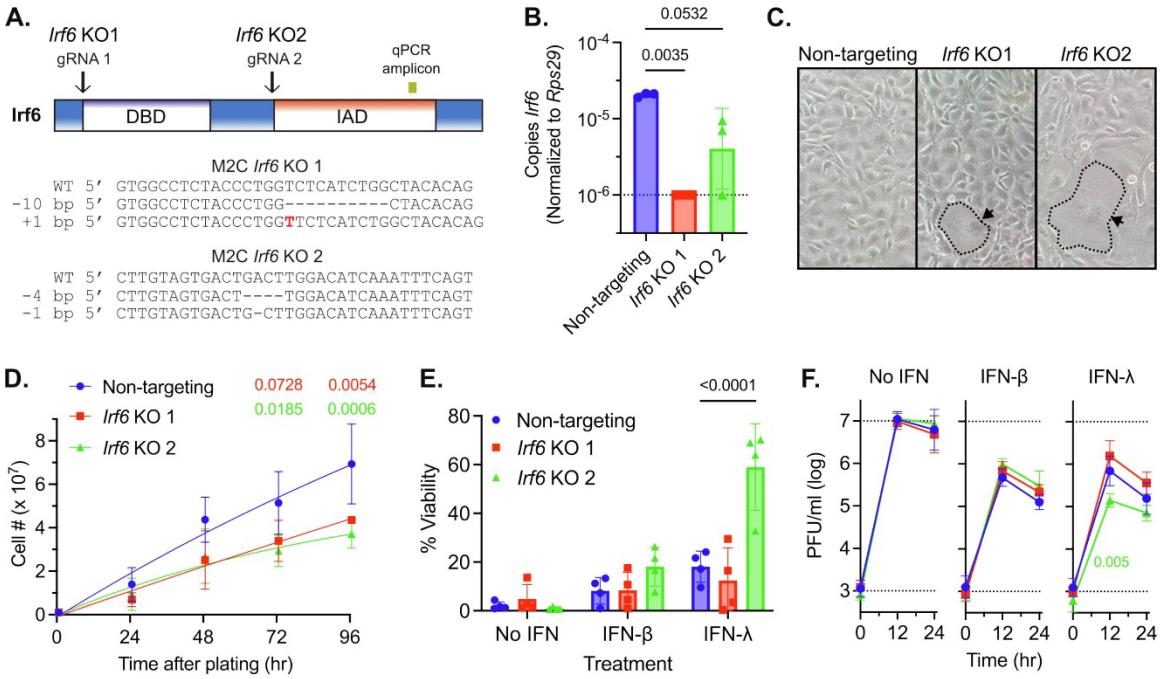

Figure 2.4 Irf6 knockout slows growth and alters interferon-stimulated protection in an intestinal epithelial cell line.

(A) Graphical representation of targeting sites for each Irf6 gRNA in the context of resulting protein domains, and sequences of monoclonal cell lines selected for further study. The region of the protein encoded by the qPCR amplicon sequence is indicated. Irf6 KO1 had a 10 bp deletion and a 1 bp insert resulting in early stop codons. Irf6 KO2 had a 4 bp deletion and a 1 bp deletion resulting in early stop codons. (B) qPCR of Irf6 from three replicate samples. Dashed line indicates limit of detection. P-values were calculated by one-way ANOVA. (C) Representative images of M2C cultures. Large multinucleated Irf6 KO M2Cs are outlined by the dashed lines and indicated by arrows. (D) Growth curves of uninfected and untreated M2C cells from three experimental replicates. P-values are shown above for 72- and 96-hour time points, calculated by two-way ANOVA. (E) ATP-Glo viability assay 24 hours after MNV infection of cells pretreated for 24 hours with no IFN, 0.01 ng/mL IFN-β, or 10 ng/mL IFN-λ. Data points represent four experimental replicates. P-values calculated by two-way ANOVA. (F) Growth curves for PFU following infection with MNV (MOI = 5). Cells were pre-treated for 24 hours with no IFN, 0.01 ng/mL IFN-β, or 10 ng/mL IFN-λ, as indicated. Data represents mean and standard deviation from three experimental replicates. P-values calculated by two-way ANOVA. ANOVA = analysis of variance; ATP = adenosine triphosphate; bp = base pair; gRNA = guide ribonucleic acid; IEC = intestinal epithelial cell; IFN = interferon; KO = knockout; MNV = murine norovirus; MOI = multiplicity of infection; PFU = plaque forming unit; qPCR = quantitative polymerase chain reaction.

and we were unable to detect Irf6 protein by western blot. However, we observed

phenotypic alterations following clonal isolation of the *Irf6* KO cells, with fewer cells

harvested during expansion compared to non-targeting controls, and several instances of large and multinucleated cells within *Irf6* KO isolates (**Fig. 2.4C**). These observations suggested monoclonal isolates may be selected for adaptation to *Irf6* deficiency. To quantitate the growth phenotype, we counted cells over time after plating and found that that both *Irf6* KO M2C cell lines had a decreased growth rate, with significantly fewer cells recovered compared to non-targeting controls (**Fig. 2.4D**).

We tested IFN-stimulated protection of KO cells by measuring viability after MNV infection, with or without IFN pretreatments (**Fig. 2.4E**). Additionally, we quantified viral replication by plaque assay (**Fig. 2.4F**). To ensure uniform susceptibility of monoclonal isolates to MNV infection, we re-transduced them with lentivirus encoding the receptor for MNV CD300lf. The resulting cell lines were equally susceptible to MNV-triggered death (**Fig. 2.4E**) and hosted equivalent viral replication with no IFN treatment (**Fig. 2.4F**). IFN-β and IFN-λ pretreatment increased viability and decreased viral titer of all cell lines after MNV infection (**Fig. 2.4E-F**). There were no significant differences in IFN-β-stimulated protection between the cell lines. In contrast, IFN-λ stimulated significantly greater protection of *Irf6* KO2, with viability increased to 60% average after IFN-λ treatment, compared to 20% average viability in control cells (**Fig. 2.4E**). IFN-λ treatment of *Irf6* KO2 correspondingly resulted in five-fold lower viral titer (**Fig. 2.4F**). *Irf6* KO1 did not have significantly different viability or viral titer compared to controls after either type of IFN pretreatment (**Fig. 2.4E-F**). Thus, there was an inconsistent effect of *Irf6* KO on IFN-stimulated protection from MNV in M2C-CD300lf cells, with only *Irf6* KO2 confirming the increased efficacy of IFN-λ treatment observed in the initial screen (**Fig.**

2.2E-F). However, there was a consistent reduction in growth rate for both *Irf6* KOs, suggesting that Irf6 plays an important homeostatic role in these cells.

Irf6 KO alters baseline and IFN-stimulated gene expression

To better understand the baseline and IFN-stimulated growth and viability phenotypes, we performed RNA sequencing on the *Irf6* KO and control cell lines. We harvested RNA from cells plated and treated in parallel to the viability assay in **figure 2.4E**, including both untreated and IFN-treated groups. Principal component analysis of the RNA sequencing results clustered groups with primary separation based on cell identity (PC1, 50% variance) and secondary separation based on IFN treatment (PC2, 20% variance) (**Fig. 2.5A**). Consistent with PCA analysis, there were hundreds of significantly different genes at baseline in *Irf6* KO cell lines compared to non-targeting controls. In *Irf6* KO1 we saw 103 up-regulated differentially expressed genes (DEGs), and 247 down-regulated DEGs; in *Irf6* KO2 we saw 1274 up-regulated DEGs and 1088 down regulated DEGs; both *Irf6* KO cell lines shared 31 up-regulated DEGs and 93 down-regulated DEGs (**Fig. 2.5B**). There was a notable cluster of DEGs that were uniformly down-regulated in both *Irf6* KO cell lines (**Fig. 2.5C**, box), and additional baseline DEGs that were unique to KO2. Pathway analysis of DEGs for each *Irf6* KO cell line revealed shared significant changes in pathways that regulate cell differentiation and growth (**Fig. 2.5D**). These enriched pathways are consistent with the decreased growth rate of these *Irf6* KO cell lines (**Fig. 2.4D**). Several genes decreased in both *Irf6* KO cell lines are part of

the “cell differentiation” GO pathway, including fibroblast growth factor 13 (*Fgf13*), Fms related receptor tyrosine kinase 4 (*Flt4*), *Notch1*, Lymphoid enhancer binding factor 1 (*Lef1*), Microtubule-associated protein 2 (*Map2*), and Slit guidance ligand 2 (*Slit2*) (**Fig. 2.5E**). Notably, previous ChIP-seq experiments from human keratinocytes [280] identified IRF6-bound loci in 12 human orthologs of genes down-regulated at baseline in both *Irf6* KO M2C cell lines (*SLIT2*, *CELSR1*, *SMARCA1*, *CAMK1D*, *PEG10*, *KPNA3*, *LTBP1*, *JAM2*, *KDR*, *AIG1*, *PCDH17*, and *EIF4G3*). These data indicate substantial changes to baseline gene expression in *Irf6* KO IEC cell lines and suggest roles for Irf6 in growth and differentiation of IECs.

Irf6 KO2 M2C cells had additional changes in baseline gene expression beyond the growth and development genes shared between KO cell lines (**Fig. 2.5A-E**). Pathway analysis of *Irf6* KO2 DEGs indicated significant enrichment of genes in “immune system process”, “inflammatory response”, and “regulation of leukocyte migration” GO pathways (**Fig. 2.5D**). These immune-related genes upregulated at baseline in *Irf6* KO2 included *Cxcl10*, *Tnip3*, *Lbp*, *Ikbkg*, *Tnfrsf9*, *Il33*, *Ccl2*, *Ccl20*, and *Ifnlr1* (**Fig. 2.5E**). The enrichment of *Ifnlr1* is particularly notable because it correlates with the increased IFN-λ-stimulated antiviral protection seen in **figure 2.4E-F**.

Figure 2.5 Irf6 KO alters baseline and IFN stimulated gene expression.

RNA sequencing of Irf6 KO M2C cells and non targeting controls with or without 24hrs of IFN treatment. All data is from three experimental replicates. A. Principal component plot. B-E. Differential gene expression of Irf6 KO cells relative to non-targeting controls within the untreated ('No IFN') groups. B. Differentially expressed genes (adjusted p-value < 0.05 and fold-change > 1.5). C. Heatmap of DEGs from B, with data scaled and centered by row. Box highlights DEGs down-regulated in both KO cell lines. D. Selected GO pathways significantly associated with DEGs from Irf6 KO1 (red bars) and Irf6 KO2 (green bars) cell lines. E. Volcano plot of all genes; dotted line represents cut-off for DEGs. F. Heatmap of IFN-responsive genes, including genes differentially expressed in at least one IFN-treated group compared to respective no IFN control. Data scaled and centered by row. G. Log2 fold change of genes from F. P-values calculated by Kruskal-Wallis test.

To compare the expression of IFN-regulated genes in these cell lines, we compared IFN-stimulated samples to replicate untreated controls (**Fig. 2.5F-G**). A heat map of all IFN-regulated genes reveals that most of them are upregulated by IFN treatments, an expected characteristic of ISGs (**Fig. 2.5F**). To compare the magnitude of

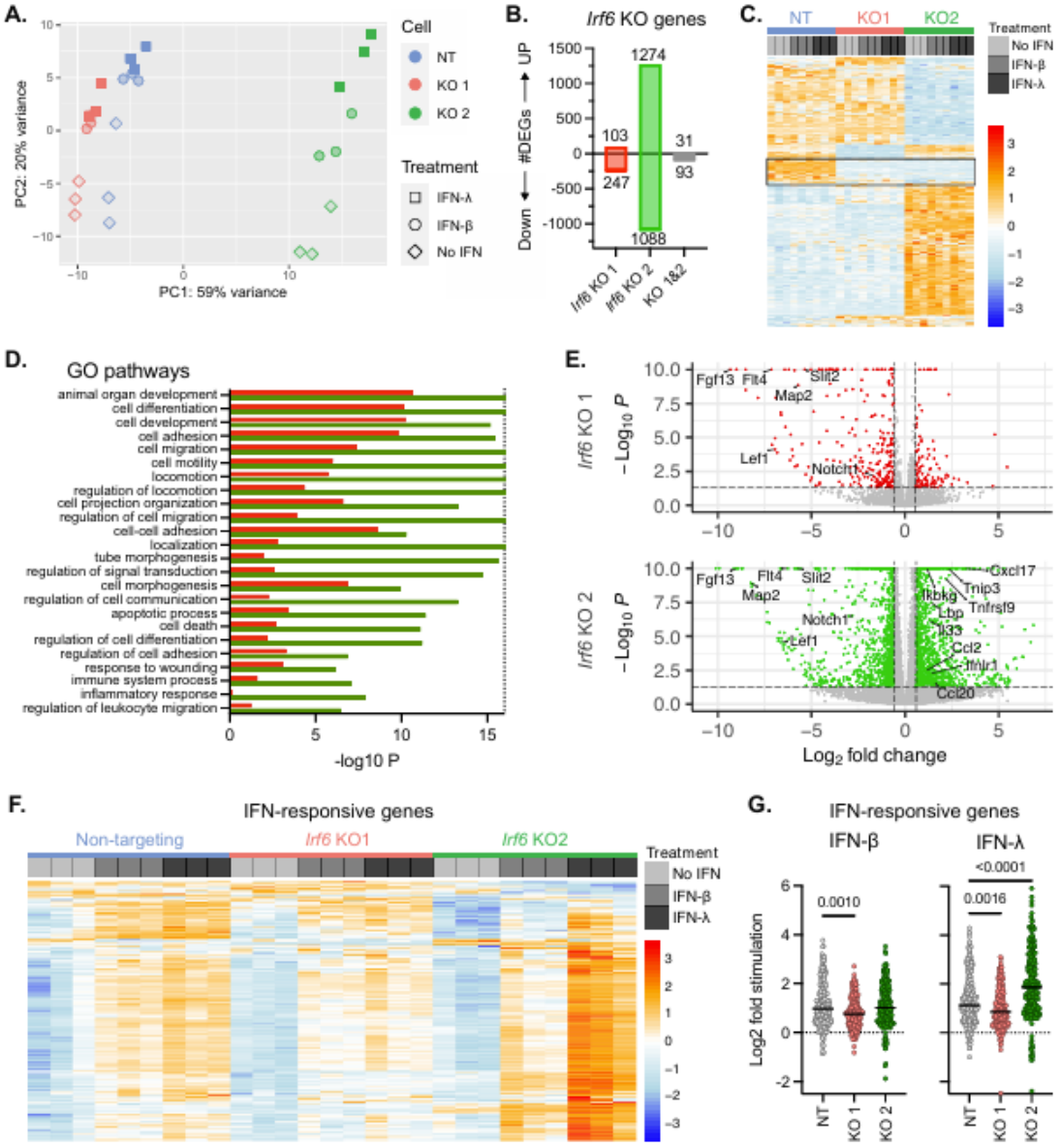

IFN responsiveness, we plotted the Log2 fold-change for the IFN-regulated genes. These comparisons show significantly higher stimulation by IFN-λ in *Irf6* KO2 compared to non-targeting controls, and significantly less stimulation of *Irf6* KO1 by both IFN-β and IFN-λ (**Fig. 2.5G**). The overall increase in ISGs seen in *Irf6* KO2 treated with IFN-λ correlates with the increased protection following MNV infection (**Fig. 2.4E-F**).

Taken together, these RNAseq data indicate a consistent down-regulation of growth and differentiation genes in *Irf6* KO cell lines. In contrast, immunity-related genes and ISGs exhibit divergent phenotypes between the *Irf6* KO cell lines that may reflect unique adaptations to *Irf6* deficiency. Although the primary goal of our CRISPR screen was to identify novel regulators of the IFN response in IECs, these data suggest that Irf6 plays more foundational roles in IEC biology at baseline.

Irf6 is expressed in primary IECs and regulates organoid homeostasis

Transformed cell lines such as M2C may selectively downregulate IRF6 due to its role as a tumor suppressor [280], [281], [282]. Indeed, we saw that *Irf6* was minimally expressed in M2C cells (**Fig. 2.4B, 2.6A**). So, we sought to test *Irf6* expression and function in primary cells. We found that *Irf6* expression in mouse small intestine and colon tissues was >10,000-fold higher than the M2C cell line, and *Irf6* in spleen tissue was significantly lower than intestinal tissues (**Fig. 2.6A**). Primary IEC organoids derived from mouse small intestine (ileum) expressed *Irf6* at levels within the same order of magnitude as intestinal tissues (**Fig. 2.6A**). These results indicate that the M2C IEC cell

line expresses sub-physiological levels of *Irf6*, so we focused subsequent study of Irf6 on primary IECs.

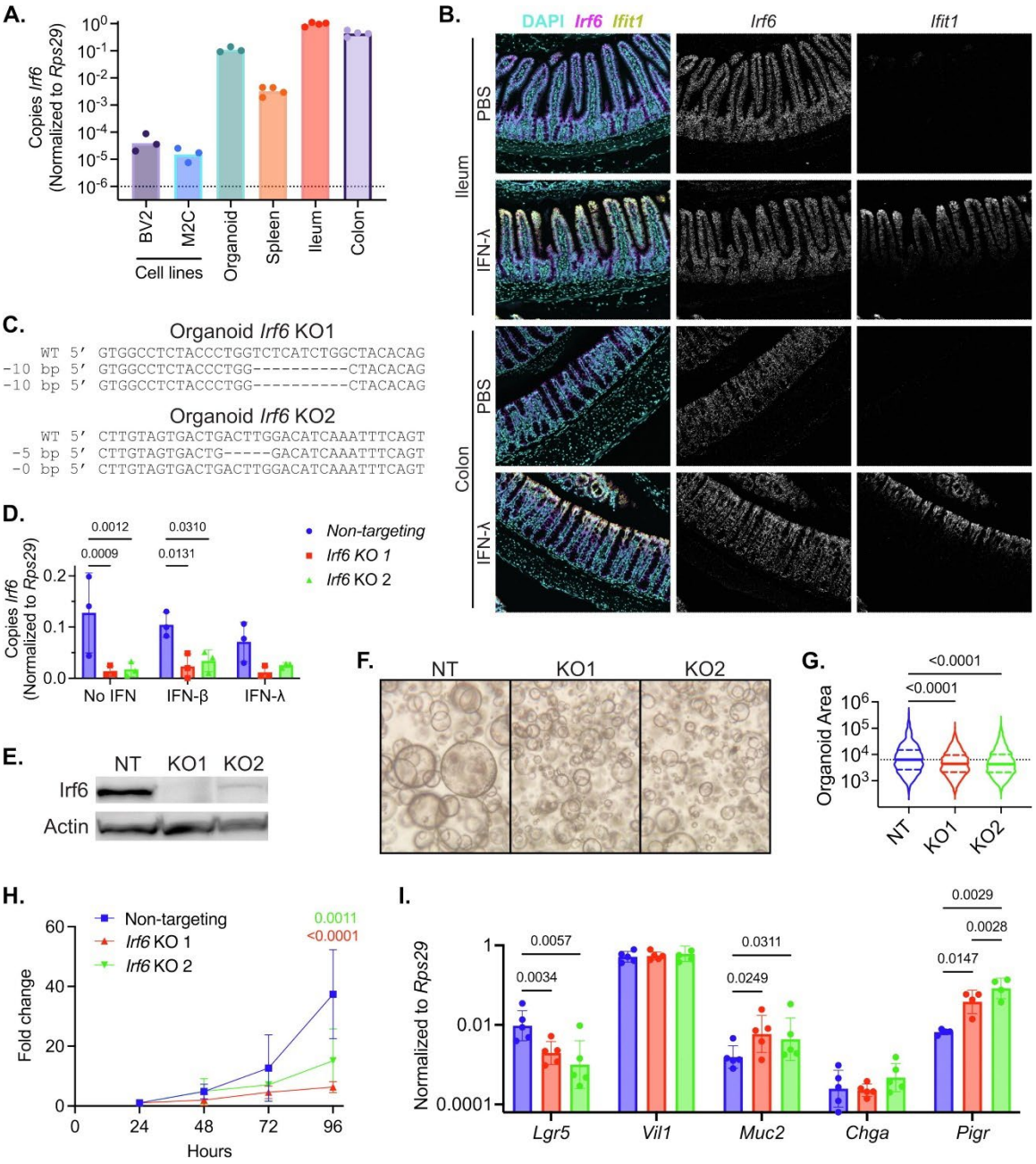

Figure 2.6 Irf6 is expressed in primary intestinal epithelial cells and regulates organoid homeostasis.

(A) Expression of Irf6 in different cells and tissues. (B) Irf6 and Ifit1 (ISG) expression in small intestine and colon of adult mice. Treatment with PBS or 3 μg peg-IFN-λ, as indicated, 24 hours prior to tissue collection. Representative of four mice per group. (C) Sequence of Irf6 locus in monoclonal IEC organoid lines transduced with CRISPR lentivirus. (D) Irf6 expression by qPCR from organoids treated with no IFN, 10 ng/mL IFN-β, or 25 ng/mL IFN-λ for 24 hours. (E) Irf6 protein expression by western blot in the non-targeting CRISPR control organoids (NT) compared to Irf6 KO organoids, representative of three replicates. (F) Representative photos of organoids 2 days after plating. (G) Cross-sectional area of organoids measured by ImageJ (arbitrary units) 2 days after plating. Violin plots show the median and quartiles of three experimental repeats (n = 1242, 1756, 1483). Dashed line indicates median of NT control. P-values calculated by Kruskal-Wallis test. (H) Growth curves of IEC organoids from three experimental replicates normalized within each replicate to cell number at 24 hours. (I) Expression of indicated genes by qPCR in Irf6 KO organoids and NT controls. Data points represent five experimental replicates. P-values calculated by two-way ANOVA. ANOVA = analysis of variance; bp = base pair; CRISPR = Clustered Regularly Interspaced Short Palindromic Repeats; DAPI = 4',6-diamidino-2-phenylindole; IEC = intestinal epithelial cell; IFN = interferon; ISG = IFN-stimulated gene; KO = knockout; NT = non-targeting; PBS = phosphate-buffered saline; qPCR = quantitative polymerase chain reaction; WT = wild type.

To visualize distribution of Irf6 within intestinal tissues we performed *in situ* hybridization for *Irf6* in ileum and colon of mice injected with PBS or IFN-λ 24 hours prior to tissue collection (**Fig. 2.6B**). In all intestinal tissues, *Irf6* was predominant within the epithelium, and was similar in abundance from crypt base to mature enterocytes and colonocytes (**Fig. 2.6B**). The ISG response in mice injected with IFN-λ was assessed by detection of *Ifit1*, and expression of this ISG was predominant within mature IECs (**Fig. 2.6B**). *Irf6* transcripts were not strikingly different between IFN-λ-treated mice and PBS controls, confirming that *Irf6* is not an ISG (**Fig. 2.6B**). This is consistent with data in the interferome database indicating that IRF6 is not upregulated by IFN treatments [283]. These imaging analyses indicated that *Irf6* is expressed in IECs of small intestine and colon, including IFN-λ-responsive cells.

We next sought to generate *Irf6* KO primary IECs by transducing organoids with *Irf6*-targeting CRISPR lentiviruses used in the screens (**Fig. 2.4A**). We selected transduced IEC organoid clones and sequenced gRNA target sites within the *Irf6* locus to assess gene disruption. We identified a homozygous *Irf6* KO in organoids transduced with CRISPR gRNA 1 (**Fig. 2.6C**, KO1). However, in organoids transduced with CRISPR gRNA 2 (cuts after DBD), we recovered only clones with heterozygous targeting of the *Irf6* gene (**Fig. 2.6C**, KO2). Analysis of *Irf6* expression by qPCR showed significant decreases in both KO organoid lines, and no significant effect of IFN treatments on *Irf6* expression (**Fig. 2.6D**). Western blot of Irf6 showed no detectable protein in KO1 organoids and a substantially decreased protein level in KO2 organoids (**Fig. 2.6E**). We speculated that homozygous targeting of *Irf6* using gRNA 2 may be more deleterious due to potential expression of a protein fragment containing the Irf6 DBD only (**Fig. 2.4A**). We were unable to visualize any such fragment on western blot, but a similar heterozygous deletion has been linked to a human orofacial clefting syndrome [284], indicating the potential for biological activity of this heterozygous truncation. So, we included both *Irf6* KO organoid lines in our subsequent studies.

During culture of *Irf6* KO IEC organoids, we noticed that they appeared smaller and darker (**Fig. 2.6F**). To quantify organoid size, we took pictures two days after plating and measured the cross-sectional area of organoids in each image. *Irf6* KO organoids were significantly smaller than the non-targeting control organoids (**Fig. 2.6G**). Additionally, counting cells over time post-plating revealed that *Irf6* KO organoids grew significantly more slowly than non-targeting controls (**Fig. 2.6H**). Thus, *Irf6* deficiency

reproducibly results in slower growth of primary IECs, similar to the baseline phenotype observed in *Irf6*-deficient M2C cell lines.

The slower growth rate of *Irf6* KO organoids, together with the earlier observation of decreased growth and development genes in *Irf6* KO M2C cell lines (**Fig. 2.6D-E**), led us to investigate the expression of IEC differentiation genes in organoids. *Lgr5* is expressed by intestinal stem cells and is reduced in expression as enterocytes mature; *Lgr5* was 5- to 10-fold lower in *Irf6* KO organoids relative to non-targeting controls (**Fig. 2.6I**). *Vil1* is an enterocyte marker and was not significantly different in *Irf6* KO organoids. *Muc2* is a mucin glycoprotein produced by goblet cells; we saw a ~5-fold increase in *Irf6* KO organoids relative to non-targeting controls (**Fig. 2.6I**). *Chga* is marker for enteroendocrine cells; *Chga* was not significantly different in *Irf6* KO organoids. *Pigr* is an Fc-receptor that facilitates translocation of immunoglobulin A into the intestinal lumen and is stimulated by innate responses to microbiota; *Pigr* was 5- to 10-fold higher in the *Irf6* KO organoids (**Fig. 2.6I**). Taken together, these data indicate that *Irf6* deficiency in primary IEC organoids results in slower growth, reduced size, and increased expression of certain differentiation genes.

Irf6 regulates development and immune response genes in primary IECs

Figure 2.7 Irf6 regulates development and immune response genes in primary intestinal epithelial cells.

NT or Irf6 KO organoids were treated with no IFN, 10 ng/mL IFN-β, or 25 ng/mL IFN-λ for 24 hours prior to preparation of single cells for scRNA-seq. (A) Diagram depicting experimental groups, multiplexing, and pooling strategy. Two pools consisted of organoid lines transduced with the MNV receptor CD300lf, with or without MNV infection. (B) UMAP multidimensional clustering of all sequenced cells, colored by cell line. Insets at bottom are split by IFN treatment group, as indicated. (C) Heatmap of Irf6-dependent DEGs arranged by preferential expression in NT control cells (top) to preferential expression in Irf6 KOs (bottom). Selected genes related to development and immunity are labeled. (D) Number of DEGs from C for each KO organoid line compared to NT control and overlapping DEGs shared by KO organoid lines. (E) Association between genes in C–D and selected GO pathways for Irf6 KO1 (red bars) and Irf6 KO2 (green bars) organoid lines. (F) Dot plot depicting expression of selected genes related to growth, differentiation, and immunity, within each organoid cell line. (G) Unsupervised clustering of all cells, with cluster names based on predominant organoid cell line represented. (H) Distribution of Pool IDs, cell cycle phase categories, IFN treatments, and organoid cell lines, within each cluster. (I) Dot plot depicting expression of marker genes for IEC subtypes within cells from each cluster. (J) Violin plots showing expression of marker genes for regulatory stem cells, secretory IEC subsets, or absorptive enterocytes within each organoid cell line. (K–L) CytoTRACE analysis of differentiation. Higher CytoTRACE score indicates more stem-like cells. All analyses were performed on integrated data from four single-cell pools (A). DEGs were defined as >1.5-fold change with adjusted $p < 0.05$ using analysis pipelines described in methods. CytoTRACE = cellular (cyto) trajectory reconstruction analysis using gene counts and expression; DEG = differentially expressed gene; GO = Gene Ontology; ID = identification; IEC = intestinal epithelial cell; IFN = interferon; KO = knockout; MNV = murine norovirus; NT = non-targeting; scRNA-seq = single-cell ribonucleic acid sequencing; UMAP = Uniform Manifold Approximation and Projection.

To define *Irf6*-dependent alterations to IEC organoid gene expression, we prepared single-cell RNA sequencing libraries from four multiplexed pools of organoid lines with experimental variables including *Irf6* KO, IFN treatment, CD300lf transduction, and MNV infection (**Fig. 2.7A, methods**). Upon demultiplexing and integration of these four single-cell pools, we ended up with 12,151 cells suitable for analysis. Dimensional reduction of

the integrated single-cell data revealed that a primary source of variation (UMAP1) was related to *Irf6* KO and a secondary source of variation (UMAP2) was due to IFN treatments (**Fig. 2.7B**). Separate clustering of the untreated groups confirmed that a

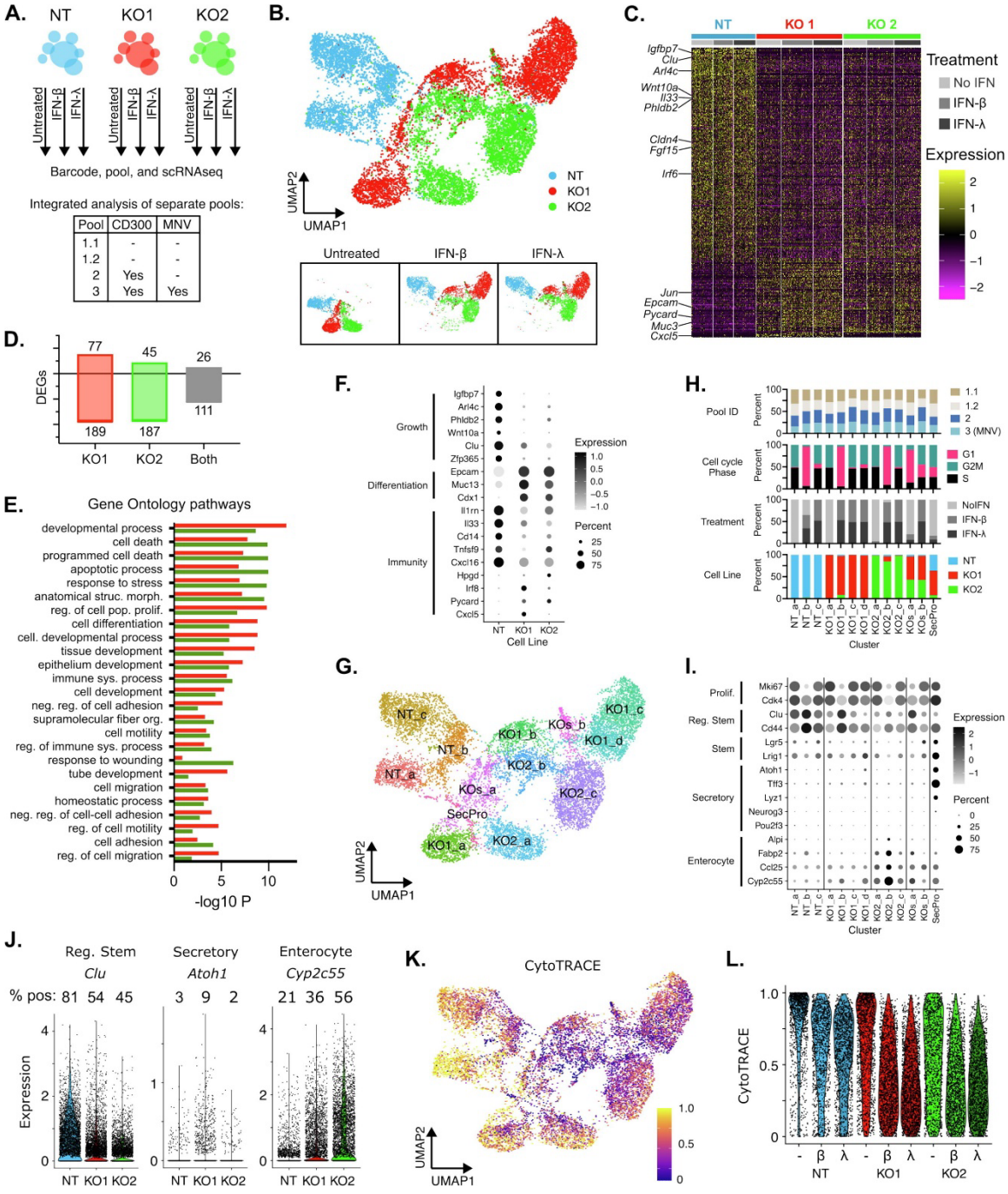

primary source of variation was related to *Irf6* KO, independent of IFN treatment (**Fig. 2.8A**).

MNV infection was not robust in CD300lf organoids at the 24hr timepoint and did not represent a significant source of variation within this dataset. The few robustly-infected cells did not cluster separately from uninfected cells (**Fig. 2.8B**). IFN treatments reduced the number of robustly-infected cells in all cases (**Fig. 2.8C**), and there were no significant differences between cell lines. Thus, we focused subsequent analyses of *Irf6* KO organoids on baseline and IFN-stimulated phenotypes.

To identify global *Irf6*-dependent transcriptional changes, we compared gene expression in each *Irf6* KO organoid line to non-targeting controls. Hundreds of genes were significantly different in each *Irf6* KO organoid line, with the majority of DEGs being downregulated relative to non-targeting control (189 for KO1, 187 for KO2) (**Fig. 2.7C-D**). There was substantial congruence in DEGs between KO lines, with 111 shared down-regulated DEGs and 26 shared up-regulated DEGs (**Fig. 2.7D**). Likewise, GO pathways associated with *Irf6* KO DEGs were shared between the two KO organoid lines, including "epithelium development," "cell death," "cell adhesion," and "regulation of immune system process" (**Fig. 2.7E**). These pathways in *Irf6* KO organoids included substantial overlap with pathways altered in *Irf6* KO in M2C cell lines (**Fig. 2.7D**), increasing confidence in the association of Irf6 with epithelial homeostasis and immunity at baseline.

To determine which genes may be direct targets of Irf6, we compared our DEGs with IRF6 binding sites in ChIP-seq data from human keratinocytes [280]. We saw 38 *Irf6*-associated DEGs were orthologs of genes from IRF6 ChIP-seq, including three of the most highly down-regulated genes in both *Irf6* KO organoid lines: insulin-like growth factor binding protein 7 (*Igfbp7*), ADP ribosylation factor-like GTPase 4C (*Arl4c*), and pleckstrin homology-like domain family B member 2 (*Phldb2*) (**Fig. 2.7F**). *Phldb2* is associated with growth of cancer cells [285], and *Arl4c* plays roles in epithelial morphogenesis [286], which is consistent with the reduced proliferation and size of *Irf6* KO organoids (**Fig. 2.6G-H**).

Figure 2.8 Supplemental analysis of scRNAseq related to Figure 2.7

(A) UMAP clustering of untreated cells only. (B) Feature plot of MNV genome count distribution among all groups. (C) Violin plot of MNV counts within the MNV-infected pool only. (D) Heatmap of 10 genes with the greatest fold-change increase in expression within each cluster (Fig. 6G) relative to all other clusters. (E) Feature plots depicting the distribution of expression for the top gene for each cluster. (F) Feature plots depicting genes enriched in SecPro cluster. (G-H) CytoTRACE analysis of differentiation in untreated cells only. Higher CytoTRACE score indicates more stem-like cells. I. Gene-set enrichment of lrf6 DEGs from this study within the ranked list of genes differently expressed in WT small intestinal stem cells relative to lrf2 KO stem cells (GSE137190). Leading edge genes shown are upregulated in lrf6 KO organoids (lrf6_up) and upregulated in lrf2 KO stem cells (Enrichment score= -0.42, adjusted p-val = 0.0038).

To further identify highest-confidence Irf6-regulated genes, we compared organoid DEGs to M2C cell line DEGs (**Fig. 2.5B-C**). 83 DEGs were shared between organoid KO and M2C KO lines, including downregulation of genes associated with Wnt signaling (*Wnt10a*), regenerative stem cells (*Clu*), and maintenance of genome stability (*Zfp365*, also shared

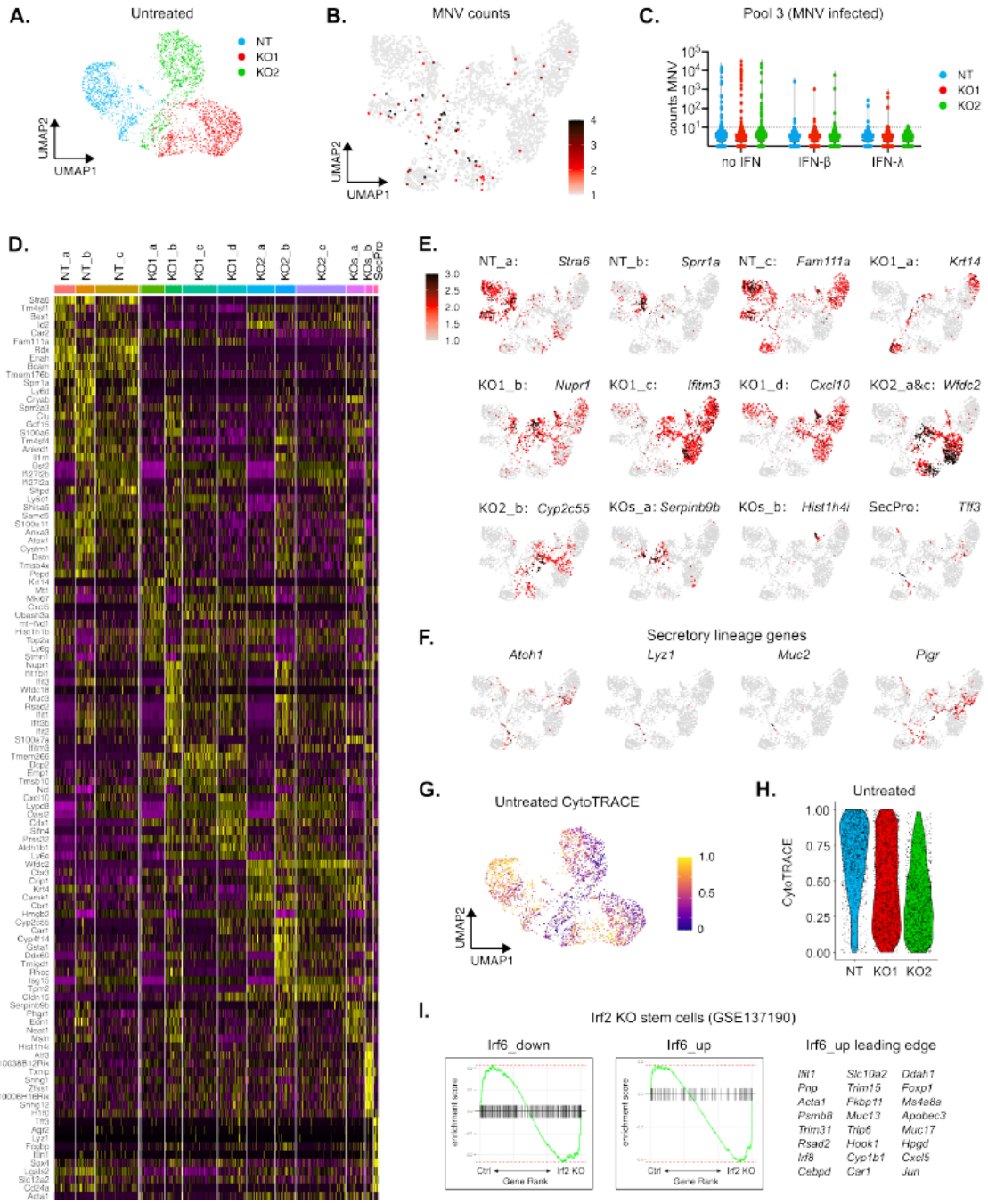

with IRF6 ChIP-seq) (**Fig. 2.7F**). Relatively few DEGs in *Irf6* KO organoids were

upregulated, but some upregulated DEGs were indicative of increased differentiation: epithelial cell adhesion molecule (*Epcam*), mucin 13 (*Muc13*), and differentiation-promoting transcription factor caudal type homeobox 1 (*Cdx1*) (**Fig. 2.7F**).

To identify subtypes within each experimental group, we performed unsupervised clustering of integrated single-cell data. We identified 13 clusters of differential gene expression (**Fig. 2.7G**). The clusters distinguished *Irf6* KO organoids from non-targeting controls and identified distinct IFN-stimulated subsets (**Fig. 2.8D-E**). Clusters were predominantly distinguished by cell line, IFN treatment, and cell cycle phase, but not by the four separate single-cell pools (**Fig. 2.6H**). Clusters were named based on the predominant cell line therein: three non-targeting control clusters (NT_a, NT_b, NT_c), four KO1 clusters (KO1_a, KO1_b, KO1_c, KO1_d), three KO2 clusters (KO2_a, KO2_b, KO2_c), and two clusters with equal representation of both KO lines (KOs_a, KOs_b) (**Fig. 2.7H**). There was also a small cluster within untreated groups that expressed markers of secretory progenitor IECs (**Fig. 2.7G**, SecPro), including master transcription factor *Atoh1*, Paneth cell-associated *Lyz1*, goblet cell-associated *Muc2*, and immunoglobulin transport receptor *Pigr* (**Fig. 2.8F**). This secretory progenitor cluster was predominantly composed of *Irf6* KO1 organoids (**Fig. 2.6H**), suggesting a role of Irf6 in blocking secretory progenitor differentiation.

With the exception of the SecPro group, unsupervised clustering did not clarify IEC subtypes within our dataset. To determine *Irf6* KO effects on IEC subset differentiation pathways, we selected subset marker genes from the literature [287], [288], [289], [290] for proliferating cells, regenerative stem cells, crypt-base stem cells,

secretory subtypes (Goblet, Paneth, Enteroendocrine, and Tuft), and absorptive enterocytes (**Fig. 2.7I**). The majority of cells in NT control organoid cultures were proliferating regenerative stem cells, with relatively low expression of secretory and absorptive IEC markers (**Fig. 2.7I**). All stem cell markers were lower in *Irf6* KO organoids compared to NT controls (**Fig. 2.7I-J**). There was a small increase in goblet cell markers *Atoh1* and *Tff3*, particularly within full *Irf6* KO organoids (**Fig. 2.7I-J**) and consistent with the high representation of *Irf6* KO1 organoids in the SecPro cluster (**Fig. 2.7H**). All *Irf6* KO organoids had increased expression of absorptive enterocyte marker genes (**Fig. 2.7I-J**). Together, these data suggest a role for Irf6 in promoting regenerative stem cell identity or inhibiting expression of differentiated IEC genes.

As an orthogonal test of differentiation status, we performed CytoTRACE analysis [291], which examines transcriptional diversity to infer developmental potential. CytoTRACE analysis indicated that *Irf6* KO organoids had less differentiation potential at baseline (No IFN groups) compared to non-targeting control organoids (**Fig. 2.7K-L, S2G-H**). IFN treatment further decreased developmental potential within each group (**Fig. 2.7K-L**). Together, these data reveal a significant role for Irf6 in regulating the homeostatic transcriptome and developmental gene expression of primary IEC organoids.

Irf6 regulates ISG expression and ISRE activity in IEC organoids

Figure 2.9 Irf6 regulates the interferon response in primary intestinal epithelial cells.

(A–B) Heatmaps of ISGs arranged by greater stimulation in non-targeting (top) to greater stimulation in Irf6 KOs (bottom). (A) All ISGs are significantly increased by IFN treatment within at least one cell line. (B) ISGs are also significantly different between at least one KO line and non-targeting controls. (C) Violin plots depicting expression of selected ISGs among clusters from Fig. 6G. (D, E) Flow cytometry of Mx1-GFP expression 24 hours after treatment of indicated organoid lines with 10 ng/mL IFN-β (dashed lines) or 25 ng/mL IFN-λ (solid lines). (D) Representative plots from three experimental replicates. (E) Fold-change in median GFP expression of IFN-treated groups relative to their respective untreated controls. Data points represent replicates and significance was calculated using two-way ANOVA with Sidak multiple comparison correction. ANOVA = analysis of variance; GFP = green flourescence protein; IEC = intestinal epithelial cell; IFN = interferon; ISG = IFN-stimulated gene; KO = knockout.

To identify all IFN-regulated genes within organoid RNAseq data, we compared IFN-treated groups for each organoid line (NT, KO1, KO2) to their respective untreated controls. IFN types were combined for this analysis because there were minimal differences in clustering between IFN-β and IFN-λ treatments (**Fig. 2.7A** inset, **Fig. 2.8E**). We identified 162, 204, and 178 IFN-regulated genes for NT control, *Irf6* KO1, and *Irf6* KO2 organoids, respectively (**Fig. 2.9A**). Many antiviral ISGs were similarly upregulated across all IFN-treated groups (e.g. *Ifih1, Tlr3*), but 20 ISGs were significantly higher in *Irf6* KO organoids relative to non-targeting controls (**Fig. 2.9B**). Some of these *Irf6*-dependent ISGs were favored within distinct IFN-stimulated KO subsets (**Fig. 2.9G**): *Muc3* and *Ifit1bl1* were preferentially stimulated in KO1_b and KO2_b clusters (G1 phase); *Ifitm3* and *Psmb8* were preferentially stimulated in KO1_c, KO1_d, and KO2_c clusters (G2/S phases) (**Fig. 2.9C**). Additionally, the KOs_b cluster was shared between IFN-stimulated *Irf6* KO organoid lines and was distinguished by increased markers of apoptotic stress

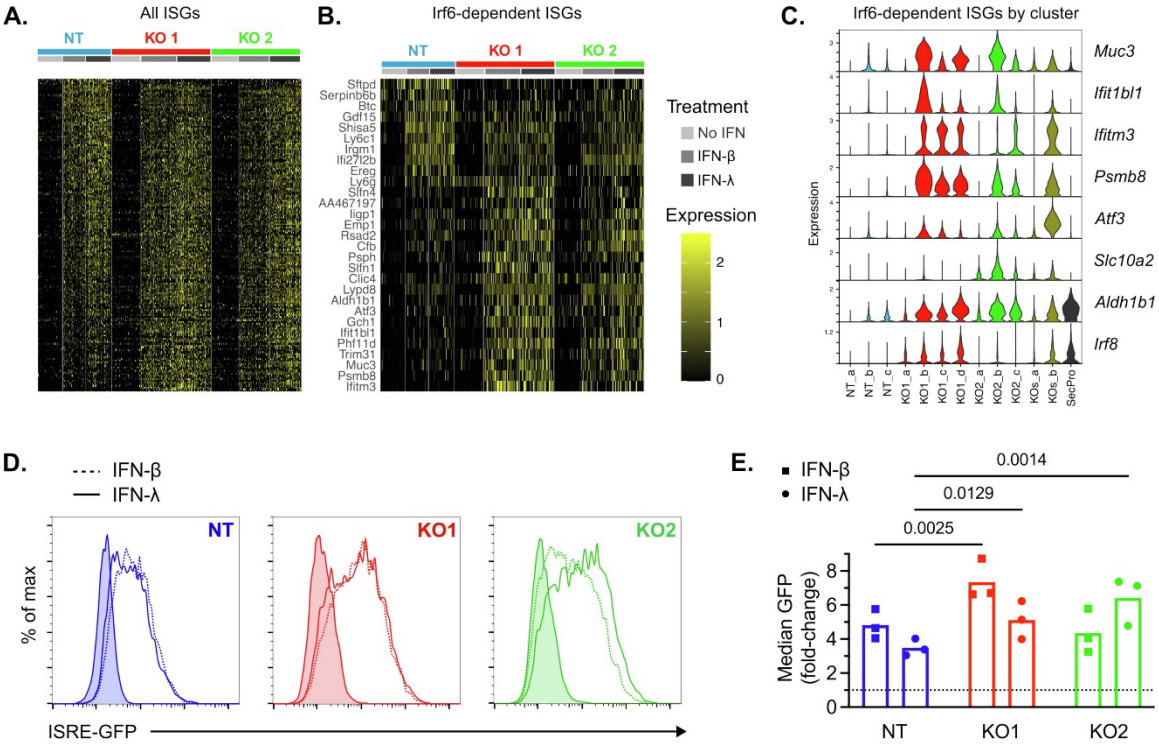

response (e.g. *Atf3*, *Atf4, Chac1*, **Fig. 2.9C**), suggesting increased IFN-stimulated stress and cytotoxicity in *Irf6* KO organoids.

Further analysis of gene clusters identified some ISGs unique to subsets of each organoid line. For example, the bile acid cotransporter *Slc10a2* was preferentially stimulated in the KO2_b cluster (**Fig. 2.9C**), which also had the highest expression of enterocyte genes (**Fig. 2.7I**). Additionally, IFN-stimulated KO1_d cluster expressed secretory-lineage transcription factor *Atoh1* (**Fig. 2.8F**), suggesting ISGs in this cluster may be preferentially IFN-stimulated within secretory-lineage cells. These KO1_d cluster ISGs included aldehyde dehydrogenase (*Aldh1b1*) and *Irf8* (**Fig. 2.9C**). Furthermore, there was increased baseline expression of *Aldh1b1* and *Irf8* within untreated secretory progenitors (**Fig. 2.9C**, SecPro), further linking these genes to IEC subsets. Together these

data revealed clusters of IFN-stimulated response genes that correlated with *Irf6* expression, cell cycle phase, and IEC subtype genes.

Differences in the ISG transcriptome of *Irf6* KO organoids may be related to differential IFN-stimulated activation of the ISRE promoter. The parental organoid line used to generate *Irf6* KOs was derived from the ileum of an ISRE-GFP reporter mouse [292]. Therefore, we used flow cytometry to quantify GFP reporter expression as an indicator of ISRE transactivation following 24 hours of treatment with either IFN-β or IFN-λ. All organoid lines had significantly higher GFP expression following IFN treatments, confirming the utility of this reporter gene (**Fig. 2.9D-E**). The median fold-increase in GFP fluorescence of *Irf6* KO1 organoids treated with either IFN type was significantly higher than non-targeting controls (**Fig. 2.9E**). *Irf6* KO2 organoids exhibited a preferential response to IFN-λ, with a significantly higher median fold-increase in GFP following treatment with IFN-λ, but not IFN-β (**Fig. 2.9E**). This IFN-λ phenotype of *Irf6* KO2 organoids was consistent with the result of preferential IFN-λ phenotype for *Irf6* in the viability CRISPR screen (**Fig. 2.2G-H**). Together, these data support the conclusion that Irf6 dampens IFN responsiveness of IEC organoids.

Increased IFN-stimulated cytotoxicity in Irf6-deficient IEC organoids

RNAseq data suggested that *Irf6* deficiency led to an increase in IFN-stimulated stress and cytotoxicity (KOs_b cluster, **Fig. 2.7G**). To quantify differences in IFN-stimulated cytotoxicity between IEC organoid lines, we treated cells with a titration of

IFN-β or IFN-λ for 48 hours and quantified viability by ATPglo cell titer assay. Treatment with IFN-β concentrations below 1 ng/mL resulted in no appreciable change in viability, but 10 ng/mL IFN-β resulted in lower viability (63%) for each *Irf6* KO organoid line compared to non-targeting controls (95% viability) (**Fig. 2.10A**). Treatment with IFN-λ concentrations below 10 ng/mL resulted in no appreciable change in viability for non-targeting control cells, but concentrations as low as 0.1 ng/mL IFN-λ resulted in 85% viability for *Irf6* KO organoids (**Fig. 2.10B**). Viability decreased to 31-42% for *Irf6* KO organoids treated with 1000 ng/mL IFN-λ, whereas non-targeting controls were only reduced to 77% viability at this maximum concentration of IFN-λ (**Fig. 2.10B**). These data indicated that IFN treatment of IEC organoids results in a greater loss of viability in the absence of *Irf6*, particularly for IFN-λ treatment, which is usually not cytotoxic.

In addition to IFN-stimulated cytotoxicity, we hypothesized that other cytotoxic stimuli may be more active in the absence of *Irf6*. We noted that the inflammasome adaptor ASC (*Pycard*) and inflammasome effector *Casp1* were significantly upregulated in *Irf6* KO organoids at baseline (**Fig. 2.7F, 2.10C**). To test whether inflammasomes were differentially active in *Irf6*-deficient IECs, we quantified inflammasome-driven lysis of IEC organoid lines by stimulating the NAIP-NLRC4 inflammasome with agonist delivery to the cytosol (FlaTox), and monitoring lysis by uptake of the DNA stain propidium iodide [293],

[294]. *Irf6* KO organoids exhibited significantly greater lysis following FlaTox addition compared to non-targeting control organoids (**Fig. 2.10D**).

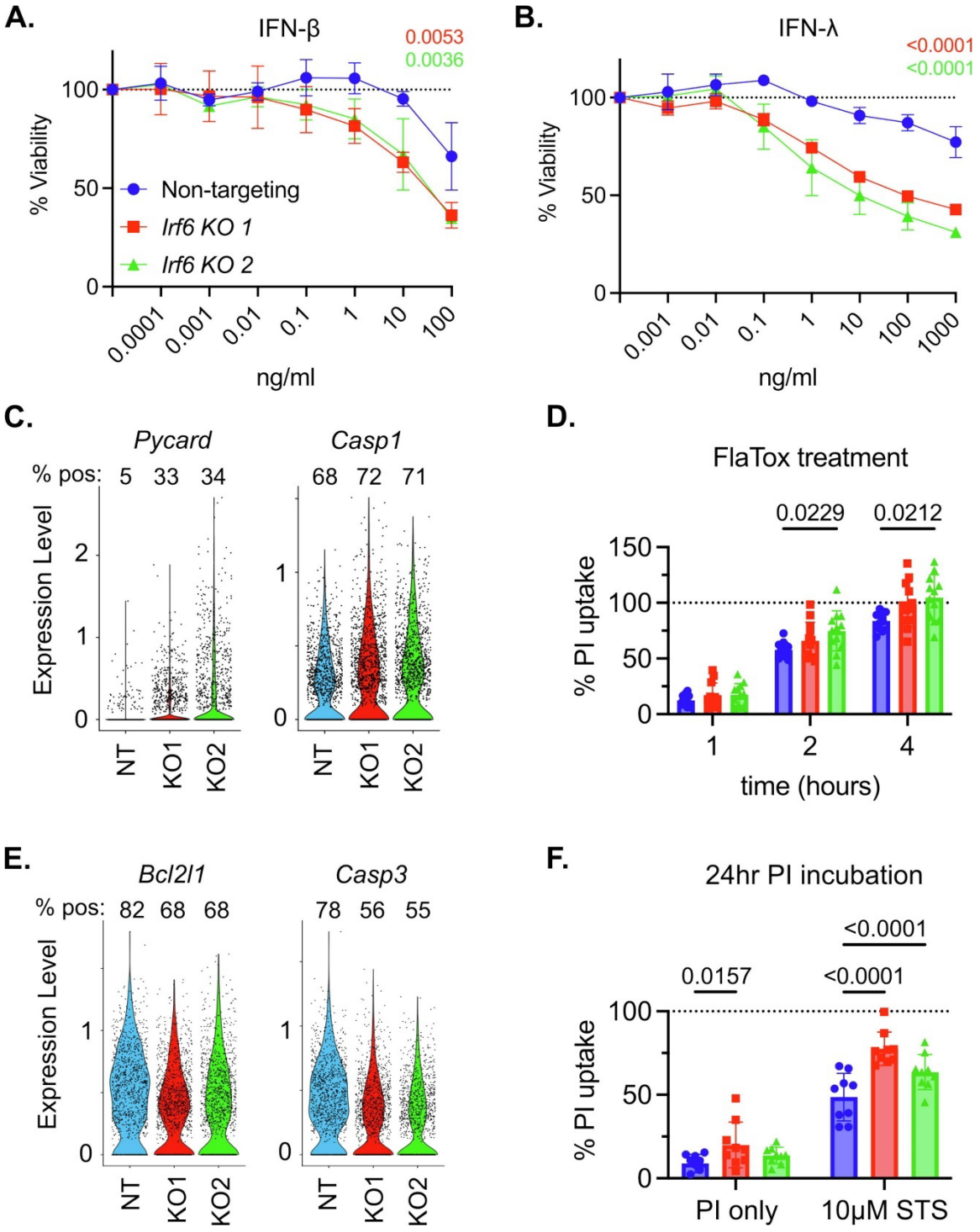

Figure 2.10 Increased innate immune cytotoxicity in Irf6-deficient intestinal epithelial cell organoids.

(A) Irf6 KO and non-targeting control organoids were treated with indicated concentrations of IFN-β (A) or IFN-λ (B) for 48 hours, and viable cells were quantified by ATP-Glo assay relative to no IFN treatment controls. Two independent replicates with statistical significance by two-way ANOVA. (C) Gene expression for Pycard and Casp1 from untreated cells in single-cell RNAseq data. (D) Organoids were treated with PI viability stain in the presence or absence of FlaTox, and the percent of maximum PI fluorescence was measured relative to untreated control wells. (E) Gene expression for Bcl2l1 and Casp3 from untreated cells in single-cell RNAseq data. (F) Organoids were treated with PI viability stain in the presence or absence of STS, and the percent of maximum PI fluorescence was measured relative to 0-hour time point values. Data points in C–F are combined from three independent experiments, with statistical significance by two-way ANOVA. ANOVA = analysis of variance; ATP = adenosine triphosphate; IEC = intestinal epithelial cell; IFN = interferon; KO = knockout; PI = propidium iodide; RNAseq = ribonucleic acid sequencing; STS = staurosporine.

Apoptosis pathway genes were also significantly different in *Irf6* KO organoids, including reduced expression of anti-apoptotic Bcl-XL (*Bcl2l1*) as well as pro-apoptotic *Casp3* (**Fig. 2.10E**). To test the functional outcome of apoptosis pathway gene changes, we treated cells with the model apoptosis inducer staurosporine (STS) and monitored late apoptotic death by uptake of propidium iodide (PI). Both *Irf6* KOs exhibited significantly greater death than non-targeting controls in the presence of STS (**Fig. 2.10F**). *Irf6* KO1 also had significantly greater PI uptake in the absence of STS (**Fig. 2.10F**), which may reflect increased turnover of differentiated cells. Taken together with IFN-stimulated cytotoxicity, these data indicate that IRF6-dependent gene expression programs can directly or indirectly moderate cytotoxicity of IECs following activation of cell death pathways.

Discussion

We set out to identify novel regulators of the IFN response in IECs through the use of complementary CRISPR screens and discovered that targeting *Irf6* in M2C IEC cells (but not BV2 macrophages) led to increased IFN-stimulated protection against MNV infection (**Figs. 2.2-3**). We found that monoclonal isolates of *Irf6* KO M2C cells had a slower growth rate and decreased expression of epithelial development pathway genes (**Figs. 2.4 & 2.6**). Primary IECs express substantially more Irf6 than transformed M2C cells (**Fig. 2.6A**), and Irf6-deficient IEC organoids had a reproducible reduction in growth and differentiation genes as well as consistent alterations to ISG profile (**Figs. 2.7 & 2.9**). In particular, increased IFN-stimulated expression of stress genes (**Fig. 2.7**) was correlated with a greater cytotoxicity of IFN-treated *Irf6* KO IEC organoids (**Fig. 2.10A-B**). Thus, we have identified a novel role for IRF6 in shaping the biology of IECs at baseline, with attendant roles in regulating the response to IFN. This role extends to other immune pathways beyond IFN because we also found greater inflammasome-stimulated death in *Irf6*-deficient organoids and greater apoptosis induced by STS (**Fig. 2.10C-F**).

IRF6 is known to be important for fidelity of orofacial development, and *Irf6* knockout mice are perinatal lethal with myriad developmental defects [271]. IRF6 has been primarily studied as a lineage-defining transcription factor within the epidermis and is known to promote expression of genes important for terminal differentiation of keratinocytes [272], [280], [295]. Our findings suggest that IRF6 may play an analogous role in the development of IECs, with keratinocyte-specific transcriptional programs

substituted for IEC-specific programs. Indeed, a recent study of human organoids identified *IRF6*-targeted cells to be significantly reduced in a pooled transcription factor screen [296], indicating an important role of IRF6 in human IECs. Additionally, a genome-wide association study of inflammatory bowel diseases identified a polymorphism within an *IRF6* intron that is associated with increased risk of disease [297] and is associated with decreased expression of IRF6 transcripts. Thus, our observation of decreased developmental potential and increased cytotoxicity in *Irf6*-deficient IECs has potential implications for human disease. Future studies in IEC-specific conditional knockout mouse models will definitively test *Irf6* roles in development, immunity, and disease within intact tissues.

All IRF family transcription factors share a highly conserved DBD, and members of this transcription factor family with developmental roles could also participate in regulation of IFN-stimulated response genes. A dual role of IRF6 in development and immunity may be a beneficial strategy for shaping the immune response of epithelia to suit their physiological roles within tissues. Our data suggests that IRF6 restricts the IFN response of IECs, with increased stress and apoptosis pathway genes stimulated by IFN when IRF6 is absent (**Fig. 2.7**). This activity of IRF6 may be beneficial in reducing damage to epithelial cells during an active immune response in the intestine. Like the IFN response, inflammasome activation thresholds need to be properly balanced within IECs to balance capacity for pathogen clearance with cytotoxicity, and our data indicates a role for IRF6 in regulating this response threshold as well (**Fig. 2.10C-D**).

Increased expression of epithelial development genes such as *Muc2* in *Irf6* KO organoids suggests that secretory progenitor development may be limited by *Irf6* (**Fig. 2.6I**). Single-cell RNAseq data supports this possibility, with increased expression of secretory IEC transcription factor *Atoh1* and reduced expression of Notch ligand *Jag1* in *Irf6* KO organoids (**Fig. 2.7**). Irf6 is expressed in all epithelial cells *in vivo* (**Fig. 2.6B**) but is likely to be regulated at the post-translational level by RIPK4, which was shown to activate Irf6 as well as Wnt signaling [298], [299]. Organoid culture conditions used in this study maintain cells in high Wnt, which favors maintenance of stem cells. So, future studies testing organoid phenotypes under differentiation culture conditions that remove Wnt will be of interest.

The large, growth-arrested M2C cells observed within *Irf6* KO M2C cell isolation, and the significant increase in apoptosis pathway genes, suggests that these cells are experiencing greater genotoxic stress at baseline than non-targeting control cells. The selection pressure of genomic stress may have resulted in variable adaptations between KO lines. Alternatively, distinct phenotypes may result from the site targeted by each gRNA. *Irf6* gRNA 2 targets a sequence downstream of the DBD-encoding region, and it is possible that there is leaky expression of the resulting DBD-only truncated protein isoform. Such a DBD-only isoform would be predicted to act in a dominant-negative manner, with potential impacts extending to other IRF family members. This distinction between gRNA target sites may explain why we were unable to recover a homozygous knockout with *Irf6* gRNA 2 in IEC organoids as well as the substantially increased number of DEGs in the M2C cell line targeted with this gRNA.

We selected *Irf6* for further study from our screen, but *Irf2* was also found to play a substantial role in regulating the IFN-stimulated antiviral response in IEC cell lines (**Figs. 2.2-2.3**). IRF2 has been shown to bind ISRE elements and block IFN responses [300]. Additional recent studies have implicated *Irf2* in IEC development, suggesting that it blocks IFN cytotoxicity of colonic stem cells [301] or restricts differentiation into secretory lineages [302]. It is intriguing to speculate that IRF6 and IRF2 may participate cooperatively or antagonistically in regulatory circuits related to IEC development and immunity. Enrichment analysis of *Irf2* KO stem cell data [302] suggests overlap in up-regulated genes following *Irf2* or *Irf6* KO (**Fig. 2.8I**), but no significant association between *Irf6*-dependant downregulated genes (**Fig. 2.8I**). It will be interesting to define interaction between IRFs and other post-translational regulatory mechanisms for IRF6 in IECs. Regulation of IRF6 dimerization and nuclear translocation have been studied in keratinocytes, but it remains to be determined whether distinct mechanisms are at play in IECs. Further definition of these and other aspects of IRF6 regulation may have wide-ranging implications for intestinal homeostasis, immunity, and disease.

Chapter 3: Discussion, impact, and future directions

Discussion

The research presented in this dissertation focuses on the discovery of the non-canonical role of Irf6 in regulating IFN responsiveness, differentiation of intestinal epithelial cells, and cell death. We sought to find non-canonical cell type specific regulatory factors to elucidate why IECs respond preferentially to type III IFNs instead of type I IFNs. To answer this question, we designed a CRISPR screen that involved the homologs within gene families of all the canonical IFN signaling factors. This includes all of the IRFs, JAK/Tyk2, Rel/NfκB, and STAT gene families. By treating the KO cells with IFN followed by MNV challenge, we were able to compare the IFN induced survival and viral protein inhibition between macrophages and IECs.

The results of our screens indicated that deletion of Irf6 caused an increase in type III IFN responsiveness in IEC but had no effect on IFN signaling in macrophages. Further investigation into the gene expression and phenotypes of Irf6 deletion in IECs presented a more complex role of Irf6 in the homeostasis, growth, differentiation, and cells death. Irf6 had primarily been studied in keratinocytes due to its role in the developmental diseases Van der Woude syndrome and popliteal pterygium syndrome, but no study had yet looked at its role in the intestinal epithelium. The novel discovery of Irf6's role in cell development and IFN signaling in the intestinal epithelium presented

in this dissertation is only the beginning and many future experiments are required to better understand its regulatory role.

Expression of Irf6 is very high in the intestinal epithelium (**Fig. 2.2A**), with levels being similar to the house keeping gene *Rps29*. Irf6 has previously been shown to be regulated by p63 in keratinocytes but p63 is not expressed in the IECs [237], [242], [243]. To investigate which genes regulate Irf6 expression, I would perform a genome-wide CRISPR screen, stain for Irf6 protein production, and flow sort the cells for loss or gain of Irf6 protein. Confirmation of candidate genes would be required. Over-expression and deletion of candidate genes, followed by qPCR or western blot analysis would confirm if the candidate genes were regulating the expression of Irf6 in IECs.

Previously, it has been shown that Irf6 activity is regulated at the protein level. This is common with IRFs to be regulated post translationally and require binding partners or homodimerization. Using immunoprecipitation pull downs and mass spec analysis I would find candidate genes for protein-protein interactions of Irf6 and compare the binding partners of Irf6 in IECs to binding partners in keratinocytes. Confirmation of these candidate genes would be done by developing tagged candidate proteins and performing immunoprecipitation experiments. Using catalytically dead or activated versions of the candidate proteins, I would investigate the phosphorylation patterns of Irf6 when co-expressed with the catalytic versions of the potential binding partners.

Irf6 is a transcription factor and has previously been shown to bind DNA regions. The DNA binding region of all IRFs is highly conserved but the ISRE element that IRFs bind to are abundantly found in the genome and the binding partners of IRFs allow for more specific binding of the genome to precisely regulate gene expression depending on cell type and situation. ChIP sequencing of Irf6 with and without its potential binding partners, with and without IFN stimulation would allow us to determine the binding sites within the genome and how these sites may change depending on the binding partners. To complicate these studies, it is possible that during differentiation of IECs the binding region and binding partners of Irf6 changes depending on cell subset. Determining the binding partners and binding regions in intestinal stem cells would give more insight into the mechanism involved in the loss of differentiation potential shown in our *Irf6* KO organoids (Fig. 2.6K-L).

Irf6 appears to have an inhibitory and inducive roles in the IECs. The Irf6 KOs were more responsive to interferons indicating that Irf6 is likely an inhibitor of IFN signaling (**Fig. 2.9**). Treatment with IFNs had higher cytotoxicity in the *Irf6* KO organoids which correlates with higher baseline apoptotic genes *Casp3* and *Pycard* (**Fig. 2.10**). *Irf6* may possibly directly inhibit the expression of *Casp3* and *Pycard* but their increased baseline expression could be a secondary effect of a different *Irf6* target gene. Additionally, we were able to identify Irf6 dependent ISGs (**Fig. 2.9B**). We do not know if Irf6 is directly activating the transcription of this subset of ISGs, but it is evidence of Irf6 having an inducive role during IFN signaling. This dual function of Irf6 is likely dependent on the binding partners and activated state of Irf6. Comparing the activation state and

binding partners of Irf6 at the beginning, peak, and inhibitory phases of type I and type III IFN signaling may allow us to identify new regulatory pathways of IFN signaling in IECs.

The expression of Irf6 appears to be important for stem cell maintenance and disrupting one or both alleles resulted in less differentiation potential (**Fig. 7I-L**). The Wnt and Notch signaling pathways play a major role in IEC differentiation. The Notch ligand *Jag1* has previously appeared on ChIP sequencing experiments for Irf6 and our *Irf6* KO organoids had less *Jag1* RNA transcripts [244]. Additionally, in keratinocytes Irf6 was shown to be a primary target of Notch signaling [281].

RIPK4 has been shown to activate Irf6 and RIPK4 is an important regulator of Wnt signaling [240], [270], [295], [299], [303]. To present a potential model for future experimentation I propose that Irf6 is an important regulatory factor of intestinal stem cells being regulated by both Wnt and Notch signaling. Notch signaling induces the expression of Irf6 and Wnt stimulation activates RIPK4 which activates Irf6. The target genes of Irf6 contribute to the maintenance of the stem cell state. One potential target of activated Irf6 is the Notch ligand Jagged1 generating a feedback loop involving Notch, Wnt, and Irf6. Deletion of *Irf6* likely disrupted Notch and Wnt signaling leading to a loss of differentiation potential of the KO organoids.

A preprint study investigating the role of glucose binding to transcription factors found that the binding regions of Irf6 change depending on the concentrations of glucose indicating that the glucose gradient in the epidermis modifies the transcriptional activity of Irf6 [304]. The implications of a glucose gradient on the roe of irf6 in the

intestinal epithelium is very interesting. When taken together with the differences in nutrient absorption gene expression shown through scRNAseq and laser capture RNA sequencing discussed in the introduction, the role of glucose regulated Irf6 binding patterns becomes very complicated [79]. Looking at the binding partners and binding regions of Irf6 between cell types, IFN treatments, and glucose concentrations is fascinating but will require many discovery and confirmation studies.

In light of the recent glucose binding preprint, I hypothesize that if there is a glucose gradient in the intestinal villi, it would be dependent on the presence of glucose transporters, which were shown to be most highly expressed in the middle of the villus [79]. The enterocytes specialized for glucose transport into the blood stream will either have the highest concentrations or the lowest concentrations of glucose in the cytoplasm. I think that the transport of glucose through these cells will occur so quickly that it would not have time to interact with Irf6, and these cells will behave more closely to a glucose-starved cell, driving further differentiation of the IECs as they travel towards the villi. The crypt-based stem cells would likely have the highest concentrations of glucose in the cytoplasm, similar to what is shown in the epidermis [304]. Expression of sodium/glucose cotransporter 1 (Slc5a1) decreases at the top of the villi where the IEC begin their subcellular shedding [79].

Near the tip of the villi where the cells begin their departure from the epithelium the role of Irf6 becomes especially interesting because we see the highest responsiveness to IFN-λ at the tip and the cells begin to die as well. Partial inhibition of Irf6 expression caused our organoids to become more responsive to IFN-λ (**Fig. 2.9**) and

more sensitive to cell death (**Fig. 2.10**). I hypothesize that Irf6 activity at the tip of the villi is partially responsible for the increased sensitivity to IFN-λ signaling and the cell death occurring. I further hypothesize that the role of Irf6 is changing, depending on the location of the cell within the villi. It may not be possible to test this *in vivo,* but organoid models with differing concentrations of glucose and at different stages of differentiation may allow us to look for binding partners and DNA-binding region changes for Irf6 under these different conditions.

The complexities of the differentiation pathways, zonal gene expression, and immunological context of the intestinal epithelium complicate the experiments required to determine what Irf6 is doing but give context for the requirement of a gene that can quickly respond to the changing environment.

The role of Irf6 in the development of IECs, responsiveness to IFNs, and cell death are likely linked (**Fig. 3.1**). Given that we saw differentiation occur when our organoids were treated with IFNs (**Fig. 6K-L**), and that we see an increase in cell death as IFN responsiveness reaches a tipping point (**Fig. 2.10A-B**), it would make sense that pathway Irf6 is regulating is involved in all these phenotypes.

Irf6 KO M2C cell line

Both of our CRISPR screens indicated that deletion of Irf6 resulted in increased interferon signaling in IECs but not in macrophages. With the individual KO cell

line screen, we saw an increase in IFN-stimulated survival following viral infection (**Fig. 2.2**). The increase in survival was more pronounced with IFN-λ stimulation than IFN-β, and this difference became more obvious when we compared the viability of the KO lines by IFN type (**Fig. 2.2 G-H**). The pooled FACS-based CRISPR screen indicated that there was a decrease in production of viral protein NS1/2 when Irf6 was deleted in the M2Cs as well. This decrease in viral protein production is a result of the IFN-β treatment, as shown by the FACS plots in **Figure 2.3B**. Our analysis of the pooled screen showed similar results to that we saw in the individual KO screen of **Figure 2.2**, increasing our confidence in the results of both CRISPR screens.

Unfortunately, the IFN-λ treatment did not decrease the viral protein production in the pooled CRISPR screen. When we did not see any decrease in viral protein production after IFN-λ treatment, we were surprised by this. One possible explanation of this could be that IFN-λ does not inhibit the spread of MNV by inhibiting the production of viral proteins. Further research on this topic is required to determine this mechanism, but the dosage used during the pooled screen was higher than the dose used in the survival screen which showed increased survival.

Despite our inability to confidently analyze the IFN-λ-treated cells in our pooled CRISPR screen, we decided to move forward with our top candidate gene Irf6. To our knowledge, no research project had yet been published on the role of Irf6 in the intestinal epithelium. The sequence of monoclonal isolates confirmed M2C Irf6 KO cell lines had shared and divergent phenotypes. Both Irf6 KO M2C lines showed a decreased

growth rate (**Fig 2.4D**) and the presence of large multi nucleated cells (**Fig 2.4C**). Irf6 KO 2 had a massive increase in IFN-λ induced MNV survival, but Irf6 KO1 had no difference when compared to the non-targeting control (**Fig 2.4E**). The RNA sequencing analysis of the Irf6 KO M2Cs indicated that both KOs shared disrupted growth and differentiation pathways consistent with our growth inhibition phenotype (**Fig. 2.5**). Only Irf6 KO2 had immune process GO pathways significantly enriched (**Fig. 2.5**). However, at baseline nearly 10% of the genome was differentially expressed in KO2.

When we analyzed the differences in ISG expression between the KOs and the NT controls we saw that all ISGs were more highly expressed in KO2 when treated with IFN-λ (**Fig. 2.5**). The overall increase in ISG expression and a slight increase in the IFNLR expression led us to hypothesize that the increased responsiveness to IFN-λ was a result of increased receptor expression. However, qPCR analysis did not confirm this increased transcription of IFNLR.

The divergent phenotypes observed between the two Irf6 KO M2C cell lines raised the question of whether this discrepancy was due to an experimental artifact or if it stemmed from the specific site where guide RNA 2 targeted Irf6. To address this uncertainty, we initiated the construction of an overexpression plasmid. However, we hesitated due to concerns that artificially elevating Irf6 levels might introduce its own phenotype. Consequently, we planned to create two variants: a full-length Irf6 construct and a partial one containing only the DNA-binding domain. This approach aimed to elucidate whether the observed differences in phenotype were linked to the absence of

the IRF association domain in KO2. Additionally, we considered employing the organoid model and generating CRISPR Irf6 KO organoids using the same guide RNAs as an alternative strategy. One challenge in studying Irf6 in the M2Cs was their low expression levels, but it was found that organoids and freshly isolated intestinal epithelial cells, as illustrated in **Fig. 2.6A**, exhibit much higher levels of Irf6 expression. The increased expression, more biological relevance, and higher sensitivity to IFN treatment made the organoid strategy the better option for confirmation of the Irf6 phenotypes we were seeing.

Irf6 KO organoids

Due to the divergence between the two Irf6 KO M2Cs we decided to look in a more biologically relevant model, the intestinal epithelial organoid. By removing the stem cells from the intestinal crypt, we can grow small intestinal epithelial organoids in a 3D matrix. This allows us to do experiments on primary IECs rather than the transformed M2C IEC cell line. I made the organoids from a mouse that had a GFP cassette with the promoter from the ISG *MX1*. The MX1-GFP expression allows us to monitor IFN stimulation by looking at GFP production. I deleted Irf6 in the organoids using the same guides I used in the M2C CRISPR screen and sequence confirmed monoclonal isolates. I was able to get a full knock out using guide 1 which cuts at the beginning of the DBD (**Fig. 2.6C**). For guide 2, I was only able to get a KO that only had one allele disrupted (**Fig. 2.6C**). Guide 2 cuts at the beginning of IAD domain. We decided to continue with our heterogenous KO of guide 2 because mutations that result in an early stop codon at

the beginning of the IAD region of Irf6 have been shown to cause VWS in humans. It is possible that a full knockout of Irf6 at the beginning of the IAD domain is lethal to the cell, and all the organoid isolates we screened had silenced their CRISPR expression before the second allele could be disrupted.

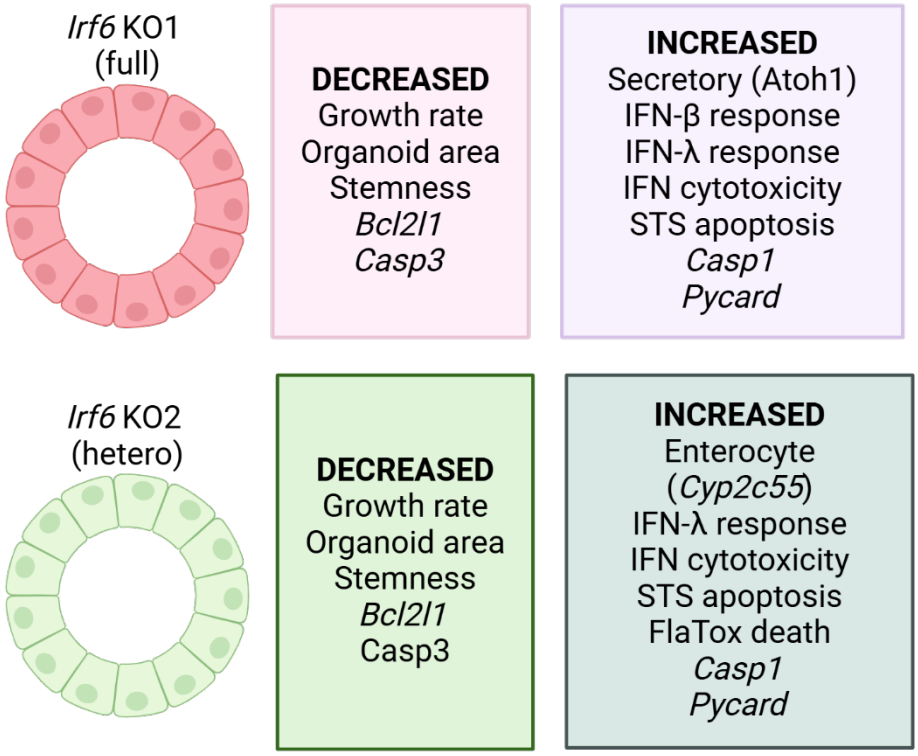

Figure 3.1 Summary of *Irf6* KO organoid phenotypes.

The two *Irf6* KO organoids differed in genotype with KO1 having an early stop codon occurring on both alleles and KO2 only having an early stop codon on a single allele. Most of the phenotypes observed were shared between the two different mutants. However, KO1 had secretory progenitors identified by the expression of *Atoh1* and KO2 had more enterocyte progenitors identified by *Cyp2c55* expression. Both KOs were more sensitive to IFN cytotoxicity and STS induced apoptosis, but only KO2 was more sensitive to Flatox. Image was created using BioRender.

While growing the Irf6 KO organoids, I quickly noticed that they were not getting as large, would appear darker, and fill up with dead cells (**Fig. 2.6 F-G**). The organoids

were growing slower (**Fig. 2.6H**), and would take up more P.I. (**Fig. 2.10F**). Unlike the large multinucleated cells seen in the M2C KOs, I noticed the Irf6 KO organoids were smaller when I would disrupt them and count them. I also noticed they were more difficult to disrupt, indicating that they may be stickier, which coincides with the increased epithelial cell adhesion molecule (*Epcam*) expression seen in the scRNAseq (**Fig. 2.7C**).

The intestinal epithelium is made up of several different types of epithelial cells, and one of the benefits of studying organoids is that they allow us to look for different cell types. We hypothesized that the slower growth rate may be an indication that the Irf6 KO organoids were less stem-like. When we looked for different cell type markers, we saw decreased expression of the stem cell marker *Lgr5*, and increased *Muc2,* which is a marker for goblet cells (**Fig. 2.6I**).

When we treated the organoids with IFNs, we saw increased expression of GFP by the Irf6 KO organoids compared to the non-targeting control, indicating that the organoids were more sensitive to IFN stimulation. However, Irf6 KO1 showed increased GFP expression when stimulated with both IFN-β and IFN-λ, but Irf6 KO2 only showed an increase in GFP expression when treated with IFN-λ (**Fig. 2.9D-E**). In addition to these differences, we saw a wider range in GFP expression indicating that there was a heterogenous response that may be dependent on differences in cell type population in the organoids.

To determine if the deletion of Irf6 was causing cell subpopulation differences we performed scRNAseq. The results from scRNAseq indicated that, although the Irf6 KO cells were less stem-like (**Fig. 2.7K**), there were not any fully differentiated cells in our organoids. The full Irf6 KO1 had an increased population of secretory progenitors expressing *Atoh1* and the heterogeneous Irf6 KO2 had an increased population of enterocyte progenitors expressing *Cyp2c55* (**Fig 2.7J**). These results indicate that Irf6 expression may play a role in determining if IEC stem cells become secretory or absorptive progenitors. One possible explanation for the increased *Atoh1* expression is the decreased expression of the Notch ligand Jag1 as the strength of Notch signaling has been shown to affect cell type lineages of TA cells. Jag1 has previous appeared on ChIP sequencing experiments of Irf6 [244].

Further differentiation experiments are required for proof of Irf6's role in differentiation. qPCR analysis of *Atoh1* in an organoid that has an inducible Irf6 would allow us to determine at which concentration of Irf6 the differentiation goes toward secretory or absorptive lineages. The expression of Irf6 does not change throughout the villi (**Fig. 2.6B**), but the activation of Irf6 might. The inducible model would allow us to finely tune Irf6 expression in an organoid, but after discovery of the Irf6 activation partners, further experiments controlling the activation of Irf6 would define the role of Irf6 in the differentiation of IECs.

Cell death

Interferons are pivotal in the immune response to viral pathogens. They inhibit viral replication, increase survival of cells challenged by viruses, and play a major role in activating the adaptive immune response. The three different types of IFNs have been shown to play specialized roles despite signaling through similar canonical pathways. Since the discovery of type III interferons, it has been shown that epithelial cells preferentially utilize type III IFN signaling during viral infection, but the cell type-specific mechanisms that regulate differential gene expression stimulated by type I and type III IFNs still requires further research.

One explanation for the utilization of type III IFNs by epithelial cells is that they exhibit less cytotoxicity. Since epithelial cells at barrier sites need to stay alive to maintain the barrier function, it makes sense that responses to a cytotoxic cytokine would be down-regulated. The differences of ISG expression elicited by type I and type III IFN in IECs has been investigated, but because IECs in adult mice don't respond to type I IFNs, we can only look ex *vivo*. When the IECs are removed from an adult mouse and grown as organoids, they regain their responsiveness to type I interferons, allowing us to look at the differences between type I and type III IFNs. In these organoid models, we see that type I IFNs are more cytotoxic (**Fig. 2.10**). When we disrupted Irf6 expression in these IEC organoids, we saw an increase in cytotoxicity from both type I and type III IFN stimulation. The two different types of IFNs showed similar levels of cytotoxicity in the Irf6 KO organoids.

We only see Irf6 expression in the epithelium in the intestine (**Fig. 2.6**), and it is possible that this cell type specific expression of Irf6 regulates the cytotoxicity of type III IFNs. Further investigation into the role of Irf6 in IECs during IFN signaling is required to determine this possibility. It is also possible the increased cytotoxicity we see in Irf6 KO organoids stimulated with IFNs may be a secondary phenotype to the primary role of Irf6 that we have yet to understand. To further investigate this, we would need to analyze the signaling that occurs in the Irf6 KO that leads to cell death. Utilizing flow cytometry and plate reader assays to investigate the type of cell death occurring, we could investigate the function role of Irf6 in a more specific manner. Interestingly, several papers have indicated that expression of Irf6 is important for apoptosis [227], [234], [305], [306]. During palatal fusion Irf6 expression is important for p21 dependent apoptosis by inhibiting the p21 inhibitor Δp63 [234]. However, the rs2205986 variant, previously linked to differential expression of IRF6, was linked to IFN-β-induced liver damage in multiple sclerosis patients receiving IFN treatment [307].

The previous experiments showed that Irf6 was regulating apoptosis at the protein level. Proteins Irf6 interact with to inhibit IFN-induced cytotoxicity in IECs could be investigated through co-immunoprecipitation pull down and mass spectrophotometry analysis. Follow-up analysis of IFN-stimulated cytotoxicity with knock-down of genes enriched in the mass-spec pull downs would allow us to map out the cell death pathways.

Our scRNAseq data indicated that deletion of Irf6 resulted in higher *Pycard* and *Casp1* expression (**Fig. 2.10**). It is possible that the increased expression of

inflammasome proteins before IFN stimulation leads to dysregulated inflammasome activation resulting in increased IFN-induced cytotoxicity. Mass-spec pull downs and chromatin immunoprecipitation sequencing would allow us to identify potential protein interactions and genome interactions that are responsible for the increased expression of *Pycard* and *Casp1*.

It is possible that the Irf6 KO organoids are more sensitive to death because of cellular stress. Previously it was shown that Irf6 regulates glycolysis and lipid metabolism [240], [250], [305]. Irf6 has been shown to regulate the glucose metabolism regulator Peroxisome proliferator-activated receptor gamma (PPARγ) through direct binding [308]. Investigations into a keratinocyte conditional Irf6 KO mouse showed dysregulated lipid metabolism [295]. Lipidomic and metabolomic analysis of Irf6 KO organoids may give insight into potential cellular stress that could correlate with the slowed growth rate (**Fig. 2.4**) and the increased cell death from IFNs, FlaTox, and STS (**Fig. 2.10**).

Interferon Signaling

The initial purpose of the project in this dissertation was to find non-canonical cell type specific signaling factors that determine IFN responsiveness in IECs. Our CRISPR screen indicated that deletion of Irf6 or Irf2 increased IFN responsiveness in IECs (**Fig. 2.2 and 2.3**). Irf2 has previously been shown to be inhibitory, but Irf6 has not [309]. Irf6 has been shown to promote IFN-β production in epithelial cells but the role of Irf6 in response to IFNs has not yet been investigated [246]. We hypothesized that Irf6 may be an inhibitor of IFN signaling in IECs as we were seeing increased responsiveness to IFNs

in our Irf6 KO cell lines and organoids. However, it is possible that baseline disruptions to the M2Cs and organoids led to increased sensitivity to the interferons as a secondary effect. It is likely though, that the presence of Irf6 in IECs is directly inhibiting the IFN responsiveness in IECs to dampen the cytotoxicity that IFNs are known to produce. This would be consistent with the increased cytotoxicity we see in the Irf6 KO organoids (**Fig. 2.10A-B**).

To further investigate the role of Irf6 during IFN signaling in a cell type specific manner we would need to directly compare Irf6 KOs in other cell types that are also responsive to IFN-λ. I would compare Irf6 KO IFN responsiveness between IECs, lung epithelium, liver, and keratinocytes. Transcriptional profiling of the different cell types would be informative as well.

The small number of Irf6-dependent ISGs we were able to find in our scRNAseq data (**Fig. 2.9B**) does not fully explain the increased responsiveness we see in our IRF6 KO organoids. This is likely due to the lack of depth we get from scRNAseq, and I would like to see the Irf6-dependent ISGs we get from bulk RNA sequencing at a much higher sequencing depth. I would hypothesize that Irf6 is directly binding to the genomic DNA, inhibiting the expression of ISGs in a competitive manner like what has been shown with Irf2. Essentially, as the concentrations of ISGF3 begin to wane, Irf6 would be able to compete for the ISRE binding regions turning all the ISG expression. To test this hypothesis, we can perform a competition assay with a known promoter region regulating a reporter gene. By putting the ISRE promoter region of Ifit1 before a GFP reporter gene, we could increase the dose of a Irf6 to monitor the expression of GFP in

the presence of the ISGF3 complex. If the GFP expression begins to go down past a certain concentration of Irf6 this would indicate it is competing for the binding region.

The role of Irf6 in inhibiting IFN signaling may also be a secondary result of an inhibitory gene that Irf6 promotes. To test this hypothesis ChIP sequencing analysis of Irf6 during different stages of the IFN response would be informative. The candidate gene list from the IFN dependent ChIP sequencing would allow us to determine if a known inhibitor of IFN signaling (e.g. SOCS1) is being regulated by Irf6. This would easily explain the increased responsiveness we see in out Irf6 KO organoids and a rescue experiment where we restore the expression of the inhibitory gene in Irf6 KOs should restore the wild type responsiveness to IFNs.

The making of an IEC conditional KO mouse is currently in process, and the IFN responsiveness in the intestines of these mice will be very interesting to see. It is possible that these Vil-Cre KO mice will not survive, and an inducible KO may be required to study Irf6 in the adult intestine. If the mice survive, I would first look at their responsiveness to IFN injection of IFN-λ and IFN-β. I would hypothesize that their intestinal epithelium is more responsive to IFNs and have increased cytotoxicity when treated with IFNs. I would also hypothesize that these conditional KO mice are more resistant to MNV infections because of the increased responsiveness to IFNs. IEC enriched RNA sequencing and scRNAseq analysis of the Irf6 conditional KO mice will be very informative regarding the IFN response and Irf6-dependent ISGs.

The Vil-Cre Irf6 KO mice will be very important for future experiments and determining the role Irf6 in the intestine. At homeostasis the loss of *Irf6* will likely result in dysregulated differentiation of IECs and potentially a complete loss of the stem cell niche. As previous research has connected Irf6, Wnt, and Notch in keratinocytes and the deletion of *Irf6* in keratinocytes causes dysregulated keratinocyte differentiation, the *Irf6* Vil-Cre KO mice will likely not develop intestines properly. However, heterozygous mice may give more insight into the role of Irf6 in the intestines as gene dosage clearly plays a major role in the function of Irf6. If this is the case looking at embryos during development may be the best option for analyzing the defects resulting for Irf6 ablation until an inducible KO mouse is generated. With an inducible Irf6 KO mouse, we would be able to monitor whether the stem cell niche is lost and identify the specific types of IECs into which all the stem cells differentiate.

It would also be informative to generate organoids from humans who have Van der Woude syndrome. With so much unknown the role of Irf6 in the intestinal epithelium, many of the basic characterization experiments still need to be done. It is exciting to see what future papers come out of the Nice lab investigating Irf6, and I cannot wait to see what the Vil-Cre KO mice teach us.

Closing remarks

Barrier immunity serves as our primary defense against invading pathogens, forming the defining boundary between self and the external world. Throughout my scientific journey, I've often pondered the rigid classification of organisms and the

intricate role of our microscopic companions in shaping our existence. Our barrier immunity is profoundly influenced by these "beneficial" microbes, yet we also contribute significantly to their sustenance. Despite the relentless assault of antimicrobial proteins, digestive enzymes, and a constant flow of mucus, commensal microorganisms persist in close proximity. Our immune responses, cognitive functions, and digestive processes are intricately intertwined with the microbial products surrounding us. However, the biochemical, physical, and immunological facets of barrier immunity tirelessly guard against microbial invasion, recognizing that not all microbes are benign, and even friendly ones may pose risks beyond the barrier. Thus, we have evolved a complex and redundant system to maintain the integrity of our internal environment and confine the external world to its rightful place. In the intricate ecosystem of the intestines, this defense mechanism becomes even more intricate. The ingestion of food and water introduces not only essential nutrients but also a plethora of potential threats, including pathogens, chemicals, toxins, and foreign objects. As a parent, raising a young child has heightened my awareness of the myriad of dangers that humans can unwittingly ingest, extending beyond the microscopic realm. Yet, despite our best efforts, we inevitably become nourishment for the very microbes we strive to repel, underscoring the remarkable efficacy of the immune system.

Chapter 4: Methods

Cell Culture

BV2 (macrophage) cells and HEK 293T cells (ATCC #CRL-3216) were maintained in DMEM (Gibco #11995065) with 5% fetal bovine serum (FBS), 1x penicillin/streptomycin/glutamine solution (Gibco #10378016), and 10 mM HEPES (HyClone #SH30237). M2C transformed colon epithelial cells [274] were maintained with Advanced DMEM/F12 blend (Gibco #12634010) supplemented with 10% FBS, 1x penicillin/streptomycin/glutamine solution, and 10 mM HEPES. All cells and organoids were lifted and disrupted using trypsin/EDTA (Gibco #2500).

Organoids were generated, as previously described [310], from the ileum of a female MX1-GFP mouse (B6.Cg-*Mx1*$^{tm1.1Agsa}$/J, Jackson Laboratory strain #033219). L-WRN cells (ATCC #CRL3276) were cultured for collection of conditioned supernatants containing Wnt3a, R spondin 3, and Noggin as previously described [310]. Organoid cultures were grown in Matrigel (Corning #354234) with 50% L-WRN conditioned media (CM) supplemented with 10 µm Y-27632 (MedChemExpress #HY10583) and 10 µm SB-431542 (MedChemExpress #HY10431).

Mice

Animal protocols were approved by the Institutional Animal Care and Use Committee at OHSU (protocol #IP00000228) in accordance with standards provided in the *Animal Welfare Act*. MX1-GFP mice (JAX stock #033219) were bred and maintained in specific pathogen-free facilities at Oregon Health & Science University (OHSU). C57BL6/J mice (JAX stock #000664) were purchased from Jackson Laboratories, and littermates were equally distributed among experimental groups with equal distribution of males and females. Adult mice were used at 7-10 weeks of age and injected intraperitoneally with 3 μg peg-IFN-λ (Bristol-Myers Squibb) or an equal volume of PBS vehicle as indicated in figure legends.

Lentiviral production and cell transduction.

Lentiviruses were produced from the following vectors: lentiCRISPRv2 hygro (Addgene #98291), pLenti CMV Blast empty (w263-1) (addgene #17486), and pCDH-MSCV CD300lf-T2A-GFP (gift from Dr. Craig Wilen). Insertion of gRNAs into the lentiCRISPRv2 hygro backbone was done as previously described [311]. CD300lf was cloned from a gene block (IDT) by amplifying with primers that included restriction site for XbaI and XhoI. Vector backbone and CD300lf amplicon were restriction digested following manufacturer's protocol. Fragments were gel purified and cloned using T4 DNA ligase. Chemically competent STBL3 *E. coli* was heat shock transformed with the ligated

constructs and plated on ampicillin plates for selection. The resulting plasmid sequence was confirmed by sanger sequencing.

To produce the lentiviral particles, 293T cells were plated at 500,000 cells per well in a 6-well plate with 600 ng psPAX2, 300 ng pVSVg, 1000 ng lentiviral vector, 100 µl of Optimem (Gibco #31985-062) and 6 µl of Transit-LT1 (Mirus #MIR2300). Two days after transfection lentivirus was harvested and mixed with equal parts fresh media before overlaying on top of target cell lines. For transduction, BV2 cells were seeded at 20,000 cells per well and M2C cells were seeded at 1e4 cells per well in a 6-well plate. Two days after transduction lentivirus was removed and antibiotic selection media was added. After confirming death of untransduced control cells, transduced cell lines were cryogenically frozen in nine parts FBS one-part DMSO.

Monoclonal cell lines were isolated by diluting polyclonal populations to 0.5 cells per 100 µl of media and 100 µl was plated in a 96-well plate. Wells were monitored for single cell colonies and CRISPR mutations were confirmed using NGS amplicon sequencing (Genewiz). Amplicons were PCR amplified for sequencing using Q5 polymerase with the corresponding primers. Analysis of NGS sequencing data was done using CRISPResso2 [312].

Lentiviruses for the pooled CRISPR screen were produced as described above with equal proportions of all CRISPR/gRNA plasmids added to the transfection mix and the twelve wells of transfected 293T cells. The pooled lentiviral prep was used to infect 1000 cells per gRNA, at an MOI=0.5, as empirically determined for M2C and BV2 cells.

Lentiviral transduction of organoids was done after trypsinization to liberate from Matrigel and separate into single cells. The single cells were resuspended in a 1:1 mixture of 50% CM and lentiviral supernatant. The bottom of a 24-well plate was coated with 80 µl of Matrigel and solidified. The Cell/lentiviral mixture was then overlayed on top of the layer of Matrigel. Lentivirus was removed after 24hrs and replaced with 50% CM. Organoids were cultured and expanded for one week after transduction to allow for accumulation of the resistance gene within clonal organoids. After one week of culture, antibiotics were added to select for the transduced organoids. During selection, the surviving organoids were expanded. Selection antibiotics were removed for two days after each expansion to favor recovery after disruption of organoids and plating. Monoclonal organoids were generated by pipetting a single organoid into a new well and expanding. Mutations to the gRNA target site were determined as for cell lines above.

Murine norovirus production, infection, and viability CRISPR screen

MNV was produced from molecular clones as previously described [276]. A chimeric strain CR6-VP1^{CW3} was used because it was shown to have the greatest lytic potential [275], increasing the dynamic range of the survival screen. M2C and BV2 cell lines were seeded at 10,000 or 5,000 cells per well, respectively, in 96-well flat bottom black plates. At the time of plating, cells were treated with the indicated dosage of IFN-β (PBL #12405-1) or IFN-λ3 (PBL #12820-1). 24hrs after plating, cells were challenged with murine norovirus strain CR6-VP1^{CW3} at a MOI of either 50 for M2C cells or 10 for BV2

cells. 24 hours after infection, cell viability was quantified using the ATP-Glo™ Bioluminometric Cell Viability Assay (Biotium #30020-2) on a CLARIOstar plate reader.

For each CRISPR ko cell group, we calculated % viability compared to untreated controls, and calculated "% protection" attributed to IFN pretreatments by subtracting the viability of untreated conditions from viability of paired IFN-treatment conditions. We initially observed significant variance in % viability between CRISPR-transduced M2C-CD300lf cell lines after MNV infection (no IFN) that was independent of the specific gene targeted. To limit potential confounding effects of baseline variance in MNV susceptibility and maximize the effect-size of IFN-treatment, we excluded poorly infected cells in which % viability following MNV infection was >50% in the absence of IFN pretreatment.

Infections for growth curves were performed on ice at an MOI = 5, followed by two washes with PBS, replacement of growth media, and freezing of plates at each time point. Plaque assays were performed using BV2 cells, essentially as previously described [276]. Briefly, BV2 cells were infected with serial dilutions of each well from thawed plates, consisting of combined cell and supernatant virions. After one hour incubation at room temperature, the inoculum was removed, and cells were overlaid with 1% methylcellulose in BV2 culture media and cultured for three days. Cells were fixed and stained with 20% ethanol and 0.1% crystal violet for visualization and enumeration of plaques.

Pooled CRISPR screen and FACS

Pooled populations of CRISPR cell lines were plated at 500,000 cells per 10 cm dish. After plating, BV2 cells were treated with 1 ng/ml IFN-β and M2C cells were treated with either 1 ng/ml IFN-β or 100 ng/ml IFN-λ. After 24hrs of IFN treatment, the cells were inoculated with MNV CR6-VP1^{CW3}. BV2 cells were challenged with an MOI=10 and M2C cells were challenged with an MOI=100. After 8hrs the cells were lifted using trypsin. All the media and PBS used to wash the cells were collected and combined with the lifted cells to ensure any cells that died during infection were included in the sorting. Cells were stained with Zombie Aqua™ Fixable Viability Kit (Biolegend # 423102) and Fc receptors were blocked using the CD16/32 antibody (Biolegend #101302) for 20min on ice. Cells were washed with PBS and fixed in 2% paraformaldehyde for 20min at room temperature (RT). Cells were washed with PBS and permeabilized in PBS with 0.2% Triton X-100, 3%FBS, 1% normal goat serum (perm/block) for 30min RT. Cells were stored in perm/block at 4 degrees until both replicates had been collected. Immediately before sorting, cells were stained with a MNV NS1/2 polyclonal rabbit antibody (generous gift of Dr. Vernon Ward) for 30 minutes at room temperature. After washing two times, cells were stained with a goat anti-rabbit IgG antibody conjugated to Alexa 647 (ThermoFisher #A21244) in perm/block for 30 minutes at room temperature. Cells were washed twice with PBS 0.2% Triton X-100 and resuspended in FACS buffer for sorting.

The top 10% of cells stained with NS1/2 for each sample were sorted on the BD InFlux cell sorter for sequencing. DNA extraction was done using the Quick-DNA FFPE Miniprep (Zymo #D3067). Genome counts were determined through qPCR of the CRISPR insert and PCR amplification of the gRNA insert was done on 2000 genomes per sample using Q5® Hot Start High-Fidelity DNA Polymerase (NEB # M0493) with P5 and P7 primers that included the Genewiz partial adapter sequence. Amplicons were purified with AMPure XP beads (Beckman Coulter # A63880) and submitted for amplicon sequencing (Genewiz). Analysis of gRNA sequences was done using MAGeCK [313], [314].

Bulk RNA sequencing and analysis

RNA was extracted using the Zymo Quick-DNA/RNA Viral 96 Kit (ZymoResearch #D7023) from three M2C cell lines and three treatment groups each in triplicate experimental replicates (27 total samples). Quality of RNA samples were assessed using a TapeStation (Agilent) and mRNA sequencing libraries were prepared by the OHSU Massively Parallel Sequencing Shared Resource (MPSSR) using the TruSeq Stranded Poly(A)+ Library Prep Kit (Illumina). Barcoded libraries were pooled, paired-end sequencing was performed using the Illumina NovaSeq platform, reads were trimmed of adaptors, and reads were demultiplexed. Adaptor-trimmed and demultiplexed reads were mapped to the mouse genome (GRCm39) using the STAR aligner [315], and mapping quality was evaluated using RSeQC [316] and MultiQC [317]. All samples had

between 16 million and 27 million uniquely mapped reads with similar distributions across genomic features and uniform gene body coverage. Read counts per gene were determined using the featureCounts program [318], and differential expression analysis was performed using DEseq2 [319], with each cell/treatment combination representing a different group in the study design (9 total comparison groups). PCA was performed on DEseq2 regularized logarithm (rlog)-transformed data. Heat maps were generated using either rlog-transformed raw counts or counts normalized to control samples ("Non-targeting" cells or "No IFN" treatment group), as indicated in figure legends. Heatmap clustering is based on Euclidean distance. Volcano plots were generated using the EnhancedVolcano program (https://github.com/kevinblighe/EnhancedVolcano).

Single-cell RNA sequencing

For some experimental groups, clonal lentiCRISPR-transduced organoid lines (non-targeting, *Irf6* KO1, *Irf6* KO2) were further transduced with CD300lf using pCDH-MSCV CD300lf-T2A-GFP and transduction methods described above (**Fig. 2.7A**, pools 3 and 4).

Each IEC organoid line was treated with 10 ng/mL IFN-β, 25 ng/mL IFN-λ, or media only. One group of replicate CD300lf-transduced organoids additionally received 9e5 PFU of MNV strain CR6-VP1^{CW3} at the same time as IFN treatments. 24 hours after treatments, single cells were prepared by incubation in trypsin/EDTA for 20 minutes, with pipetting every 5 minutes to disrupt organoids. The nine groups of cell lines (NT,

KO1, KO2) and treatment conditions (no IFN, IFN-β, IFN-λ) were incubated with separate oligonucleotide-tagged antibodies (HTO) for multiplexing (Biolegend TotalSeq, A0301 - A0309). Groups were counted and pooled in equal abundance, with four separate pools of cells: two groups without CD300lf transduction or MNV infection, a CD300lf-transduced group without MNV infection, and a CD300lf-transduced group with MNV infection (**Fig. 2.7A**). Pools were submitted to the OHSU Gene Profiling Shared Resource for preparation of 10x chromium next GEM 3' single cell gene expression v3 libraries and HTO libraries. Libraries from the four pools were prepared separately and sequenced on an Illumina NovaSeq by the OHSU MPSSR. Adaptor-trimmed and demultiplexed reads from the libraries of each pool were mapped with Cell Ranger Count v7.1.0 to the mouse genome (mm10-2020-A), with addition of MNV genome as a custom gene definition.

Gene counts from Cell Ranger were read into Seurat version 4.1.3 [320]. Each pool was filtered for cells with less-than 10% mitochondrial reads, greater than 1000 genes, and greater than 5000 counts. Gene counts were normalized and variable features identified within each pool using the default parameters. Pools were integrated using FindIntegrationAnchors and IntegrateData functions (50 dimensions). HTO data was normalized using centered log-ratio (CLR) transformation, and groups were de-multiplexed using the HTODemux function (positive.quantile = 0.999). 12,151 demultiplexed singlets were clustered by gene expression using the following functions: ScaleData, RunPCA, FindNeighbors (dims = 1:15), FindClusters (resolution = 1), and RunUMAP (dims = 1:15). One small cluster of 31 cells ("NT_d") was not considered further due to lower than average read counts. Experimental groups were identified by

HTO, and differentially expressed genes between groups were identified using DESeq2 [319] via the FindMarkers function. DEGs were defined as having a greater than 1.5 fold-change and adjusted p-value < 0.05. Marker genes for clusters were identified by Wilcoxon Rank Sum test using the FindAllMarkers function (min.pct = 0.25). Cell cycle phase was determined using the CellCycleScoring() function.

Quantitative PCR

RNA was extracted using the Zymo Quick-RNA Viral Kit (ZymoResearch #R1035). DNA contamination was removed using the Turbo DNAfree kit (ThermoFisher #AM1907). cDNA was generated with the ImPromII reverse transcription system (Promega #A3800). Quantitative PCR was performed using PerfeCTa qPCR FasMix II (QuantaBio #95119) and the pre-designed primer and probe assays from Integrated DNA Technologies (IDT). Absolute copy number was determined by comparing Ct values to a standard curve generated using DNA of known copy number encoding the target sequences. Samples are graphed as absolute copy number of the indicated target divided by the absolute copy number of the housekeeping gene, *Rps29*, with log-transformation and normalization as indicated in figure legends.

Western blot

Two days after plating, organoids were dissociated from Matrigel using trypsin/EDTA (Gibco #2500), washed with PBS, and lysed in RIPA buffer (NaCl 150mM, Tris-HCl 50mM [pH 8.0], sodium deoxycholate 0.5%, and SDS 0.1%) supplemented with cOmplete mini, EDTA-free protease inhibitor cocktail (Sigma #4693159001). Each sample was mixed with Bolt LDX buffer (ThermoFisher), Bolt reducing agent (ThermoFisher), and incubated at 70C for 10 min. Samples were run on a 12% Bis-Tris Bolt Mini protein gel (ThermoFisher) and transferred to a PVDF membrane using Bolt transfer buffer (ThermoFisher). IRF6 antibody (BioLegend #674502) was diluted 1:500 and the secondary antibody goat anti-mouse conjugated to horseradish peroxidase (ThermoFisher #62-6720) was diluted 1:5000.

Fluorescence *in situ* hybridization

FISH was performed using the Advanced Cell Diagnostics (Newark, CA) manual RNAscope assay following manufacturer protocol from FFPE tissue sections. Probes specific for *Mus musculus* genes *Irf6* (ACD, #462931) and *Ifit1* (ACD, #500071-C2) were purchased from Advanced Cell Diagnostics. Slides were counter-stained with DAPI and mounted with ProLong Gold antifade reagent (ThermoFisher). Fluorescent micrographs were captured using a Zeiss ApoTome2 on an Axio Imager, with a Zeiss AxioCam 506 (Zeiss) detector.

FlaTox inflammasome assay

Organoids were seeded into 5µL Matrigel domes in 96-well plates, at least 3 wells per treatment. After 2-3 days, organoids were treated with FlaTox (comprised of flagellin from *V. parahemolyticus* (16µg/mL) and protective antigen (1µg/mL)) and propidium iodide (1:100 dilution) in complete media. Absorbance was measured on a CLARIOstar plate reader each hour following treatment. Absorbance readings were first normalized to untreated controls (0%) and then normalized to maximum PI uptake in replicate wells for each organoid line treated with 1% Triton-X (100%).

Staurosporine apoptosis assay

Organoids were seeded 20,000 cells per 5µL Matrigel domes in 96-well plates, at least 3 wells per treatment. 48 hrs after seeding organoids were treated with 10µM staurosporine (Cell Signaling Technology) and propidium iodide in 50% L-WRN conditioned media supplemented with 10 µm Y-27632 and 10 µm SB-431542. Replicate wells were treated with propidium iodide only. Absorbance was measured on a CLARIOstar plate reader at 0 and 24 hours following treatments. Absorbance readings for each well were first normalized to their respective 0 hr timepoint values (0%) and then normalized to maximum PI uptake in replicate wells for each organoid line treated with 1% Triton-X (100%).

Statistical Analyses

Sample size estimation was performed based on historical data. Data were analyzed with Prism software (GraphPad Prism Software), with specified tests as noted in the figure legends.

Data availability

RNA sequencing data obtained in this study have been deposited in the NCBI gene expression omnibus (GEO) under series number GSE245972.

References

[1] G. K. Menon, G. W. Cleary, and M. E. Lane, “The structure and function of the stratum corneum,” *Int J Pharm*, vol. 435, no. 1, pp. 3–9, Oct. 2012, doi: 10.1016/j.ijpharm.2012.06.005.

[2] F. Niyonsaba, C. Kiatsurayanon, P. Chieosilapatham, and H. Ogawa, “Friends or Foes? Host defense (antimicrobial) peptides and proteins in human skin diseases,” *Exp Dermatol*, vol. 26, no. 11, pp. 989–998, Nov. 2017, doi: 10.1111/exd.13314.

[3] I. R. Scott, “Factors controlling the expressed activity of histidine ammonia-lyase in the epidermis and the resulting accumulation of urocanic acid,” *Biochemical Journal*, vol. 194, no. 3, pp. 829–838, Mar. 1981, doi: 10.1042/bj1940829.

[4] R. Bansil and B. S. Turner, “The biology of mucus: Composition, synthesis and organization,” *Adv Drug Deliv Rev*, vol. 124, pp. 3–15, Jan. 2018, doi: 10.1016/j.addr.2017.09.023.

[5] M. Faderl, M. Noti, N. Corazza, and C. Mueller, “Keeping bugs in check: The mucus layer as a critical component in maintaining intestinal homeostasis,” *IUBMB Life*, vol. 67, no. 4, pp. 275–285, Apr. 2015, doi: 10.1002/iub.1374.

[6] B. L. Kagan, M. E. Selsted, T. Ganz, and R. I. Lehrer, “Antimicrobial defensin peptides form voltage-dependent ion-permeable channels in planar lipid bilayer membranes.,” *Proceedings of the National Academy of Sciences*, vol. 87, no. 1, pp. 210–214, Jan. 1990, doi: 10.1073/pnas.87.1.210.

[7] R. I. Lehrer, A. Barton, K. A. Daher, S. S. Harwig, T. Ganz, and M. E. Selsted, "Interaction of human defensins with Escherichia coli. Mechanism of bactericidal activity.," *Journal of Clinical Investigation*, vol. 84, no. 2, pp. 553–561, Aug. 1989, doi: 10.1172/JCI114198.

[8] E. de Leeuw *et al.*, "Functional interaction of human neutrophil peptide-1 with the cell wall precursor lipid II," *FEBS Lett*, vol. 584, no. 8, pp. 1543–1548, Apr. 2010, doi: 10.1016/j.febslet.2010.03.004.

[9] C. Kim *et al.*, "Human α-defensins neutralize anthrax lethal toxin and protect against its fatal consequences," *Proceedings of the National Academy of Sciences*, vol. 102, no. 13, pp. 4830–4835, Mar. 2005, doi: 10.1073/pnas.0500508102.

[10] E. Leikina *et al.*, "Carbohydrate-binding molecules inhibit viral fusion and entry by crosslinking membrane glycoproteins," *Nat Immunol*, vol. 6, no. 10, pp. 995–1001, Oct. 2005, doi: 10.1038/ni1248.

[11] J. G. Smith and G. R. Nemerow, "Mechanism of Adenovirus Neutralization by Human α-Defensins," *Cell Host Microbe*, vol. 3, no. 1, pp. 11–19, Jan. 2008, doi: 10.1016/j.chom.2007.12.001.

[12] L. Antoni *et al.*, "Human colonic mucus is a reservoir for antimicrobial peptides," *J Crohns Colitis*, vol. 7, no. 12, pp. e652–e664, Dec. 2013, doi: 10.1016/j.crohns.2013.05.006.

[13] D. Xhindoli, S. Pacor, M. Benincasa, M. Scocchi, R. Gennaro, and A. Tossi, “The human cathelicidin LL-37 — A pore-forming antibacterial peptide and host-cell modulator,” *Biochimica et Biophysica Acta (BBA) - Biomembranes*, vol. 1858, no. 3, pp. 546–566, Mar. 2016, doi: 10.1016/j.bbamem.2015.11.003.

[14] K. A. Sochacki, K. J. Barns, R. Bucki, and J. C. Weisshaar, “Real-time attack on single *Escherichia coli* cells by the human antimicrobial peptide LL-37,” *Proceedings of the National Academy of Sciences*, vol. 108, no. 16, Apr. 2011, doi: 10.1073/pnas.1101130108.

[15] M. Demirci, A. Yigin, and C. Demir, “Efficacy of antimicrobial peptide LL-37 against biofilm forming Staphylococcus aureus strains obtained from chronic wound infections,” *Microb Pathog*, vol. 162, p. 105368, Jan. 2022, doi: 10.1016/j.micpath.2021.105368.

[16] S. Tripathi, T. Tecle, A. Verma, E. Crouch, M. White, and K. L. Hartshorn, “The human cathelicidin LL-37 inhibits influenza A viruses through a mechanism distinct from that of surfactant protein D or defensins,” *Journal of General Virology*, vol. 94, no. 1, pp. 40–49, Jan. 2013, doi: 10.1099/vir.0.045013-0.

[17] C. Ye *et al.*, “Cathelicidin CATH-B1 Inhibits Pseudorabies Virus Infection via Direct Interaction and TLR4/JNK/IRF3-Mediated Interferon Activation,” *J Virol*, vol. 97, no. 7, Jul. 2023, doi: 10.1128/jvi.00706-23.

[18] J. Yu *et al.*, “Cathelicidin antimicrobial peptides suppress EV71 infection via regulating antiviral response and inhibiting viral binding,” *Antiviral Res*, vol. 187, p. 105021, Mar. 2021, doi: 10.1016/j.antiviral.2021.105021.

[19] T. Takahashi, N. N. Kulkarni, E. Y. Lee, L. Zhang, G. C. L. Wong, and R. L. Gallo, “Cathelicidin promotes inflammation by enabling binding of self-RNA to cell surface scavenger receptors,” *Sci Rep*, vol. 8, no. 1, p. 4032, Mar. 2018, doi: 10.1038/s41598-018-22409-3.

[20] A. Fleming, V. D. Allison, and A. Fleming, “OBSERVATIONS ON A BACTERIOLYTIC SUBSTANCE (" LYSOZYME ") FOUND IN SECRETIONS AND TISSUES”.

[21] M. R. J. Salton, “THE PROPERTIES OF LYSOZYME AND ITS ACTION ON MICROORGANISMS,” *Bacteriol Rev*, vol. 21, no. 2, pp. 82–100, Jun. 1957, doi: 10.1128/br.21.2.82-100.1957.

[22] Z. Wei, S. Wu, J. Xia, P. Shao, P. Sun, and N. Xiang, “Enhanced Antibacterial Activity of Hen Egg-White Lysozyme against *Staphylococcus aureus* and *Escherichia coli* due to Protein Fibrillation,” *Biomacromolecules*, vol. 22, no. 2, pp. 890–897, Feb. 2021, doi: 10.1021/acs.biomac.0c01599.

[23] P. Markart, T. R. Korfhagen, T. E. Weaver, and H. T. Akinbi, “Mouse Lysozyme M Is Important in Pulmonary Host Defense against *Klebsiella pneumoniae* Infection,” *Am J Respir Crit Care Med*, vol. 169, no. 4, pp. 454–458, Feb. 2004, doi: 10.1164/rccm.200305-669OC.

[24] T. Ganz *et al.*, “Increased inflammation in lysozyme M–deficient mice in response to Micrococcus luteus and its peptidoglycan,” *Blood*, vol. 101, no. 6, pp. 2388–2392, Mar. 2003, doi: 10.1182/blood-2002-07-2319.

[25] T. Ganz, “Iron and infection,” *Int J Hematol*, vol. 107, no. 1, pp. 7–15, Jan. 2018, doi: 10.1007/s12185-017-2366-2.

[26] G. C. CHEESEMAN and D. J. JAYNE-WILLIAMS, “An inhibitory Substance present in Milk,” *Nature*, vol. 204, no. 4959, pp. 688–689, Nov. 1964, doi: 10.1038/204688a0.

[27] E. M. Redwan, V. N. Uversky, E. M. El-Fakharany, and H. Al-Mehdar, “Potential lactoferrin activity against pathogenic viruses,” *C R Biol*, vol. 337, no. 10, pp. 581–595, Oct. 2014, doi: 10.1016/j.crvi.2014.08.003.

[28] E. Bard *et al.*, “New Sensitive Method for the Measurement of Lysozyme and Lactoferrin for the Assessment of Innate Mucosal Immunity. Part I: Time-Resolved Immunofluorometric Assay in Serum and Mucosal Secretions,” *Clin Chem Lab Med*, vol. 41, no. 2, Jan. 2003, doi: 10.1515/CCLM.2003.021.

[29] M. E. Kelver, A. Kaul, B. Nowicki, W. E. Findley, T. W. Hutchens, and M. Nagamani, “Estrogen Regulation of Lactoferrin Expression in Human Endometrium,” *American Journal of Reproductive Immunology*, vol. 36, no. 5, pp. 243–247, Nov. 1996, doi: 10.1111/j.1600-0897.1996.tb00171.x.

[30] K. Clayton, A. F. Vallejo, J. Davies, S. Sirvent, and M. E. Polak, “Langerhans Cells—Programmed by the Epidermis,” *Front Immunol*, vol. 8, Nov. 2017, doi: 10.3389/fimmu.2017.01676.

[31] A. M. G. van der Aar *et al.*, “Langerhans Cells Favor Skin Flora Tolerance through Limited Presentation of Bacterial Antigens and Induction of Regulatory T Cells,” *Journal of Investigative Dermatology*, vol. 133, no. 5, pp. 1240–1249, May 2013, doi: 10.1038/jid.2012.500.

[32] J. Seneschal, R. A. Clark, A. Gehad, C. M. Baecher-Allan, and T. S. Kupper, “Human Epidermal Langerhans Cells Maintain Immune Homeostasis in Skin by Activating Skin Resident Regulatory T Cells,” *Immunity*, vol. 36, no. 5, pp. 873–884, May 2012, doi: 10.1016/j.immuni.2012.03.018.

[33] C. Hauser, “The Interaction between Langerhans Cells and CD4 $^{+}$ T Cells,” *J Dermatol*, vol. 19, no. 11, pp. 722–725, Nov. 1992, doi: 10.1111/j.1346-8138.1992.tb03768.x.

[34] C. L. Bennett *et al.*, “Langerhans cells regulate cutaneous injury by licensing CD8 effector cells recruited to the skin,” *Blood*, vol. 117, no. 26, pp. 7063–7069, Jun. 2011, doi: 10.1182/blood-2011-01-329185.

[35] M. Rescigno *et al.*, “Dendritic cells express tight junction proteins and penetrate gut epithelial monolayers to sample bacteria,” *Nat Immunol*, vol. 2, no. 4, pp. 361–367, Apr. 2001, doi: 10.1038/86373.

[36] A. Dillon and D. D. Lo, “M Cells: Intelligent Engineering of Mucosal Immune Surveillance,” *Front Immunol*, vol. 10, Jul. 2019, doi: 10.3389/fimmu.2019.01499.

[37] I. R. Williams and R. L. Owen, “M Cells,” in *Mucosal Immunology*, Elsevier, 2015, pp. 211–229. doi: 10.1016/B978-0-12-415847-4.00013-6.

[38] N. Y. Lycke and M. Bemark, “The role of Peyer’s patches in synchronizing gut IgA responses,” *Front Immunol*, vol. 3, 2012, doi: 10.3389/fimmu.2012.00329.

[39] S. W. Craig and J. J. Cebra, “PEYER’S PATCHES: AN ENRICHED SOURCE OF PRECURSORS FOR I <scp>G</scp> A-PRODUCING IMMUNOCYTES IN THE RABBIT,” *J Exp Med*, vol. 134, no. 1, pp. 188–200, Jul. 1971, doi: 10.1084/jem.134.1.188.

[40] Tomio. Okada, Hiroaki. Konishi, Masafumi. Ito, Hiroshi. Nagura, and Junpei. Asai, “Identification of Secretory Immunoglobulin A in Human Sweat and Sweat Glands,” *Journal of Investigative Dermatology*, vol. 90, no. 5, pp. 648–651, May 1988, doi: 10.1111/1523-1747.ep12560807.

[41] D. Metze, W. Jurecka, W. Gebhart, J. Schmidt, M. Mainitz, and G. Niebauer, “Immunohistochemical Demonstration of Immunoglobulin A in Human Sebaceous and Sweat Glands,” *Journal of Investigative Dermatology*, vol. 92, no. 1, pp. 13–17, Jan. 1989, doi: 10.1111/1523-1747.ep13070402.

[42] A. Reboldi, T. I. Arnon, L. B. Rodda, A. Atakilit, D. Sheppard, and J. G. Cyster, “IgA production requires B cell interaction with subepithelial dendritic cells in Peyer’s

patches," *Science (1979)*, vol. 352, no. 6287, May 2016, doi: 10.1126/science.aaf4822.

[43] H. Wei and J.-Y. Wang, "Role of Polymeric Immunoglobulin Receptor in IgA and IgM Transcytosis," *Int J Mol Sci*, vol. 22, no. 5, p. 2284, Feb. 2021, doi: 10.3390/ijms22052284.

[44] H. L. Dupont, Z.-D. Jiang, A. W. Dupont, and N. S. Utay, "THE INTESTINAL MICROBIOME IN HUMAN HEALTH AND DISEASE.," *Trans Am Clin Climatol Assoc*, vol. 131, pp. 178–197, 2020.

[45] J. M. Sasso *et al.*, "Gut Microbiome–Brain Alliance: A Landscape View into Mental and Gastrointestinal Health and Disorders," *ACS Chem Neurosci*, vol. 14, no. 10, pp. 1717–1763, May 2023, doi: 10.1021/acschemneuro.3c00127.

[46] Y. Zeng and J. Q. Liang, "Nasal Microbiome and Its Interaction with the Host in Childhood Asthma," *Cells*, vol. 11, no. 19, p. 3155, Oct. 2022, doi: 10.3390/cells11193155.

[47] B. Zhu, Z. Tao, L. Edupuganti, M. G. Serrano, and G. A. Buck, "Roles of the Microbiota of the Female Reproductive Tract in Gynecological and Reproductive Health," *Microbiology and Molecular Biology Reviews*, vol. 86, no. 4, Dec. 2022, doi: 10.1128/mmbr.00181-21.

[48] R. L. Marsh *et al.*, "Recent advances in understanding the natural history of the otitis media microbiome and its response to environmental pressures," *Int J*

Pediatr Otorhinolaryngol, vol. 130, p. 109836, Mar. 2020, doi: 10.1016/j.ijporl.2019.109836.

[49] C. Milani *et al.*, "The First Microbial Colonizers of the Human Gut: Composition, Activities, and Health Implications of the Infant Gut Microbiota," *Microbiology and Molecular Biology Reviews*, vol. 81, no. 4, Dec. 2017, doi: 10.1128/MMBR.00036-17.

[50] D. Zheng, T. Liwinski, and E. Elinav, "Interaction between microbiota and immunity in health and disease," *Cell Res*, vol. 30, no. 6, pp. 492–506, Jun. 2020, doi: 10.1038/s41422-020-0332-7.

[51] F. Petrillo *et al.*, "Current Evidence on the Ocular Surface Microbiota and Related Diseases," *Microorganisms*, vol. 8, no. 7, p. 1033, Jul. 2020, doi: 10.3390/microorganisms8071033.

[52] E. Rath and D. Haller, "Intestinal epithelial cell metabolism at the interface of microbial dysbiosis and tissue injury," *Mucosal Immunol*, vol. 15, no. 4, pp. 595–604, Apr. 2022, doi: 10.1038/s41385-022-00514-x.

[53] A. G. Solis, M. Klapholz, J. Zhao, and M. Levy, "The bidirectional nature of microbiome-epithelial cell interactions," *Curr Opin Microbiol*, vol. 56, pp. 45–51, Aug. 2020, doi: 10.1016/j.mib.2020.06.007.

[54] I. Bourdeau-Julien *et al.*, “The diet rapidly and differentially affects the gut microbiota and host lipid mediators in a healthy population,” *Microbiome*, vol. 11, no. 1, p. 26, Feb. 2023, doi: 10.1186/s40168-023-01469-2.

[55] Howard. H. Chauncey, “Salivary enzymes,” *The Journal of the American Dental Association*, vol. 63, no. 3, pp. 360–368, Sep. 1961, doi: 10.14219/jada.archive.1961.0215.

[56] C. Peyrot des Gachons and P. A. S. Breslin, “Salivary Amylase: Digestion and Metabolic Syndrome,” *Curr Diab Rep*, vol. 16, no. 10, p. 102, Oct. 2016, doi: 10.1007/s11892-016-0794-7.

[57] J. J. Zakowski and D. E. Bruns, “Biochemistry of Human Alpha Amylase Isoenzymes,” *CRC Crit Rev Clin Lab Sci*, vol. 21, no. 4, pp. 283–322, Jan. 1985, doi: 10.3109/10408368509165786.

[58] P. J. Keller and B. J. Allan, “The protein composition of human pancreatic juice.,” *Journal of Biological Chemistry*, vol. 242, no. 2, pp. 281–287, Jan. 1967, doi: 10.1016/s0021-9258(19)81461-8.

[59] H. Brockerhoff, “On the function of bile salts and proteins as cofactors of lipase.,” *Journal of Biological Chemistry*, vol. 246, no. 18, pp. 5828–5831, Sep. 1971, doi: 10.1016/s0021-9258(18)61880-0.

[60] B. Borgström, “On the interactions between pancreatic lipase and colipase and the substrate, and the importance of bile salts.,” *J Lipid Res*, vol. 16, no. 6, pp. 411–7, Nov. 1975.

[61] K. Schneeberger, S. Roth, E. E. S. Nieuwenhuis, and S. Middendorp, “Intestinal epithelial cell polarity defects in disease: lessons from microvillus inclusion disease,” *Dis Model Mech*, vol. 11, no. 2, Feb. 2018, doi: 10.1242/dmm.031088.

[62] L. J. Klunder, K. N. Faber, G. Dijkstra, and S. C. D. van IJzendoorn, “Mechanisms of Cell Polarity–Controlled Epithelial Homeostasis and Immunity in the Intestine,” *Cold Spring Harb Perspect Biol*, vol. 9, no. 7, p. a027888, Jul. 2017, doi: 10.1101/cshperspect.a027888.

[63] A. Fatehullah, P. L. Appleton, and I. S. Näthke, “Cell and tissue polarity in the intestinal tract during tumourigenesis: cells still know the right way up, but tissue organization is lost,” *Philosophical Transactions of the Royal Society B: Biological Sciences*, vol. 368, no. 1629, p. 20130014, Nov. 2013, doi: 10.1098/rstb.2013.0014.

[64] A. W. Overeem, C. Posovszky, E. H. M. M. Rings, B. N. G. Giepmans, and S. C. D. van IJzendoorn, “The role of enterocyte defects in the pathogenesis of congenital diarrheal disorders,” *Dis Model Mech*, vol. 9, no. 1, pp. 1–12, Jan. 2016, doi: 10.1242/dmm.022269.

[65] B.-K. Koo *et al.*, “Tumour suppressor RNF43 is a stem-cell E3 ligase that induces endocytosis of Wnt receptors,” *Nature*, vol. 488, no. 7413, pp. 665–669, Aug. 2012, doi: 10.1038/nature11308.

[66] H.-X. Hao *et al.*, “ZNRF3 promotes Wnt receptor turnover in an R-spondin-sensitive manner,” *Nature*, vol. 485, no. 7397, pp. 195–200, May 2012, doi: 10.1038/nature11019.

[67] N. Barker *et al.*, “Identification of stem cells in small intestine and colon by marker gene Lgr5,” *Nature*, vol. 449, no. 7165, pp. 1003–1007, Oct. 2007, doi: 10.1038/nature06196.

[68] R. Aoki *et al.*, “Foxl1-expressing mesenchymal cells constitute the intestinal stem cell niche.,” *Cell Mol Gastroenterol Hepatol*, vol. 2, no. 2, pp. 175–188, Feb. 2016, doi: 10.1016/j.jcmgh.2015.12.004.

[69] X. Yin, H. F. Farin, J. H. van Es, H. Clevers, R. Langer, and J. M. Karp, “Niche-independent high-purity cultures of Lgr5+ intestinal stem cells and their progeny,” *Nat Methods*, vol. 11, no. 1, pp. 106–112, Jan. 2014, doi: 10.1038/nmeth.2737.

[70] M. Yousefi, L. Li, and C. J. Lengner, “Hierarchy and Plasticity in the Intestinal Stem Cell Compartment,” *Trends in Cell Biology*, vol. 27, no. 10. Elsevier Ltd, pp. 753–764, Oct. 01, 2017. doi: 10.1016/j.tcb.2017.06.006.

[71] P. H. Vachon, “Integrin Signaling, Cell Survival, and Anoikis: Distinctions, Differences, and Differentiation,” *J Signal Transduct*, vol. 2011, pp. 1–18, Jul. 2011, doi: 10.1155/2011/738137.

[72] A. S. Darwich, U. Aslam, D. M. Ashcroft, and A. Rostami-Hodjegan, “Meta-Analysis of the Turnover of Intestinal Epithelia in Preclinical Animal Species and Humans,” *Drug Metabolism and Disposition*, vol. 42, no. 12, pp. 2016–2022, Dec. 2014, doi: 10.1124/dmd.114.058404.

[73] J. Maury, C. Nicoletti, L. Guzzo-Chambraud, and S. Maroux, “The Filamentous Brush Border Glycocalyx, a Mucin-like Marker of Enterocyte Hyper-Polarization,” *Eur J Biochem*, vol. 228, no. 2, pp. 323–331, Mar. 1995, doi: 10.1111/j.1432-1033.1995.0323n.x.

[74] S. H. Lee, “Intestinal Permeability Regulation by Tight Junction: Implication on Inflammatory Bowel Diseases,” *Intest Res*, vol. 13, no. 1, p. 11, 2015, doi: 10.5217/ir.2015.13.1.11.

[75] L. Shen, C. R. Weber, D. R. Raleigh, D. Yu, and J. R. Turner, “Tight Junction Pore and Leak Pathways: A Dynamic Duo,” *Annu Rev Physiol*, vol. 73, no. 1, pp. 283–309, Mar. 2011, doi: 10.1146/annurev-physiol-012110-142150.

[76] B. N. G. Giepmans and S. C. D. van IJzendoorn, “Epithelial cell–cell junctions and plasma membrane domains,” *Biochimica et Biophysica Acta (BBA) - Biomembranes*, vol. 1788, no. 4, pp. 820–831, Apr. 2009, doi: 10.1016/j.bbamem.2008.07.015.

[77] M. G. Farquhar and G. E. Palade, “JUNCTIONAL COMPLEXES IN VARIOUS EPITHELIA,” *J Cell Biol*, vol. 17, no. 2, pp. 375–412, May 1963, doi: 10.1083/jcb.17.2.375.

[78] L. Borradori and A. Sonnenberg, “Structure and Function of Hemidesmosomes: More Than Simple Adhesion Complexes,” *Journal of Investigative Dermatology*, vol. 112, no. 4, pp. 411–418, Apr. 1999, doi: 10.1046/j.1523-1747.1999.00546.x.

[79] A. E. Moor *et al.*, “Spatial Reconstruction of Single Enterocytes Uncovers Broad Zonation along the Intestinal Villus Axis,” *Cell*, vol. 175, no. 4, pp. 1156-1167.e15, Nov. 2018, doi: 10.1016/j.cell.2018.08.063.

[80] J. Qu, C.-W. Ko, P. Tso, and A. Bhargava, “Apolipoprotein A-IV: A Multifunctional Protein Involved in Protection against Atherosclerosis and Diabetes,” *Cells*, vol. 8, no. 4, p. 319, Apr. 2019, doi: 10.3390/cells8040319.

[81] S. Ghoshal, J. Witta, J. Zhong, W. de Villiers, and E. Eckhardt, “Chylomicrons promote intestinal absorption of lipopolysaccharides,” *J Lipid Res*, vol. 50, no. 1, pp. 90–97, Jan. 2009, doi: 10.1194/jlr.M800156-JLR200.

[82] Y. Akiba *et al.*, “Lipopolysaccharides transport during fat absorption in rodent small intestine,” *American Journal of Physiology-Gastrointestinal and Liver Physiology*, vol. 318, no. 6, pp. G1070–G1087, Jun. 2020, doi: 10.1152/ajpgi.00079.2020.

[83] A. C. E. Vreugdenhil, C. H. Rousseau, T. Hartung, J. W. M. Greve, C. van ‘t Veer, and W. A. Buurman, “Lipopolysaccharide (LPS)-Binding Protein Mediates LPS Detoxification by Chylomicrons,” *The Journal of Immunology*, vol. 170, no. 3, pp. 1399–1405, Feb. 2003, doi: 10.4049/jimmunol.170.3.1399.

[84] V. Snoeck, B. Goddeeris, and E. Cox, “The role of enterocytes in the intestinal barrier function and antigen uptake,” *Microbes Infect*, vol. 7, no. 7–8, pp. 997–1004, Jun. 2005, doi: 10.1016/j.micinf.2005.04.003.

[85] A. Monaco, B. Ovryn, J. Axis, and K. Amsler, “The Epithelial Cell Leak Pathway,” *Int J Mol Sci*, vol. 22, no. 14, p. 7677, Jul. 2021, doi: 10.3390/ijms22147677.

[86] R. L. Owen and A. L. Jones, “Epithelial Cell Specialization within Human Peyer’s Patches: An Ultrastructural Study of Intestinal Lymphoid Follicles,” *Gastroenterology*, vol. 66, no. 2, pp. 189–203, Feb. 1974, doi: 10.1016/S0016-5085(74)80102-2.

[87] K. Nagashima *et al.*, “Targeted deletion of RANKL in M cell inducer cells by the Col6a1-Cre driver,” *Biochem Biophys Res Commun*, vol. 493, no. 1, pp. 437–443, Nov. 2017, doi: 10.1016/j.bbrc.2017.09.004.

[88] I. N. Farstad, T. S. Halstensen, O. Fausa, and P. Brandtzaeg, “Heterogeneity of M-cell-associated B and T cells in human Peyer’s patches.,” *Immunology*, vol. 83, no. 3, pp. 457–64, Nov. 1994.

[89] T. V. Golovkina, M. Shlomchik, L. Hannum, and A. Chervonsky, “Organogenic Role of B Lymphocytes in Mucosal Immunity,” *Science (1979)*, vol. 286, no. 5446, pp. 1965–1968, Dec. 1999, doi: 10.1126/science.286.5446.1965.

[90] A. Iwasaki and B. L. Kelsall, “Unique Functions of CD11b+, CD8α+, and Double-Negative Peyer’s Patch Dendritic Cells,” *The Journal of Immunology*, vol. 166, no. 8, pp. 4884–4890, Apr. 2001, doi: 10.4049/jimmunol.166.8.4884.

[91] J. Rey, N. Garin, F. Spertini, and B. Corthésy, “Targeting of Secretory IgA to Peyer’s Patch Dendritic and T Cells after Transport by Intestinal M Cells,” *The Journal of Immunology*, vol. 172, no. 5, pp. 3026–3033, Mar. 2004, doi: 10.4049/jimmunol.172.5.3026.

[92] D. Rios, M. B. Wood, J. Li, B. Chassaing, A. T. Gewirtz, and I. R. Williams, “Antigen sampling by intestinal M cells is the principal pathway initiating mucosal IgA production to commensal enteric bacteria,” *Mucosal Immunol*, vol. 9, no. 4, pp. 907–916, Jul. 2016, doi: 10.1038/mi.2015.121.

[93] P. Andreu *et al.*, “A genetic study of the role of the Wnt/β-catenin signalling in Paneth cell differentiation,” *Dev Biol*, vol. 324, no. 2, pp. 288–296, Dec. 2008, doi: 10.1016/j.ydbio.2008.09.027.

[94] J. H. van Es *et al.*, “Wnt signalling induces maturation of Paneth cells in intestinal crypts,” *Nat Cell Biol*, vol. 7, no. 4, pp. 381–386, Apr. 2005, doi: 10.1038/ncb1240.

[95] X. Yin, H. F. Farin, J. H. van Es, H. Clevers, R. Langer, and J. M. Karp, “Niche-independent high-purity cultures of Lgr5+ intestinal stem cells and their progeny,” *Nat Methods*, vol. 11, no. 1, pp. 106–112, Jan. 2014, doi: 10.1038/nmeth.2737.

[96] A. Durand *et al.*, “Functional intestinal stem cells after Paneth cell ablation induced by the loss of transcription factor Math1 (Atoh1),” *Proceedings of the National Academy of Sciences*, vol. 109, no. 23, pp. 8965–8970, Jun. 2012, doi: 10.1073/pnas.1201652109.

[97] Y. Mori–Akiyama *et al.*, “SOX9 Is Required for the Differentiation of Paneth Cells in the Intestinal Epithelium,” *Gastroenterology*, vol. 133, no. 2, pp. 539–546, Aug. 2007, doi: 10.1053/j.gastro.2007.05.020.

[98] T. Ayabe *et al.*, “Activation of Paneth Cell α-Defensins in Mouse Small Intestine,” *Journal of Biological Chemistry*, vol. 277, no. 7, pp. 5219–5228, Feb. 2002, doi: 10.1074/jbc.M109410200.

[99] Q.-J. Tang *et al.*, “Expression of Polymeric Immunoglobulin Receptor mRNA and Protein in Human Paneth Cells: Paneth Cells Participate in Acquired Immunity,” *Am J Gastroenterol*, vol. 101, no. 7, pp. 1625–1632, Jul. 2006, doi: 10.1111/j.1572-0241.2006.00605.x.

[100] T. Peeters and G. Vantrappen, “The Paneth cell: A source of intestinal lysozyme’,” 1975.

[101] P. Cray, B. J. Sheahan, and C. M. Dekaney, “Secretory Sorcery: Paneth Cell Control of Intestinal Repair and Homeostasis,” *Cell Mol Gastroenterol Hepatol*, vol. 12, no. 4, pp. 1239–1250, 2021, doi: 10.1016/j.jcmgh.2021.06.006.

[102] H. Schneider, T. Pelaseyed, F. Svensson, and M. E. V. Johansson, “Study of mucin turnover in the small intestine by in vivo labeling,” *Sci Rep*, vol. 8, no. 1, p. 5760, Apr. 2018, doi: 10.1038/s41598-018-24148-x.

[103] A. Macierzanka, A. R. Mackie, and L. Krupa, “Permeability of the small intestinal mucus for physiologically relevant studies: Impact of mucus location and ex vivo treatment,” *Sci Rep*, vol. 9, no. 1, p. 17516, Nov. 2019, doi: 10.1038/s41598-019-53933-5.

[104] J. K. Gustafsson and M. E. V. Johansson, “The role of goblet cells and mucus in intestinal homeostasis,” *Nat Rev Gastroenterol Hepatol*, vol. 19, no. 12, pp. 785–803, Dec. 2022, doi: 10.1038/s41575-022-00675-x.

[105] M. R. Howitt *et al.*, “Tuft cells, taste-chemosensory cells, orchestrate parasite type 2 immunity in the gut,” *Science (1979)*, vol. 351, no. 6279, pp. 1329–1333, Mar. 2016, doi: 10.1126/science.aaf1648.

[106] B. Schütz *et al.*, “Distribution pattern and molecular signature of cholinergic tuft cells in human gastro-intestinal and pancreatic-biliary tract,” *Sci Rep*, vol. 9, no. 1, p. 17466, Nov. 2019, doi: 10.1038/s41598-019-53997-3.

[107] F. Gerbe *et al.*, “Distinct ATOH1 and Neurog3 requirements define tuft cells as a new secretory cell type in the intestinal epithelium,” *Journal of Cell Biology*, vol. 192, no. 5, pp. 767–780, Mar. 2011, doi: 10.1083/jcb.201010127.

[108] J. Beumer, H. Gehart, and H. Clevers, “Enteroendocrine Dynamics – New Tools Reveal Hormonal Plasticity in the Gut,” *Endocr Rev*, vol. 41, no. 5, Oct. 2020, doi: 10.1210/endrev/bnaa018.

[109] S. Afroze *et al.*, “The physiological roles of secretin and its receptor.,” *Ann Transl Med*, vol. 1, no. 3, p. 29, Oct. 2013, doi: 10.3978/j.issn.2305-5839.2012.12.01.

[110] M. Jenny *et al.*, “Neurogenin3 is differentially required for endocrine cell fate specification in the intestinal and gastric epithelium,” *EMBO J*, vol. 21, no. 23, pp. 6338–6347, Dec. 2002, doi: 10.1093/emboj/cdf649.

[111] L. López-Díaz *et al.*, “Intestinal Neurogenin 3 directs differentiation of a bipotential secretory progenitor to endocrine cell rather than goblet cell fate,” *Dev Biol*, vol. 309, no. 2, pp. 298–305, Sep. 2007, doi: 10.1016/j.ydbio.2007.07.015.

[112] X. Zhang *et al.*, “Global Burden and Trends of Norovirus-Associated Diseases From 1990 to 2019: An Observational Trend Study,” *Front Public Health*, vol. 10, Jun. 2022, doi: 10.3389/fpubh.2022.905172.

[113] S. Ghosh *et al.*, “Enteric viruses replicate in salivary glands and infect through saliva,” *Nature*, vol. 607, no. 7918, pp. 345–350, Jul. 2022, doi: 10.1038/s41586-022-04895-8.

[114] V. Costantini *et al.*, “Human Norovirus Replication in Human Intestinal Enteroids as Model to Evaluate Virus Inactivation.,” *Emerg Infect Dis*, vol. 24, no. 8, pp. 1453–1464, Aug. 2018, doi: 10.3201/eid2408.180126.

[115] D. Zhang, M. Tan, W. Zhong, M. Xia, P. Huang, and X. Jiang, “Human intestinal organoids express histo-blood group antigens, bind norovirus VLPs, and support limited norovirus replication,” *Sci Rep*, vol. 7, no. 1, p. 12621, Oct. 2017, doi: 10.1038/s41598-017-12736-2.

[116] C. Mirabelli *et al.*, “Human Norovirus Efficiently Replicates in Differentiated 3D-Human Intestinal Enteroids,” *J Virol*, vol. 96, no. 22, Nov. 2022, doi: 10.1128/jvi.00855-22.

[117] K. Ettayebi *et al.*, “Replication of human noroviruses in stem cell-derived human enteroids.,” *Science*, vol. 353, no. 6306, pp. 1387–1393, Sep. 2016, doi: 10.1126/science.aaf5211.

[118] J. Vinjé *et al.*, “ICTV Virus Taxonomy Profile: Caliciviridae,” *Journal of General Virology*, vol. 100, pp. 1469–1470, 2019.

[119] N. Winder, S. Gohar, and M. Muthana, “Norovirus: An Overview of Virology and Preventative Measures,” *Viruses*, vol. 14, no. 12, p. 2811, Dec. 2022, doi: 10.3390/v14122811.

[120] X. Jiang, M. Wang, K. Wang, and M. K. Estes, “Sequence and Genomic Organization of Norwalk Virus,” *Virology*, vol. 195, no. 1, pp. 51–61, Jul. 1993, doi: 10.1006/viro.1993.1345.

[121] N. McFadden *et al.*, “Norovirus Regulation of the Innate Immune Response and Apoptosis Occurs via the Product of the Alternative Open Reading Frame 4,” *PLoS Pathog*, vol. 7, no. 12, p. e1002413, Dec. 2011, doi: 10.1371/journal.ppat.1002413.

[122] T. J. Nice, D. W. Strong, B. T. McCune, C. S. Pohl, and H. W. Virgin, “A Single-Amino-Acid Change in Murine Norovirus NS1/2 Is Sufficient for Colonic Tropism and Persistence,” *J Virol*, vol. 87, no. 1, pp. 327–334, Jan. 2013, doi: 10.1128/JVI.01864-12.

[123] S. Lee *et al.*, “A Secreted Viral Nonstructural Protein Determines Intestinal Norovirus Pathogenesis,” *Cell Host Microbe*, vol. 25, no. 6, pp. 845-857.e5, Jun. 2019, doi: 10.1016/j.chom.2019.04.005.

[124] T. Pfister and E. Wimmer, “Polypeptide p41 of a Norwalk-Like Virus Is a Nucleic Acid-Independent Nucleoside Triphosphatase,” *J Virol*, vol. 75, no. 4, pp. 1611–1619, Feb. 2001, doi: 10.1128/JVI.75.4.1611-1619.2001.

[125] T. M. Sharp, S. Guix, K. Katayama, S. E. Crawford, and M. K. Estes, “Inhibition of Cellular Protein Secretion by Norwalk Virus Nonstructural Protein p22 Requires a Mimic of an Endoplasmic Reticulum Export Signal,” *PLoS One*, vol. 5, no. 10, p. e13130, Oct. 2010, doi: 10.1371/journal.pone.0013130.

[126] G. Belliot, S. V. Sosnovtsev, K.-O. Chang, P. McPhie, and K. Y. Green, "Nucleotidylylation of the VPg protein of a human norovirus by its proteinase-polymerase precursor protein," *Virology*, vol. 374, no. 1, pp. 33–49, Apr. 2008, doi: 10.1016/j.virol.2007.12.028.

[127] C. P. Campillay-Véliz *et al.*, "Human Norovirus Proteins: Implications in the Replicative Cycle, Pathogenesis, and the Host Immune Response," *Front Immunol*, vol. 11, Jun. 2020, doi: 10.3389/fimmu.2020.00961.

[128] S. Vongpunsawad, B. V. Venkataram Prasad, and M. K. Estes, "Norwalk Virus Minor Capsid Protein VP2 Associates within the VP1 Shell Domain," *J Virol*, vol. 87, no. 9, pp. 4818–4825, May 2013, doi: 10.1128/JVI.03508-12.

[129] C. Borg, A. S. Jahun, L. Thorne, F. Sorgeloos, D. Bailey, and I. G. Goodfellow, "Murine norovirus virulence factor 1 (VF1) protein contributes to viral fitness during persistent infection," *Journal of General Virology*, vol. 102, no. 9, Sep. 2021, doi: 10.1099/jgv.0.001651.

[130] N. McFadden *et al.*, "Norovirus Regulation of the Innate Immune Response and Apoptosis Occurs via the Product of the Alternative Open Reading Frame 4," *PLoS Pathog*, vol. 7, no. 12, p. e1002413, Dec. 2011, doi: 10.1371/journal.ppat.1002413.

[131] A. Gerondopoulos, T. Jackson, P. Monaghan, N. Doyle, and L. O. Roberts, "Murine norovirus-1 cell entry is mediated through a non-clathrin-, non-caveolae-,

dynamin- and cholesterol-dependent pathway," *Journal of General Virology*, vol. 91, no. 6, pp. 1428–1438, Jun. 2010, doi: 10.1099/vir.0.016717-0.

[132] R. C. Orchard *et al.*, "Discovery of a proteinaceous cellular receptor for a norovirus," *Science (1979)*, vol. 353, no. 6302, pp. 933–936, Aug. 2016, doi: 10.1126/science.aaf1220.

[133] J. W. Perry and C. E. Wobus, "Endocytosis of Murine Norovirus 1 into Murine Macrophages Is Dependent on Dynamin II and Cholesterol," *J Virol*, vol. 84, no. 12, pp. 6163–6176, Jun. 2010, doi: 10.1128/JVI.00331-10.

[134] I. Goodfellow *et al.*, "Calicivirus translation initiation requires an interaction between VPg and eIF4E," *EMBO Rep*, vol. 6, no. 10, pp. 968–972, Oct. 2005, doi: 10.1038/sj.embor.7400510.

[135] K. F. Daughenbaugh, "The genome-linked protein VPg of the Norwalk virus binds eIF3, suggesting its role in translation initiation complex recruitment," *EMBO J*, vol. 22, no. 11, pp. 2852–2859, Jun. 2003, doi: 10.1093/emboj/cdg251.

[136] M. Amir Yunus, "Molecular Mechanisms for Norovirus Genome Replication," in *Norovirus*, IntechOpen, 2021. doi: 10.5772/intechopen.96032.

[137] J. Rohayem, I. Robel, K. Jäger, U. Scheffler, and W. Rudolph, "Protein-Primed and De Novo Initiation of RNA Synthesis by Norovirus 3D ^{pol}," *J Virol*, vol. 80, no. 14, pp. 7060–7069, Jul. 2006, doi: 10.1128/JVI.02195-05.

[138] P. Simmonds, I. Karakasiliotis, D. Bailey, Y. Chaudhry, D. J. Evans, and I. G. Goodfellow, “Bioinformatic and functional analysis of RNA secondary structure elements among different genera of human and animal caliciviruses,” *Nucleic Acids Res*, vol. 36, no. 8, pp. 2530–2546, May 2008, doi: 10.1093/nar/gkn096.

[139] M. A. Yunus *et al.*, “The Murine Norovirus Core Subgenomic RNA Promoter Consists of a Stable Stem-Loop That Can Direct Accurate Initiation of RNA Synthesis,” *J Virol*, vol. 89, no. 2, pp. 1218–1229, Jan. 2015, doi: 10.1128/JVI.02432-14.

[140] G. Wang, D. Zhang, R. C. Orchard, D. C. Hancks, and T. A. Reese, “Norovirus MLKL-like protein initiates cell death to induce viral egress,” *Nature*, vol. 616, no. 7955, pp. 152–158, Apr. 2023, doi: 10.1038/s41586-023-05851-w.

[141] C. E. Wobus, L. B. Thackray, and H. W. Virgin, “Murine Norovirus: a Model System To Study Norovirus Biology and Pathogenesis,” *J Virol*, vol. 80, no. 11, pp. 5104–5112, Jun. 2006, doi: 10.1128/JVI.02346-05.

[142] H. L. Koo, N. Ajami, R. L. Atmar, and H. L. DuPont, “Noroviruses: The leading cause of gastroenteritis worldwide.,” *Discovery medicine*, vol. 10, no. 50. NIH Public Access, pp. 61–70, 2010.

[143] R. I. Glass, U. D. Parashar, and M. K. Estes, “Norovirus Gastroenteritis,” *New England Journal of Medicine*, vol. 361, no. 18, pp. 1776–1785, Oct. 2009, doi: 10.1056/NEJMra0804575.

[144] A. S. Jahun and I. G. Goodfellow, “Interferon responses to norovirus infections: current and future perspectives,” *Journal of General Virology*, vol. 102, no. 10, Nov. 2021, doi: 10.1099/jgv.0.001660.

[145] S. M. Karst, C. E. Wobus, M. Lay, J. Davidson, and H. W. Virgin, “STAT1-Dependent Innate Immunity to a Norwalk-Like Virus,” *Science (1979)*, vol. 299, no. 5612, pp. 1575–1578, Mar. 2003, doi: 10.1126/science.1077905.

[146] M. T. Baldridge *et al.*, “Expression of Ifnlr1 on Intestinal Epithelial Cells Is Critical to the Antiviral Effects of Interferon Lambda against Norovirus and Reovirus,” *J Virol*, vol. 91, no. 7, Apr. 2017, doi: 10.1128/JVI.02079-16.

[147] R. Savan, S. Ravichandran, J. R. Collins, M. Sakai, and H. A. Young, “Structural conservation of interferon gamma among vertebrates,” *Cytokine Growth Factor Rev*, vol. 20, no. 2, pp. 115–124, Apr. 2009, doi: 10.1016/j.cytogfr.2009.02.006.

[148] M. Syedbasha and A. Egli, “Interferon Lambda: Modulating Immunity in Infectious Diseases,” *Front Immunol*, vol. 8, p. 119, Feb. 2017, doi: 10.3389/fimmu.2017.00119.

[149] A. Lasfar *et al.*, “Characterization of the Mouse IFN-λ Ligand-Receptor System: IFN-λs Exhibit Antitumor Activity against B16 Melanoma,” *Cancer Res*, vol. 66, no. 8, pp. 4468–4477, Apr. 2006, doi: 10.1158/0008-5472.CAN-05-3653.

[150] G. Kak, M. Raza, and B. K. Tiwari, “Interferon-gamma (IFN-γ): Exploring its implications in infectious diseases,” *Biomol Concepts*, vol. 9, no. 1, pp. 64–79, May 2018, doi: 10.1515/bmc-2018-0007.

[151] G. Tau and P. Rothman, “Biologic functions of the IFN-gamma receptors.,” *Allergy*, vol. 54, no. 12, pp. 1233–51, Dec. 1999, doi: 10.1034/j.1398-9995.1999.00099.x.

[152] R. P. Donnelly and S. V. Kotenko, “Interferon-lambda: A new addition to an old family,” *Journal of Interferon and Cytokine Research*, vol. 30, no. 8, pp. 555–564, 2010, doi: 10.1089/jir.2010.0078.

[153] M. S. Diamond and M. Farzan, “The broad-spectrum antiviral functions of IFIT and IFITM proteins,” *Nat Rev Immunol*, vol. 13, no. 1, pp. 46–57, Jan. 2013, doi: 10.1038/nri3344.

[154] Y.-C. Perng and D. J. Lenschow, “ISG15 in antiviral immunity and beyond,” *Nat Rev Microbiol*, vol. 16, no. 7, pp. 423–439, Jul. 2018, doi: 10.1038/s41579-018-0020-5.

[155] L. Ji *et al.*, “The crucial regulatory role of type I interferon in inflammatory diseases,” *Cell Biosci*, vol. 13, no. 1, p. 230, Dec. 2023, doi: 10.1186/s13578-023-01188-z.

[156] E. V. Mesev, R. A. LeDesma, and A. Ploss, “Decoding type I and III interferon signalling during viral infection,” *Nat Microbiol*, vol. 4, no. 6, pp. 914–924, Apr. 2019, doi: 10.1038/s41564-019-0421-x.

[157] J. J. Babon *et al.*, “Suppression of Cytokine Signaling by SOCS3: Characterization of the Mode of Inhibition and the Basis of Its Specificity,” *Immunity*, vol. 36, no. 2, pp. 239–250, Feb. 2012, doi: 10.1016/j.immuni.2011.12.015.

[158] N. Honke, N. Shaabani, D.-E. Zhang, C. Hardt, and K. S. Lang, “Multiple functions of USP18,” *Cell Death Dis*, vol. 7, no. 11, pp. e2444–e2444, Nov. 2016, doi: 10.1038/cddis.2016.326.

[159] A. Broggi, Y. Tan, F. Granucci, and I. Zanoni, “IFN-λ suppresses intestinal inflammation by non-translational regulation of neutrophil function,” *Nat Immunol*, vol. 18, no. 10, pp. 1084–1093, Oct. 2017, doi: 10.1038/ni.3821.

[160] A. A. Alase, Y. M. El-Sherbiny, E. M. Vital, D. J. Tobin, N. A. Turner, and M. Wittmann, “IFNλ Stimulates MxA Production in Human Dermal Fibroblasts via a MAPK-Dependent STAT1-Independent Mechanism,” *Journal of Investigative Dermatology*, vol. 135, no. 12, pp. 2935–2943, Dec. 2015, doi: 10.1038/jid.2015.317.

[161] H. M. Lazear *et al.*, “Interferon-λ restricts West Nile virus neuroinvasion by tightening the blood-brain barrier,” *Sci Transl Med*, vol. 7, no. 284, Apr. 2015, doi: 10.1126/scitranslmed.aaa4304.

[162] C. Mazewski, R. E. Perez, E. N. Fish, and L. C. Platanias, “Type I Interferon (IFN)-Regulated Activation of Canonical and Non-Canonical Signaling Pathways,” *Front Immunol*, vol. 11, Nov. 2020, doi: 10.3389/fimmu.2020.606456.

[163] A. H. H. Van Boxel-Dezaire, M. R. Sandhya Rani, and G. R. Stark, “Review Complex Modulation of Cell Type-Specific Signaling in Response to Type I Interferons,” *Immunity*, vol. 25, pp. 361–372, 2006, doi: 10.1016/j.immuni.2006.08.014.

[164] G. R. Stark, I. M. Kerr, B. R. G. Williams, R. H. Silverman, and R. D. Schreiber, “How cells respond to interferons,” *Annual Review of Biochemistry*, vol. 67, no. 1. Annual Reviews 4139 El Camino Way, P.O. Box 10139, Palo Alto, CA 94303-0139, USA, pp. 227–264, Jun. 28, 1998. doi: 10.1146/annurev.biochem.67.1.227.

[165] J. E. Darnell, “STATs and gene regulation,” *Science (1979)*, vol. 277, no. 5332, pp. 1630–1635, Sep. 1997, doi: 10.1126/science.277.5332.1630.

[166] F. Seif, M. Khoshmirsafa, H. Aazami, M. Mohsenzadegan, G. Sedighi, and M. Bahar, “The role of JAK-STAT signaling pathway and its regulators in the fate of T helper cells,” *Cell Communication and Signaling*, vol. 15, no. 1. BioMed Central Ltd., pp. 1–13, Jun. 21, 2017. doi: 10.1186/s12964-017-0177-y.

[167] K. Blaszczyk, H. Nowicka, K. Kostyrko, A. Antonczyk, J. Wesoly, and H. A. R. Bluyssen, “The unique role of STAT2 in constitutive and IFN-induced transcription and antiviral responses,” *Cytokine Growth Factor Rev*, vol. 29, pp. 71–81, Jun. 2016, doi: 10.1016/j.cytogfr.2016.02.010.

[168] M. L. Stanifer, K. Pervolaraki, and S. Boulant, “Differential Regulation of Type I and Type III Interferon Signaling,” *Int J Mol Sci*, vol. 20, no. 6, p. 1445, Mar. 2019, doi: 10.3390/ijms20061445.

[169] Y. J. Lou *et al.*, “Ifr-9/stat2 functional interaction drives Retinoic acid-induced gene g expression independently of stat1,” *Cancer Res*, vol. 69, no. 8, pp. 3673–3680, Apr. 2009, doi: 10.1158/0008-5472.CAN-08-4922.

[170] J. J. Ghislain, T. Wong, M. Nguyen, and E. N. Fish, “The interferon-inducible Stat2:Stat1 heterodimer preferentially binds in vitro to a consensus element found in the promoters of a subset of interferon-stimulated genes,” *Journal of Interferon and Cytokine Research*, vol. 21, no. 6, pp. 379–388, 2001, doi: 10.1089/107999001750277853.

[171] S. Gupta, M. Jiang, and A. B. Pernis, “IFN-alpha activates Stat6 and leads to the formation of Stat2:Stat6 complexes in B cells.,” *J Immunol*, vol. 163, no. 7, pp. 3834–41, Oct. 1999.

[172] E. N. Fish, S. Uddin, M. Korkmaz, B. Majchrzak, B. J. Druker, and L. C. Platanias, “Activation of a CrkL-Stat5 Signaling Complex by Type I Interferons,” *Journal of Biological Chemistry*, vol. 274, no. 2, pp. 571–573, Jan. 1999, doi: 10.1074/jbc.274.2.571.

[173] H. M. Lazear, J. W. Schoggins, and M. S. Diamond, “Shared and Distinct Functions of Type I and Type III Interferons,” *Immunity*, vol. 50, no. 4, pp. 907–923, Apr. 2019, doi: 10.1016/J.IMMUNI.2019.03.025.

[174] T. A. Selvakumar *et al.*, “Identification of a predominantly interferon-λ-induced transcriptional profile in murine intestinal epithelial cells,” *Front Immunol*, vol. 8, no. OCT, p. 1302, 2017, doi: 10.3389/fimmu.2017.01302.

[175] E. A. Caine *et al.*, “Interferon lambda protects the female reproductive tract against Zika virus infection,” *Nat Commun*, vol. 10, no. 1, p. 280, Dec. 2019, doi: 10.1038/s41467-018-07993-2.

[176] J. A. Van Winkle, D. A. Constant, L. Li, and T. J. Nice, “Selective interferon responses of intestinal epithelial cells minimize TNFα cytotoxicity,” *bioRxiv*, Mar. 2020, doi: 10.1101/2020.03.20.000604.

[177] S. Bhushal *et al.*, “Cell Polarization and Epigenetic Status Shape the Heterogeneous Response to Type III Interferons in Intestinal Epithelial Cells,” *Front Immunol*, vol. 8, p. 12, Jun. 2017, doi: 10.3389/fimmu.2017.00671.

[178] S. Matikainen, T. Sareneva, T. Ronni, A. Lehtonen, P. J. Koskinen, and I. Julkunen, “Interferon-□Activates Multiple STAT Proteins and Upregulates Proliferation-Associated IL-2R□,c-myc, and pim-1 Genes in Human T Cells,” *Blood*, vol. 93, no. 6, pp. 1980–1991, Mar. 1999, doi: 10.1182/blood.V93.6.1980.406k20_1980_1991.

[179] S. Gupta, M. Jiang, and A. B. Pernis, “IFN-α Activates Stat6 and Leads to the Formation of Stat2:Stat6 Complexes in B Cells,” *The Journal of Immunology*, vol. 163, no. 7, pp. 3834–3841, Oct. 1999, doi: 10.4049/jimmunol.163.7.3834.

[180] M. Kim *et al.*, “Interferon-β activates multiple signaling cascades in primary human microglia,” *J Neurochem*, vol. 81, no. 6, pp. 1361–1371, Jun. 2002, doi: 10.1046/j.1471-4159.2002.00949.x.

[181] T. J. Nice *et al.*, “Interferon- cures persistent murine norovirus infection in the absence of adaptive immunity,” *Science (1979)*, vol. 347, no. 6219, pp. 269–273, Jan. 2015, doi: 10.1126/science.1258100.

[182] J. A. Van Winkle, D. A. Constant, L. Li, and T. J. Nice, “Selective Interferon Responses of Intestinal Epithelial Cells Minimize Tumor Necrosis Factor Alpha Cytotoxicity.,” *J Virol*, vol. 94, no. 21, pp. 1–16, Aug. 2020, doi: 10.1128/JVI.00603-20.

[183] D. A. Constant *et al.*, “Transcriptional and Cytotoxic Responses of Human Intestinal Organoids to IFN Types I, II, and III,” *Immunohorizons*, vol. 6, no. 7, pp. 416–429, Jul. 2022, doi: 10.4049/immunohorizons.2200025.

[184] T. Mahlakõiv, P. Hernandez, K. Gronke, A. Diefenbach, and P. Staeheli, “Leukocyte-Derived IFN-α/β and Epithelial IFN-λ Constitute a Compartmentalized Mucosal Defense System that Restricts Enteric Virus Infections,” *PLoS Pathog*, vol. 11, no. 4, p. e1004782, Apr. 2015, doi: 10.1371/journal.ppat.1004782.

[185] H. M. Lazear, T. J. Nice, and M. S. Diamond, “Interferon-λ: Immune Functions at Barrier Surfaces and Beyond,” *Immunity*, vol. 43, no. 1, pp. 15–28, 2015, doi: 10.1016/j.immuni.2015.07.001.

[186] T. J. Nice *et al.*, “Interferon- cures persistent murine norovirus infection in the absence of adaptive immunity,” *Science (1979)*, vol. 347, no. 6219, pp. 269–273, Jan. 2015, doi: 10.1126/science.1258100.

[187] S. T. Peterson *et al.*, “Disruption of Type III Interferon (IFN) Genes *Ifnl2* and *Ifnl3* Recapitulates Loss of the Type III IFN Receptor in the Mucosal Antiviral Response,” *J Virol*, vol. 93, no. 22, Nov. 2019, doi: 10.1128/JVI.01073-19.

[188] S. Lee and M. T. Baldridge, “Interferon-Lambda: A Potent Regulator of Intestinal Viral Infections,” *Front Immunol*, vol. 8, Jun. 2017, doi: 10.3389/fimmu.2017.00749.

[189] J. A. Van Winkle *et al.*, “Homeostatic interferon-lambda response to bacterial microbiota stimulates preemptive antiviral defense within discrete pockets of intestinal epithelium,” *Elife*, vol. 11, Feb. 2022, doi: 10.7554/eLife.74072.

[190] A. R. Gibson *et al.*, “A genetic screen identifies a protective type III interferon response to Cryptosporidium that requires TLR3 dependent recognition,” *PLoS Pathog*, vol. 18, no. 5, p. e1010003, May 2022, doi: 10.1371/journal.ppat.1010003.

[191] A. Isaacs and J. Lindenmann, “Virus Interference. I. The Interferon,” 1957. [Online]. Available: https://www.jstor.org/stable/83104

[192] T. Fujita, J. Sakakibara, Y. Sudo, M. Miyamoto, Y. Kimura, and T. Taniguchi, “Evidence for a nuclear factor(s), IRF-1, mediating induction and silencing properties to human IFN-beta gene regulatory elements.,” *EMBO J*, vol. 7, no. 11, pp. 3397–3405, Nov. 1988, doi: 10.1002/j.1460-2075.1988.tb03213.x.

[193] J. Nehyba, R. Hrdlickova, and H. R. Bose, “Dynamic Evolution of Immune System Regulators: The History of the Interferon Regulatory Factor Family,” *Mol Biol Evol*, vol. 26, no. 11, pp. 2539–2550, Nov. 2009, doi: 10.1093/molbev/msp167.

[194] C. R. Escalante, J. Yie, D. Thanos, and A. K. Aggarwal, “Structure of IRF-1 with bound DNA reveals determinants of interferon regulation,” *Nature*, vol. 391, no. 6662, pp. 103–106, Jan. 1998, doi: 10.1038/34224.

[195] A. Antonczyk *et al.*, “Direct inhibition of IRF-dependent transcriptional regulatory mechanisms associated with disease,” *Front Immunol*, vol. 10, no. MAY, p. 1176, May 2019, doi: 10.3389/FIMMU.2019.01176/BIBTEX.

[196] K. Takahasi *et al.*, “X-ray crystal structure of IRF-3 and its functional implications,” *Nat Struct Mol Biol*, vol. 10, no. 11, pp. 922–927, Nov. 2003, doi: 10.1038/nsb1001.

[197] G.-N. Zhao, D.-S. Jiang, and H. Li, “Interferon regulatory factors: at the crossroads of immunity, metabolism, and disease,” *Biochimica et Biophysica Acta (BBA) - Molecular Basis of Disease*, vol. 1852, no. 2, pp. 365–378, Feb. 2015, doi: 10.1016/j.bbadis.2014.04.030.

[198] H. Negishi *et al.*, “Negative regulation of Toll-like-receptor signaling by IRF-4,” *Proceedings of the National Academy of Sciences*, vol. 102, no. 44, pp. 15989–15994, Nov. 2005, doi: 10.1073/pnas.0508327102.

[199] C. del Fresno *et al.*, “Interferon-β Production via Dectin-1-Syk-IRF5 Signaling in Dendritic Cells Is Crucial for Immunity to C. albicans,” *Immunity*, vol. 38, no. 6, pp. 1176–1186, Jun. 2013, doi: 10.1016/j.immuni.2013.05.010.

[200] H. Feng, Y.-B. Zhang, J.-F. Gui, S. M. Lemon, and D. Yamane, “Interferon regulatory factor 1 (IRF1) and anti-pathogen innate immune responses,” *PLoS Pathog*, vol. 17, no. 1, p. e1009220, Jan. 2021, doi: 10.1371/journal.ppat.1009220.

[201] H. Harada *et al.*, “Structurally similar but functionally distinct factors, IRF-1 and IRF-2, bind to the same regulatory elements of IFN and IFN-inducible genes,” *Cell*, vol. 58, no. 4, pp. 729–739, Aug. 1989, doi: 10.1016/0092-8674(89)90107-4.

[202] L. B. Ivashkiv and L. T. Donlin, “Regulation of type I interferon responses,” *Nat Rev Immunol*, vol. 14, no. 1, pp. 36–49, Jan. 2014, doi: 10.1038/nri3581.

[203] A. Battistini, “Interferon Regulatory Factors in Hematopoietic Cell Differentiation and Immune Regulation,” *Journal of Interferon & Cytokine Research*, vol. 29, no. 12, pp. 765–780, Dec. 2009, doi: 10.1089/jir.2009.0030.

[204] A. J. S. Rundberg Nilsson, H. Xian, S. Shalapour, J. Cammenga, and M. Karin, “IRF1 regulates self-renewal and stress responsiveness to support hematopoietic stem cell maintenance,” *Sci Adv*, vol. 9, no. 43, Oct. 2023, doi: 10.1126/sciadv.adg5391.

[205] E. M. COCCIA *et al.*, “Ectopic expression of interferon regulatory factor-1 potentiates granulocytic differentiation,” *Biochemical Journal*, vol. 360, no. 2, pp. 285–294, Dec. 2001, doi: 10.1042/bj3600285.

[206] U. Testa *et al.*, “Impaired myelopoiesis in mice devoid of interferon regulatory factor 1,” *Leukemia*, vol. 18, no. 11, pp. 1864–1871, Nov. 2004, doi: 10.1038/sj.leu.2403472.

[207] R. Nayar *et al.*, “TCR signaling via Tec kinase ITK and interferon regulatory factor 4 (IRF4) regulates CD8 $^{+}$ T-cell differentiation,” *Proceedings of the National Academy of Sciences*, vol. 109, no. 41, Oct. 2012, doi: 10.1073/pnas.1205742109.

[208] S. Yao *et al.*, “Interferon Regulatory Factor 4 Sustains CD8+ T Cell Expansion and Effector Differentiation,” *Immunity*, vol. 39, no. 5, pp. 833–845, Nov. 2013, doi: 10.1016/j.immuni.2013.10.007.

[209] M. Huber and M. Lohoff, “IRF4 at the crossroads of effector T-cell fate decision,” *Eur J Immunol*, vol. 44, no. 7, pp. 1886–1895, Jul. 2014, doi: 10.1002/eji.201344279.

[210] J. Lu, T. Liang, P. Li, and Q. Yin, “Regulatory effects of IRF4 on immune cells in the tumor microenvironment,” *Front Immunol*, vol. 14, Feb. 2023, doi: 10.3389/fimmu.2023.1086803.

[211] N. S. De Silva, G. Simonetti, N. Heise, and U. Klein, “The diverse roles of IRF4 in late germinal center B-cell differentiation,” *Immunol Rev*, vol. 247, no. 1, pp. 73–92, May 2012, doi: 10.1111/j.1600-065X.2012.01113.x.

[212] K. Ochiai *et al.*, “Transcriptional Regulation of Germinal Center B and Plasma Cell Fates by Dynamical Control of IRF4,” *Immunity*, vol. 38, no. 5, pp. 918–929, May 2013, doi: 10.1016/j.immuni.2013.04.009.

[213] A. M. Becker, D. G. Michael, A. T. Satpathy, R. Sciammas, H. Singh, and D. Bhattacharya, “IRF-8 extinguishes neutrophil production and promotes dendritic cell lineage commitment in both myeloid and lymphoid mouse progenitors,” *Blood*, vol. 119, no. 9, pp. 2003–2012, Mar. 2012, doi: 10.1182/blood-2011-06-364976.

[214] T. Holtschke *et al.*, “Immunodeficiency and Chronic Myelogenous Leukemia-like Syndrome in Mice with a Targeted Mutation of the ICSBP Gene,” *Cell*, vol. 87, no. 2, pp. 307–317, Oct. 1996, doi: 10.1016/S0092-8674(00)81348-3.

[215] S. Hambleton *et al.*, “*IRF8* Mutations and Human Dendritic-Cell Immunodeficiency,” *New England Journal of Medicine*, vol. 365, no. 2, pp. 127–138, Jul. 2011, doi: 10.1056/NEJMoa1100066.

[216] X. Xia, W. Wang, K. Yin, and S. Wang, “Interferon regulatory factor 8 governs myeloid cell development,” *Cytokine Growth Factor Rev*, vol. 55, pp. 48–57, Oct. 2020, doi: 10.1016/j.cytogfr.2020.03.003.

[217] J. Chandra, P. T. Y. Kuo, A. M. Hahn, G. T. Belz, and I. H. Frazer, “Batf3 selectively determines acquisition of CD8 $^{+}$ dendritic cell phenotype and function,” *Immunol Cell Biol*, vol. 95, no. 2, pp. 215–223, Feb. 2017, doi: 10.1038/icb.2016.83.

[218] G. E. Grajales-Reyes *et al.*, “Batf3 maintains autoactivation of Irf8 for commitment of a CD8α+ conventional DC clonogenic progenitor,” *Nat Immunol*, vol. 16, no. 7, pp. 708–717, Jul. 2015, doi: 10.1038/ni.3197.

[219] C. Bornstein *et al.*, “A Negative Feedback Loop of Transcription Factors Specifies Alternative Dendritic Cell Chromatin States,” *Mol Cell*, vol. 56, no. 6, pp. 749–762, Dec. 2014, doi: 10.1016/j.molcel.2014.10.014.

[220] Y. Zhao *et al.*, “mTOR masters monocyte development in bone marrow by decreasing the inhibition of STAT5 on IRF8,” *Blood*, vol. 131, no. 14, pp. 1587–1599, Apr. 2018, doi: 10.1182/blood-2017-04-777128.

[221] T. Tamura, T. Nagamura-Inoue, Z. Shmeltzer, T. Kuwata, and K. Ozato, “ICSBP Directs Bipotential Myeloid Progenitor Cells to Differentiate into Mature Macrophages,” *Immunity*, vol. 13, no. 2, pp. 155–165, Aug. 2000, doi: 10.1016/S1074-7613(00)00016-9.

[222] T. Elien, D. N. Kamilla, and E. I. Auerkari, “Van der woude syndrome,” *J Phys Conf Ser*, vol. 1943, no. 1, p. 012089, Jul. 2021, doi: 10.1088/1742-6596/1943/1/012089.

[223] R. L. L. F. de Lima *et al.*, “Prevalence and nonrandom distribution of exonic mutations in interferon regulatory factor 6 in 307 families with Van der Woude syndrome and 37 families with popliteal pterygium syndrome,” *Genetics in Medicine*, vol. 11, no. 4, pp. 241–247, Apr. 2009, doi: 10.1097/GIM.0b013e318197a49a.

[224] Y. A. Kousa *et al.*, “The TFAP2A–IRF6–GRHL3 genetic pathway is conserved in neurulation,” *Hum Mol Genet*, vol. 28, no. 10, pp. 1726–1737, May 2019, doi: 10.1093/hmg/ddz010.

[225] C. M. Bailey *et al.*, “Mammary Serine Protease Inhibitor (Maspin) Binds Directly to Interferon Regulatory Factor 6,” *Journal of Biological Chemistry*, vol. 280, no. 40, pp. 34210–34217, Oct. 2005, doi: 10.1074/jbc.M503523200.

[226] D. Li *et al.*, “IRF6 Is Directly Regulated by ZEB1 and ELF3, and Predicts a Favorable Prognosis in Gastric Cancer,” *Front Oncol*, vol. 9, Apr. 2019, doi: 10.3389/fonc.2019.00220.

[227] I.-K. Kim *et al.*, “Plasticity-induced repression of Irf6 underlies acquired resistance to cancer immunotherapy in pancreatic ductal adenocarcinoma,” *Nat Commun*, vol. 15, no. 1, p. 1532, Feb. 2024, doi: 10.1038/s41467-024-46048-7.

[228] S. Hong, N. Fu, S. Sang, X. Ma, F. Sun, and X. Zhang, “Identification and validation of IRF6 related to ovarian cancer and biological function and prognostic value,” *J Ovarian Res*, vol. 17, no. 1, p. 64, Mar. 2024, doi: 10.1186/s13048-024-01386-4.

[229] Y. A. Kousa and B. C. Schutte, “Toward an orofacial gene regulatory network,” *Developmental Dynamics*, vol. 245, no. 3, pp. 220–232, Mar. 2016, doi: 10.1002/dvdy.24341.

[230] R. J. Richardson *et al.*, “Irf6 is a key determinant of the keratinocyte proliferation-differentiation switch,” *Nat Genet*, vol. 38, no. 11, pp. 1329–1334, Nov. 2006, doi: 10.1038/ng1894.

[231] H. J. Little *et al.*, “Missense mutations that cause Van der Woude syndrome and popliteal pterygium syndrome affect the DNA-binding and transcriptional activation functions of IRF6,” *Hum Mol Genet*, vol. 18, no. 3, pp. 535–545, Feb. 2009, doi: 10.1093/hmg/ddn381.

[232] S. Kondo *et al.*, “Mutations in IRF6 cause Van der Woude and popliteal pterygium syndromes,” *Nat Genet*, vol. 32, no. 2, pp. 285–289, Oct. 2002, doi: 10.1038/ng985.

[233] W. D. Fakhouri *et al.*, “An etiologic regulatory mutation in IRF6 with loss- and gain-of-function effects,” *Hum Mol Genet*, vol. 23, no. 10, pp. 2711–2720, May 2014, doi: 10.1093/hmg/ddt664.

[234] C.-Y. Ke, H.-H. Mei, F.-H. Wong, and L.-J. Lo, “IRF6 and TAK1 coordinately promote the activation of HIPK2 to stimulate apoptosis during palate fusion,” *Sci Signal*, vol. 12, no. 593, Aug. 2019, doi: 10.1126/scisignal.aav7666.

[235] C.-Y. Ke, W.-L. Xiao, C.-M. Chen, L.-J. Lo, and F.-H. Wong, “IRF6 is the mediator of TGFβ3 during regulation of the epithelial mesenchymal transition and palatal fusion,” *Sci Rep*, vol. 5, no. 1, p. 12791, Aug. 2015, doi: 10.1038/srep12791.

[236] J. Iwata *et al.*, "*Smad4* - *Irf6* genetic interaction and TGFβ-mediated IRF6 signaling cascade are crucial for palatal fusion in mice," *Development*, vol. 140, no. 6, pp. 1220–1230, Mar. 2013, doi: 10.1242/dev.089615.

[237] H. A. Thomason *et al.*, "Cooperation between the transcription factors p63 and IRF6 is essential to prevent cleft palate in mice," *Journal of Clinical Investigation*, vol. 120, no. 5, pp. 1561–1569, May 2010, doi: 10.1172/JCI40266.

[238] C.-Y. Ke, W.-L. Xiao, C.-M. Chen, L.-J. Lo, and F.-H. Wong, "IRF6 is the mediator of TGFβ3 during regulation of the epithelial mesenchymal transition and palatal fusion," *Sci Rep*, vol. 5, no. 1, p. 12791, Aug. 2015, doi: 10.1038/srep12791.

[239] C. R. Ingraham *et al.*, "Abnormal skin, limb and craniofacial morphogenesis in mice deficient for interferon regulatory factor 6 (Irf6)," *Nat Genet*, vol. 38, no. 11, pp. 1335–1340, Nov. 2006, doi: 10.1038/ng1903.

[240] N. Oberbeck *et al.*, "The RIPK4–IRF6 signalling axis safeguards epidermal differentiation and barrier function," *Nature*, vol. 574, no. 7777, pp. 249–253, Oct. 2019, doi: 10.1038/s41586-019-1615-3.

[241] M. Q. Kwa *et al.*, "Receptor-interacting Protein Kinase 4 and Interferon Regulatory Factor 6 Function as a Signaling Axis to Regulate Keratinocyte Differentiation," *Journal of Biological Chemistry*, vol. 289, no. 45, pp. 31077–31087, Nov. 2014, doi: 10.1074/jbc.M114.589382.

[242] W. D. Fakhouri *et al.*, "*MCS9.7* enhancer activity is highly, but not completely, associated with expression of Irf6 and p63," *Developmental Dynamics*, vol. 241, no. 2, pp. 340–349, Feb. 2012, doi: 10.1002/dvdy.22786.

[243] F. Moretti *et al.*, "A regulatory feedback loop involving p63 and IRF6 links the pathogenesis of 2 genetically different human ectodermal dysplasias," *Journal of Clinical Investigation*, vol. 120, no. 5, pp. 1570–1577, May 2010, doi: 10.1172/JCI40267.

[244] E. Botti *et al.*, "Developmental factor IRF6 exhibits tumor suppressor activity in squamous cell carcinomas," *Proceedings of the National Academy of Sciences*, vol. 108, no. 33, pp. 13710–13715, Aug. 2011, doi: 10.1073/pnas.1110931108.

[245] J. L. Sabel *et al.*, "Maternal Interferon Regulatory Factor 6 is required for the differentiation of primary superficial epithelia in Danio and Xenopus embryos," *Dev Biol*, vol. 325, no. 1, pp. 249–262, Jan. 2009, doi: 10.1016/j.ydbio.2008.10.031.

[246] M. Q. Kwa *et al.*, "Interferon Regulatory Factor 6 Differentially Regulates Toll-like Receptor 2-dependent Chemokine Gene Expression in Epithelial Cells," *Journal of Biological Chemistry*, vol. 289, no. 28, pp. 19758–19768, Jul. 2014, doi: 10.1074/jbc.M114.584540.

[247] D. Ramnath *et al.*, "TLR3 drives IRF6-dependent IL-23p19 expression and p19/EBI3 heterodimer formation in keratinocytes," *Immunol Cell Biol*, vol. 93, no. 9, pp. 771–779, Oct. 2015, doi: 10.1038/icb.2015.77.

[248] J. Huynh *et al.*, “IRF6 Regulates the Expression of IL-36γ by Human Oral Epithelial Cells in Response to *Porphyromonas gingivalis*,” *The Journal of Immunology*, vol. 196, no. 5, pp. 2230–2238, Mar. 2016, doi: 10.4049/jimmunol.1501263.

[249] S. Joly, L. Rhea, P. Volk, J. G. Moreland, and M. Dunnwald, “Interferon Regulatory Factor 6 Has a Protective Role in the Host Response to Endotoxic Shock,” *PLoS One*, vol. 11, no. 4, p. e0152385, Apr. 2016, doi: 10.1371/journal.pone.0152385.

[250] C. Li *et al.*, “IRF6 Regulates Alternative Activation by Suppressing PPARγ in Male Murine Macrophages,” *Endocrinology*, vol. 158, no. 9, pp. 2837–2847, Sep. 2017, doi: 10.1210/en.2017-00053.

[251] W. M. Schneider, M. D. Chevillotte, and C. M. Rice, “Interferon-stimulated genes: a complex web of host defenses.,” *Annu Rev Immunol*, vol. 32, no. 4, pp. 513–45, Apr. 2014, doi: 10.1146/annurev-immunol-032713-120231.

[252] J. W. Schoggins, “Interferon-Stimulated Genes: What Do They All Do?,” *Annu Rev Virol*, vol. 6, no. 1, pp. 567–584, 2019, doi: 10.1146/annurev-virology-092818-015756.

[253] A. J. Sadler and B. R. G. Williams, “Interferon-inducible antiviral effectors,” *Nat Rev Immunol*, vol. 8, no. 7, pp. 559–68, Jul. 2008, doi: 10.1038/nri2314.

[254] C. Sommereyns, S. Paul, P. Staeheli, and T. Michiels, “IFN-Lambda (IFN-λ) Is Expressed in a Tissue-Dependent Fashion and Primarily Acts on Epithelial Cells In

Vivo," *PLoS Pathog*, vol. 4, no. 3, p. e1000017, Mar. 2008, doi: 10.1371/journal.ppat.1000017.

[255] T. Mahlakoiv, P. Hernandez, K. Gronke, A. Diefenbach, and P. Staeheli, "Leukocyte-derived IFN-alpha/beta and epithelial IFN-lambda constitute a compartmentalized mucosal defense system that restricts enteric virus infections," *PLoS Pathog*, vol. 11, no. 4, p. e1004782, 2015, doi: 10.1371/journal.ppat.1004782.

[256] M. Mordstein *et al.*, "Lambda interferon renders epithelial cells of the respiratory and gastrointestinal tracts resistant to viral infections.," *J Virol*, vol. 84, no. 11, pp. 5670–7, Jun. 2010, doi: 10.1128/JVI.00272-10.

[257] M. T. Baldridge *et al.*, "Expression of Ifnlr1 on Intestinal Epithelial Cells Is Critical to the Antiviral Effects of Interferon Lambda against Norovirus and Reovirus.," *J Virol*, vol. 91, no. 7, pp. e02079-16, Apr. 2017, doi: 10.1128/JVI.02079-16.

[258] T. J. Nice *et al.*, "Interferon-λ cures persistent murine norovirus infection in the absence of adaptive immunity.," *Science*, vol. 347, no. 6219, pp. 269–73, Jan. 2015, doi: 10.1126/science.1258100.

[259] J. A. Van Winkle *et al.*, "A homeostatic interferon-lambda response to bacterial microbiota stimulates preemptive antiviral defense within discrete pockets of intestinal epithelium," *Elife*, vol. 11, p. 2021.06.02.446828, Feb. 2022, doi: 10.7554/eLife.74072.

[260] J. Pott *et al.*, “IFN-lambda determines the intestinal epithelial antiviral host defense.,” *Proc Natl Acad Sci U S A*, vol. 108, no. 19, pp. 7944–9, May 2011, doi: 10.1073/pnas.1100552108.

[261] J. L. Mendoza *et al.*, “The IFN-λ-IFN-λR1-IL-10Rβ Complex Reveals Structural Features Underlying Type III IFN Functional Plasticity,” *Immunity*, vol. 46, no. 3, pp. 379–392, Mar. 2017, doi: 10.1016/j.immuni.2017.02.017.

[262] A. Forero *et al.*, “Differential Activation of the Transcription Factor IRF1 Underlies the Distinct Immune Responses Elicited by Type I and Type III Interferons,” *Immunity*, vol. 51, no. 3, pp. 451-464.e6, Sep. 2019, doi: 10.1016/j.immuni.2019.07.007.

[263] K. Pervolaraki *et al.*, “Differential induction of interferon stimulated genes between type I and type III interferons is independent of interferon receptor abundance,” *PLoS Pathog*, vol. 14, no. 11, p. e1007420, 2018, doi: 10.1371/journal.ppat.1007420.

[264] T. Taniguchi, K. Ogasawara, A. Takaoka, and N. Tanaka, “IRF family of transcription factors as regulators of host defense.,” *Annu Rev Immunol*, vol. 19, no. 1, pp. 623–55, Apr. 2001, doi: 10.1146/annurev.immunol.19.1.623.

[265] H. Negishi, T. Taniguchi, and H. Yanai, “The Interferon (IFN) Class of Cytokines and the IFN Regulatory Factor (IRF) Transcription Factor Family,” *Cold Spring Harb Perspect Biol*, vol. 10, no. 11, p. a028423, Nov. 2018, doi: 10.1101/cshperspect.a028423.

[266] H. Wang *et al.*, “IRF8 regulates B-cell lineage specification, commitment, and differentiation,” *Blood*, vol. 112, no. 10, pp. 4028–4038, Nov. 2008, doi: 10.1182/blood-2008-01-129049.

[267] H. Tsujimura, T. Nagamura-Inoue, T. Tamura, and K. Ozato, “IFN Consensus Sequence Binding Protein/IFN Regulatory Factor-8 Guides Bone Marrow Progenitor Cells Toward the Macrophage Lineage,” *The Journal of Immunology*, vol. 169, no. 3, pp. 1261–1269, Aug. 2002, doi: 10.4049/jimmunol.169.3.1261.

[268] A. Mancino and G. Natoli, “Specificity and Function of IRF Family Transcription Factors: Insights from Genomics,” *Journal of Interferon & Cytokine Research*, vol. 36, no. 7, pp. 462–469, Jul. 2016, doi: 10.1089/jir.2016.0004.

[269] L. Gabriele and K. Ozato, “The role of the interferon regulatory factor (IRF) family in dendritic cell development and function,” *Cytokine Growth Factor Rev*, vol. 18, no. 5–6, pp. 503–510, 2007, doi: 10.1016/j.cytogfr.2007.06.008.

[270] M. Q. Kwa, J. Huynh, E. C. Reynolds, J. A. Hamilton, and G. M. Scholz, “Disease-associated mutations in IRF6 and RIPK4 dysregulate their signalling functions,” *Cell Signal*, vol. 27, no. 7, pp. 1509–1516, 2015, doi: 10.1016/j.cellsig.2015.03.005.

[271] C. R. Ingraham *et al.*, “Abnormal skin, limb and craniofacial morphogenesis in mice deficient for interferon regulatory factor 6 (Irf6).,” *Nat Genet*, vol. 38, no. 11, pp. 1335–40, Nov. 2006, doi: 10.1038/ng1903.

[272] Y. A. Kousa, D. Moussa, and B. C. Schutte, “IRF6 expression in basal epithelium partially rescues *Irf6* knockout mice,” *Developmental Dynamics*, vol. 246, no. 9, pp. 670–681, Sep. 2017, doi: 10.1002/dvdy.24537.

[273] E. Blasi, R. Barluzzi, V. Bocchini, R. Mazzolla, and F. Bistoni, “Immortalization of murine microglial cells by a v-raf / v-myc carrying retrovirus,” *J Neuroimmunol*, vol. 27, no. 2–3, pp. 229–237, May 1990, doi: 10.1016/0165-5728(90)90073-V.

[274] H. M. Padilla-Nash *et al.*, “Spontaneous transformation of murine epithelial cells requires the early acquisition of specific chromosomal aneuploidies and genomic imbalances,” *Genes Chromosomes Cancer*, vol. 51, no. 4, pp. 353–374, Apr. 2012, doi: 10.1002/GCC.21921.

[275] J. A. Van Winkle *et al.*, “Persistence of Systemic Murine Norovirus Is Maintained by Inflammatory Recruitment of Susceptible Myeloid Cells.,” *Cell Host Microbe*, vol. 24, no. 5, pp. 665-676.e4, 2018, doi: 10.1016/j.chom.2018.10.003.

[276] B. A. Robinson, J. A. Van Winkle, B. T. McCune, A. M. Peters, and T. J. Nice, “Caspase-mediated cleavage of murine norovirus NS1/2 potentiates apoptosis and is required for persistent infection of intestinal epithelial cells,” *PLoS Pathog*, vol. 15, no. 7, p. e1007940, Jul. 2019, doi: 10.1371/journal.ppat.1007940.

[277] J. M. Deerain *et al.*, “Murine norovirus infection of macrophages induces intrinsic apoptosis as the major form of programmed cell death,” *Virology*, vol. 589, p. 109921, Jan. 2024, doi: 10.1016/j.virol.2023.109921.

[278] G. Wang, D. Zhang, R. C. Orchard, D. C. Hancks, and T. A. Reese, “Norovirus MLKL-like protein initiates cell death to induce viral egress,” *Nature*, vol. 616, no. 7955, pp. 152–158, Apr. 2023, doi: 10.1038/s41586-023-05851-w.

[279] H. Harada *et al.*, “Structurally similar but functionally distinct factors, IRF-1 and IRF-2, bind to the same regulatory elements of IFN and IFN-inducible genes,” *Cell*, vol. 58, no. 4, pp. 729–739, Aug. 1989, doi: 10.1016/0092-8674(89)90107-4.

[280] E. Botti *et al.*, “Developmental factor IRF6 exhibits tumor suppressor activity in squamous cell carcinomas,” *Proceedings of the National Academy of Sciences*, vol. 108, no. 33, pp. 13710–13715, Aug. 2011, doi: 10.1073/pnas.1110931108.

[281] G. Restivo *et al.*, “IRF6 is a mediator of Notch pro-differentiation and tumour suppressive function in keratinocytes,” *EMBO J*, vol. 30, no. 22, pp. 4571–4585, Nov. 2011, doi: 10.1038/emboj.2011.325.

[282] C. M. Bailey and M. J. C. Hendrix, “IRF6 in development and disease: A mediator of quiescence and differentiation,” *Cell Cycle*, vol. 7, no. 13, pp. 1925–1930, Jul. 2008, doi: 10.4161/cc.7.13.6221.

[283] I. Rusinova *et al.*, “INTERFEROME v2.0: An updated database of annotated interferon-regulated genes,” *Nucleic Acids Res*, vol. 41, no. D1, pp. 1040–1046, 2013, doi: 10.1093/nar/gks1215.

[284] M. Degen *et al.*, “A Novel Van der Woude Syndrome-Causing IRF6 Variant Is Subject to Incomplete Non-sense-Mediated mRNA Decay Affecting the Phenotype

of Keratinocytes," *Front Cell Dev Biol*, vol. 8, Sep. 2020, doi: 10.3389/fcell.2020.583115.

[285] M. Luo *et al.*, "PHLDB2 Mediates Cetuximab Resistance via Interacting With EGFR in Latent Metastasis of Colorectal Cancer," *Cell Mol Gastroenterol Hepatol*, vol. 13, no. 4, pp. 1223–1242, 2022, doi: 10.1016/j.jcmgh.2021.12.011.

[286] S. Matsumoto *et al.*, "A combination of Wnt and growth factor signaling induces Arl4c expression to form epithelial tubular structures," *EMBO J*, vol. 33, no. 7, pp. 702–718, Apr. 2014, doi: 10.1002/embj.201386942.

[287] G. Colozza *et al.*, "Intestinal Paneth cell differentiation relies on asymmetric regulation of Wnt signaling by Daam1/2," *Sci Adv*, vol. 9, no. 47, Nov. 2023, doi: 10.1126/sciadv.adh9673.

[288] S. L. Hansen *et al.*, "An organoid-based CRISPR-Cas9 screen for regulators of intestinal epithelial maturation and cell fate," *Sci Adv*, vol. 9, no. 28, Jul. 2023, doi: 10.1126/sciadv.adg4055.

[289] K. S. Yan *et al.*, "Non-equivalence of Wnt and R-spondin ligands during Lgr5+ intestinal stem-cell self-renewal," *Nature*, vol. 545, no. 7653, pp. 238–242, May 2017, doi: 10.1038/nature22313.

[290] J. K. Heppert, J. M. Davison, C. Kelly, G. P. Mercado, C. R. Lickwar, and J. F. Rawls, "Transcriptional programmes underlying cellular identity and microbial

responsiveness in the intestinal epithelium," *Nat Rev Gastroenterol Hepatol*, vol. 18, no. 1, pp. 7–23, Jan. 2021, doi: 10.1038/s41575-020-00357-6.

[291] G. S. Gulati *et al.*, "Single-cell transcriptional diversity is a hallmark of developmental potential," *Science (1979)*, vol. 367, no. 6476, pp. 405–411, Jan. 2020, doi: 10.1126/science.aax0249.

[292] M. B. Uccellini and A. García-Sastre, "ISRE-Reporter Mouse Reveals High Basal and Induced Type I IFN Responses in Inflammatory Monocytes," *Cell Rep*, vol. 25, no. 10, pp. 2784-2796.e3, 2018, doi: 10.1016/j.celrep.2018.11.030.

[293] J. von Moltke *et al.*, "Rapid induction of inflammatory lipid mediators by the inflammasome in vivo," *Nature*, vol. 490, no. 7418, pp. 107–111, Oct. 2012, doi: 10.1038/nature11351.

[294] I. Rauch *et al.*, "NAIP-NLRC4 Inflammasomes Coordinate Intestinal Epithelial Cell Expulsion with Eicosanoid and IL-18 Release via Activation of Caspase-1 and -8," *Immunity*, vol. 46, no. 4, pp. 649–659, Apr. 2017, doi: 10.1016/j.immuni.2017.03.016.

[295] N. Oberbeck *et al.*, "The RIPK4–IRF6 signalling axis safeguards epidermal differentiation and barrier function," *Nature*, vol. 574, no. 7777, pp. 249–253, 2019, doi: 10.1038/s41586-019-1615-3.

[296] L. Lin *et al.*, “Unbiased transcription factor CRISPR screen identifies ZNF800 as master repressor of enteroendocrine differentiation,” *Science (1979)*, vol. 382, no. 6669, pp. 451–458, Oct. 2023, doi: 10.1126/science.adi2246.

[297] K. M. de Lange *et al.*, “Genome-wide association study implicates immune activation of multiple integrin genes in inflammatory bowel disease,” *Nat Genet*, vol. 49, no. 2, pp. 256–261, Feb. 2017, doi: 10.1038/ng.3760.

[298] M. Q. Kwa *et al.*, “Receptor-interacting protein kinase 4 and interferon regulatory factor 6 function as a signaling axis to regulate keratinocyte differentiation,” *Journal of Biological Chemistry*, vol. 289, no. 45, pp. 31077–31087, 2014, doi: 10.1074/jbc.M114.589382.

[299] X. Huang *et al.*, “Phosphorylation of Dishevelled by Protein Kinase RIPK4 Regulates Wnt Signaling,” *Science (1979)*, vol. 339, no. 6126, pp. 1441–1445, Mar. 2013, doi: 10.1126/science.1232253.

[300] S. Taki, “Type I interferons and autoimmunity: lessons from the clinic and from IRF-2-deficient mice,” *Cytokine Growth Factor Rev*, vol. 13, no. 4–5, pp. 379–391, Aug. 2002, doi: 10.1016/S1359-6101(02)00023-0.

[301] K. Minamide *et al.*, “IRF2 maintains the stemness of colonic stem cells by limiting physiological stress from interferon,” *Sci Rep*, vol. 10, no. 1, p. 14639, Sep. 2020, doi: 10.1038/s41598-020-71633-3.

[302] T. Sato *et al.*, “Regulated IFN signalling preserves the stemness of intestinal stem cells by restricting differentiation into secretory-cell lineages,” *Nat Cell Biol*, vol. 22, no. 8, pp. 919–926, Aug. 2020, doi: 10.1038/s41556-020-0545-5.

[303] M. Q. Kwa, G. M. Scholz, and E. C. Reynolds, “RIPK4 activates an IRF6-mediated proinflammatory cytokine response in keratinocytes,” *Cytokine*, vol. 83, pp. 19–26, 2016, doi: 10.1016/j.cyto.2016.03.005.

[304] V. Lopez-Pajares *et al.*, “Glucose modulates transcription factor dimerization to enable tissue differentiation,” *bioRxiv*, p. 2022.11.28.518222, Jan. 2022, doi: 10.1101/2022.11.28.518222.

[305] J. Lu *et al.*, “Lin28A promotes IRF6-regulated aerobic glycolysis in glioma cells by stabilizing SNHG14,” *Cell Death Dis*, vol. 11, no. 6, p. 447, Jun. 2020, doi: 10.1038/s41419-020-2650-6.

[306] Y.-C. Jou *et al.*, “Cyproheptadine, an epigenetic modifier, exhibits anti-tumor activity by reversing the epigenetic silencing of IRF6 in urothelial carcinoma,” *Cancer Cell Int*, vol. 21, no. 1, p. 226, Dec. 2021, doi: 10.1186/s12935-021-01925-9.

[307] K. Kowalec *et al.*, “Common variation near IRF6 is associated with IFN-β induced liver injury in multiple sclerosis,” *Nat Genet*, vol. 50, no. 8, p. 1081, Aug. 2018, doi: 10.1038/S41588-018-0168-Y.

[308] R. Huang, Z. Hu, Y. Feng, L. Yu, and X. Li, “The Transcription Factor IRF6 Co-Represses PPARγ-Mediated Cytoprotection in Ischemic Cerebrovascular Endothelial Cells,” *Sci Rep*, vol. 7, no. 1, p. 2150, May 2017, doi: 10.1038/s41598-017-02095-3.

[309] S. Lukhele *et al.*, “The transcription factor IRF2 drives interferon-mediated CD8+ T cell exhaustion to restrict anti-tumor immunity,” *Immunity*, vol. 55, no. 12, pp. 2369-2385.e10, Dec. 2022, doi: 10.1016/j.immuni.2022.10.020.

[310] H. Miyoshi and T. S. Stappenbeck, “In vitro expansion and genetic modification of gastrointestinal stem cells as organoids,” *Nat Protoc*, vol. 8, no. 12, p. 2471, 2013, doi: 10.1038/NPROT.2013.153.

[311] O. Shalem *et al.*, “Genome-Scale CRISPR-Cas9 Knockout Screening in Human Cells,” *Science*, vol. 343, no. 6166, p. 84, Jan. 2014, doi: 10.1126/SCIENCE.1247005.

[312] K. Clement *et al.*, “CRISPResso2 provides accurate and rapid genome editing sequence analysis,” *Nature Biotechnology 2019 37:3*, vol. 37, no. 3, pp. 224–226, Feb. 2019, doi: 10.1038/s41587-019-0032-3.

[313] W. Li *et al.*, “MAGeCK enables robust identification of essential genes from genome-scale CRISPR/Cas9 knockout screens,” *Genome Biol*, vol. 15, no. 12, p. 554, Dec. 2014, doi: 10.1186/s13059-014-0554-4.

[314] B. Wang *et al.*, “Integrative analysis of pooled CRISPR genetic screens using MAGeCKFlute,” *Nat Protoc*, vol. 14, no. 3, pp. 756–780, Mar. 2019, doi: 10.1038/s41596-018-0113-7.

[315] A. Dobin *et al.*, “STAR: ultrafast universal RNA-seq aligner,” *Bioinformatics*, vol. 29, no. 1, pp. 15–21, Jan. 2013, doi: 10.1093/bioinformatics/bts635.

[316] L. Wang, S. Wang, and W. Li, “RSeQC: quality control of RNA-seq experiments,” *Bioinformatics*, vol. 28, no. 16, pp. 2184–2185, Aug. 2012, doi: 10.1093/bioinformatics/bts356.

[317] P. Ewels, M. Magnusson, S. Lundin, and M. Käller, “MultiQC: summarize analysis results for multiple tools and samples in a single report,” *Bioinformatics*, vol. 32, no. 19, pp. 3047–3048, Oct. 2016, doi: 10.1093/bioinformatics/btw354.

[318] Y. Liao, G. K. Smyth, and W. Shi, “featureCounts: an efficient general purpose program for assigning sequence reads to genomic features,” *Bioinformatics*, vol. 30, no. 7, pp. 923–930, Apr. 2014, doi: 10.1093/bioinformatics/btt656.

[319] M. I. Love, W. Huber, and S. Anders, “Moderated estimation of fold change and dispersion for RNA-seq data with DESeq2,” *Genome Biol*, vol. 15, no. 12, pp. 1–21, 2014, doi: 10.1186/s13059-014-0550-8.

[320] Y. Hao *et al.*, “Integrated analysis of multimodal single-cell data,” *Cell*, vol. 184, no. 13, pp. 3573-3587.e29, Jun. 2021, doi: 10.1016/j.cell.2021.04.048.